Award Number: W81XWH-14-1-0295

TITLE: Microenvironments and Signaling Pathways Regulating Early Dissemination, Dormancy, and Metastasis

PRINCIPAL INVESTIGATOR: Julio A. Aguirre-Ghiso

CONTRACTING ORGANIZATION: Mount Sinai School of Medicine
New York, NY 10029

REPORT DATE: September 2016

TYPE OF REPORT: Annual

PREPARED FOR: U.S. Army Medical Research and Materiel Command
Fort Detrick, Maryland 21702-5012

REPORT DOCUMENTATION PAGE

Form Approved
OMB No. 0704-0188

1. REPORT DATE	**2. REPORT TYPE**	**3. DATES COVERED**
September 2016	Annual	1Sep2015 - 31Aug2016

4. TITLE AND SUBTITLE
Microenvironments and Signaling Pathways Regulating Early Dissemination, Dormancy, and Metastasis.

5a. CONTRACT NUMBER

5b. GRANT NUMBER
W81XWH-14-1-0295

5c. PROGRAM ELEMENT NUMBER

6. AUTHOR(S)
Julio Aguirre-Ghiso, John Condeelis

E-Mail: Julio.aguirre-ghiso@mssm.edu

5d. PROJECT NUMBER
0010533517

5e. TASK NUMBER

5f. WORK UNIT NUMBER

7. PERFORMING ORGANIZATION NAME(S) AND ADDRESS(ES)

Mount Sinai, School of Medicine,
New York, NY, 10029

8. PERFORMING ORGANIZATION REPORT NUMBER

9. SPONSORING / MONITORING AGENCY NAME(S) AND ADDRESS(ES)
U.S. Army Medical Research and Materiel Command
Fort Detrick, Maryland 21702-5012

10. SPONSOR/MONITOR'S ACRONYM(S)

11. SPONSOR/MONITOR'S REPORT NUMBER(S)

12. DISTRIBUTION / AVAILABILITY STATEMENT
Approved for Public Release; Distribution Unlimited

13. SUPPLEMENTARY NOTES
NA

14. ABSTRACT

We devoted effort to both aims, to optimize methods and publish the first phase of efforts. **SA1** is to understand the intrinsic mechanisms of dissemination by early-progressed cancer cells and how the microenvironment in these primary sites named P-TMEM (**P**rimary **T**umor **M**icro**e**nvironment of **M**etastases) contribute to early dissemination. We now have new data suggesting that a signature of early dissemination markers consisting on $HER2^{HI}$/p-$ATF2^{LO}$/E-$cadh^{LO}$ could identify motile early-progressed tumor cells and predict for dissemination. We further show that mammary tissue macrophages and $HER2^{HI}$/p-$ATF2^{LO}$/E-$cadh^{LO}$ tumor cells cooperate to disseminate early. This further supports our hypothesis that even in early cancer lesions macrophages and tumor cells assemble with endothelial cells a TMEM structure. We have also made progress in generating a standardized triple staining that captures all these cell types in all tissues and we have used intravital imaging to document intravasation in early cancer lesions (see also partnering PI progress report). Our work revealed that the presence of intraepithelial macrophages in DCIS samples in mouse models or humans could accurately predict dissemination in 70% of the cases of patients with bone marrow DTCs (**D**isseminated **T**umor **C**ells). **SA2** focuses on elucidate how S-TMEM (**S**econdary **T**umor **M**icro**e**nvironment of **M**etastases) contributes to the dormancy phase of early DTCs. We found that early DTCs appear to undergo a p38 independent but TWIST-dependent dormancy in secondary organs revealing a new pathways for dormancy. Our new data also show that depletion of macrophages during early dissemination steps significantly reduces metastasis that develop into the late stages of progression, providing functional support for macrophages in P- and S-TMEM structures in metastasis development. This work is now part of two papers, one accepted for publication in the journal ***Nature*** and the other under review in ***Nature Communications***. Progress has also been made in the sorting protocol to isolate CFP+/HER2+ DTCs from lungs and CTCs in the MMTV-Neu-CFP model and we have also performed single cell RNA-seq which will allow us in the next year to identify the early and late gene signatures in DTCs we proposed in our grant.

15. SUBJECT TERMS

dormancy, early dissemination, EMT, macrophages, TMEM

16. SECURITY CLASSIFICATION OF:			**17. LIMITATION OF ABSTRACT**	**18. NUMBER OF PAGES**	**19a. NAME OF RESPONSIBLE PERSON**
					USAMRMC
a. REPORT	**b. ABSTRACT**	**c. THIS PAGE**			**19b. TELEPHONE NUMBER** *(include area code)*
U	U	U	UU	99	

Table of Contents

Page

INTRODUCTION

Our *hypothesis* proposes the existence of a primary tumor microenvironment of metastasis or P-TMEM, previously only detected in invasive cancers, in pre-malignant lesions. This P-TMEM is required to induce an EMT and early dissemination of ErbB2^{high}/P-p38^{low} MECs. We further hypothesize that in order to exit dormancy early DTCs need to maintain the secondary- TMEM (S-TMEM) after extravasation. If early DTCs cannot sustain the S-TMEM they then persist in dormancy. This is critical because even in patients bearing invasive lesions, early DTCs may constitute a large subpopulation of dormant DTCs that evade therapies. Our *rationale* is that by understanding early dissemination and dormancy we may find ways to eradicate dormant DTCs and prevent metastasis. Our original specific aims were:

AIM 1. To test how ErbB2^{high}/P-p38^{low} MECs assemble P-TMEM during early dissemination. Our *goals* are to 1)- use intravital imaging and *MMTV-ErbB2-CFP*, *MMTV-PyMT-EGFP-c-fms-CFP* transgenic mice and modulation of ErbB2 and p38 signaling to detect P-TMEM function during intravasation of "early" and "late" ErbB2+ MECs, 2)- obtain expression profiles from early and late CTCs to identify genes involved in MΦ recruitment and dormancy onset and 3)- perform a pilot analysis of human tissues to correlate early dissemination markers with DTCs in bone marrow of patients. We *expect* to identify how ErbB2+ MECs assemble P-TMEM, how early CTCs are predisposed to enter dormancy and that human sample analysis will correlate early dissemination markers with DTCs in bone marrow.

AIM2. To test the role of S-TMEM in regulating early DTC dormancy. The majority of pre-malignant solitary early DTCs are dormant and not associated with MΦ. In contrast, MΦ are always embedded in proliferating metastasis even if small. Our *goals* are to **A)** test the function of S-TMEM during early DTCs dormancy and **B)** isolate early and late DTCs to determine their dormancy profiles and the mechanisms that distinguish their S-TMEM assembling potential. We *expect* to identify pathways regulating dormancy of early and late DTCs and how these differ in their ability to induce metastatic-niches in target organs. We anticipate these data to reveal novel mechanisms to target dormant DTCs.

PROGRESS REPORT- DoD grant Number: W81XWH-14-1-0295

Title: Microenvironments and Signaling Pathways Regulating Early Dissemination, Dormancy, and Metastasis.

Introduction: We provide a summary of the original aims, their rationale and specific progress (see Results section) focused on the tasks set for this proposal. At the end of the Results we list the additional tasks that will be expanded for the next year.

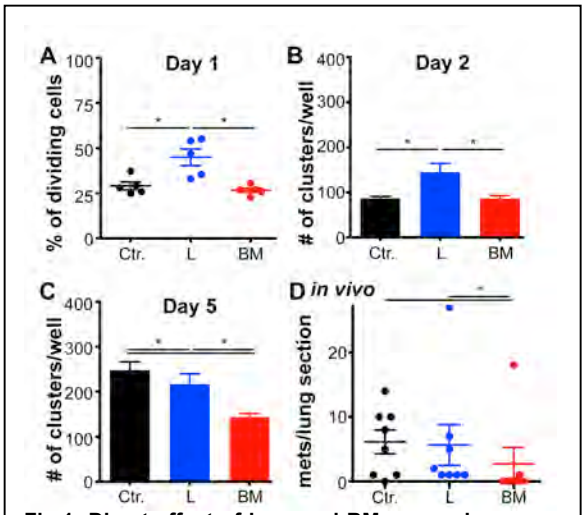

Fig.1: Direct effect of lung and BM macrophages on growth of 4T1 cells in 3D in vitro and in vivo. 4T1-GFP cells were seeded in matrigel either alone or mixed with primary lung or bone marrow MΦs. Dividing 4T1 cells were quantified after 1 day and clusters >2cells were quantified on day 2 and 5. While lung MΦs initially stimulated proliferation (A,B), BM MΦs had a long term growth inhibitory effect (C). 4T1-mCherry cells were injected into the tail vein of wild type mice wither alone or in a 1:1 ratio with either lung or BM resident MΦs.

Specific Aim 1- To test how ErbB2^{high}/P-p38^{low} MECs assemble P-TMEM during early dissemination.

SA1.1. Objective: Use intravital imaging and MMTV-ErbB2-CFP, MMTV-PyMT-EGFP-c-fms-CFP transgenic mice and modulation of ErbB2 and p38 signaling to detect P-TMEM function during intravasation of "early" and "late" ErbB2+ MECs.

Results: As described in the progress report (PR) for funding year (FY) 1, we had established and performed live imaging live to follow the intravasation of early cancer cells using MMTV-Neu-**CFP** (**c**yan **f**luorescent **p**rotein) mice. We detected the effect of p38 inhibition on early dissemination. These experiments are part of one paper (attached to this PR as Appendix 1) accepted for publication in ***Nature***.

In PR FY1 we had also described how early dissemination from pre-invasive HER2+ lesions is driven by mammary gland tissue resident macrophages a P-TMEM component. We completed these studies in FY2

and submitted a manuscript to ***Nature Communications*** where it is currently **under review** (**Appendix 2**). These findings demonstrated how macrophages enter pre-invasive lesions before any overt tumors can be detected and induce a WNT-dependent EMT and thereby drive early dissemination. In FY2 we now investigated whether these early macrophage-containing lesions also contained P-TMEM structures characterized by the interaction of early cancer cells, macrophages and the vasculature. We therefore optimized the triple staining to detect TMEM structures by IHC. This was done in collaboration with the partnering PI John Condeelis and is described in detail in his **progress report (**W81XWH-14-1-0296). Briefly, we found that P-TMEM can be found in pre-invasive HER2+ structures, supporting our novel finding that macrophage-driven dissemination occurs during these early breast cancer stages. Depletion of macrophages before overt tumor detection drastically reduced early dissemination and diminished the onset of metastasis even when macrophage depletion was stopped when tumors became invasive. Resident CCR2+/CD206+/VCAM-/Tie2+ macrophages were attracted into early lesions by CCL2 produced by early HER2+ cancer cells in an NFkB-dependent manner. Intra-epithelial macrophages and loss of E-cadherin junctions was also found in human DCIS, but not normal breast tissue. Interestingly the Tie2 is a marker of the macrophages that in large primary tumors open the endothelium for entry of tumor cells into the vasculature[1]. Thus, it seems that a population of mammary resident macrophages during very early stages of cancer are executing the same function of TAMs in invasive tumors.

Conclusions: We confirmed that P-TMEM is formed in HER2-driven tumors. This already occurs in pre-malignant lesions in the absence of invasive cancer. We also conclude that macrophages are vital for early dissemination and that macrophages and early cancer cells are critical contributors to late metastasis.

Plans for the coming year: We will increase the sample size of pre-malignant MMTV-HER2 samples of different ages and correlate the occurrence of P-TMEM structures with the amount of CTCs. We will use the mouse models available in the partnering PI's lab to image the P-TMEM formation in real time using intravital imaging. Given that early dissemination is detected in both PyMT and Her2 MMTV models[2] we will fist test the PyMT model tat is already available from the Condeelis lab[1]. In addition we will continue to work to see the paper in Nature Communications published, an essential deliverable of our efforts.

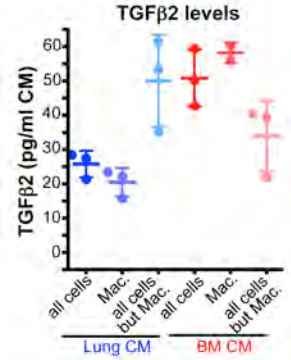

Fig.2: TGFb2 levels regulated by BM and lung resident macrophages. CM from lung or BM cell suspension was prepared (all cells). Additionally, alveolar or BM resident MΦs were FACS sorted from cell suspension and CM was made from isolated MΦs or cell suspension without macrophages. TGFβ2 levels in conditioned medium were determined by ELISA.

<u>SA1.2.</u> Objective: Obtain expression profiles from early and late CTCs to identify genes involved in MΦ recruitment and dormancy onset.

Results: In order to isolate CTCs (also termed circulating cancer cells, CCCs) by FACS, we initiated the optimization of flow cytometric detection of tumor cells in the MMTV-ErbB2-CFP model. As reported in PR of FY1, our initial experimental plan to detect MMTV-HER2-CFP cancer cells based on their CFP expression was hampered by the fact that CFP could also be detected in other host cells not expressing HER2 and when looking for rare cells in circulation or target organs with low DTC burden this was difficult to achieve. In FY2, we therefore changed our approach and optimized flow cytometric analysis of the HER2 oncogene. We were able to successfully detect HER2+ early and late cancer cells both in the primary site and the lung as a secondary site. We FACS sorted early HER2+ cancer cells from the primary site as well as CTCs and DTCs in different target organs. We then processed them using the C1 Fluidigm system and submitted these samples for RNAseq analysis. This effort was dedicated towards both SA1.2 and SA2.2 and is described in detail in SA2 below. We are currently awaiting results from the RNA seq analysis. Once we obtain the data, we will then analyze the expression of macrophage recruitment factors in early vs. late cancer cells to test the hypothesis that early cancer cells fail to attract macrophages and therefore fail to form S-TMEM and enter dormancy instead.

Additionally, we had proposed that lack of association of macrophages with DTCs may foster dormancy while interaction with macrophages might stimulate awakening from dormancy or prevent dormancy all together. We tested the hypothesis whether the interaction of DTCs with macrophages indeed fueled DTC proliferation. Interestingly, most mouse models such as the MMTV-HER2 models develop metastases mostly in the lung but never in the bone[3, 4]. Yet, DTCs are frequently observed in the bone marrow[3, 5]. This raised the question whether DTCs in the BM do not associated with macrophages or whether possibly bone resident

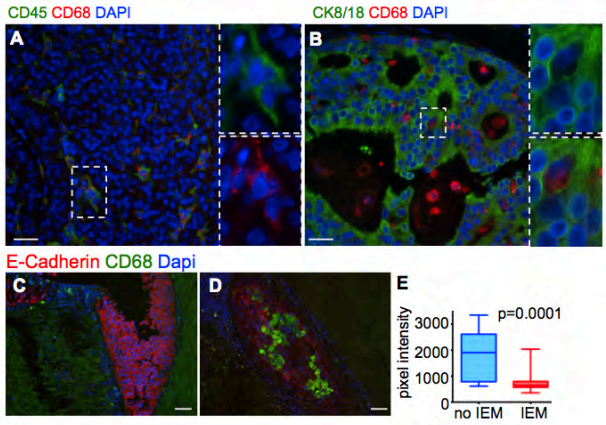

Fig3. Human DCIS sections were stained against CD68 and CD45 (**A**) and CD68 and cytokeratin 8/18 (**B**). **B,C**: Two individual ducts in one DCIS lesion of the same patient with either high E-Cadherin and low intra-epithelial macrophage (IEM) levels (**C**) or low E-Cadherin levels and high IEM levels (**D**) within the same patient. **E**: Quantification of E-Cadherin signal intensity in the region of cell junctions within ducts of the same patients with either high or low numbers of IEMs.

macrophages have a different effect on DTC proliferation than lung resident macrophages. By comparing how bone marrow and lung macrophages function we may better understand how S-TMEM functions in different target organs. To address this question in more detail, we investigated the direct effect of lung and BM resident macrophages on cancer cell proliferation by performing a direct 3D co-culture of primary alveolar and BM resident macrophages with the 4T1 cancer cell line in Matrigel (**Fig.1A-C**). We found that while lung macrophages initially stimulated proliferation (**Fig.1A,B**), BM macrophages had as a long-term effect an inhibitory capacity on the proliferation of 4T1 breast cancer cells (**Fig.1C**).

We then tested this posibility in an experimental metastasis assay *in vivo* and co-injected 4T1-mCherry cancer cells with either lung or BM resident MΦs purified via FACS. The addition of BM MΦs significantly reduced metastasis formation compared to co-injection with lung MΦs or injection of 4T1 cancer cells alone (**Fig.1D**). This led us to the conclusion that while lung resident macrophages initially stimulate proliferation, BM resident MΦs seem to have a long term growth inhibitory effect. Because in previous work we had described that dormancy of DTCs in the bone microenvironment is induced by high levels of TGFβ2[4], we tested the production of TGFβ2 by resident MΦs from either lung or BM (**Fig.2**). We found that TGFβ2 levels were higher in total BM suspension and in primary BM MΦs CM compated to total lung and lung MΦ CM. Additionally, when MΦs had been removed from the organ cell suspensions by FACS sorting (Fig.2 "all cells but macs"), this significantly increased TGFβ2 levels in lung suspension and significantly reduced TGFβ2 levels in BM suspension. This argues that macrophages in lungs may suppress the formation of dormancy inducing microenvironments and sets the stage for testing how S-TMEM in lungs functions when macrophages are affected.

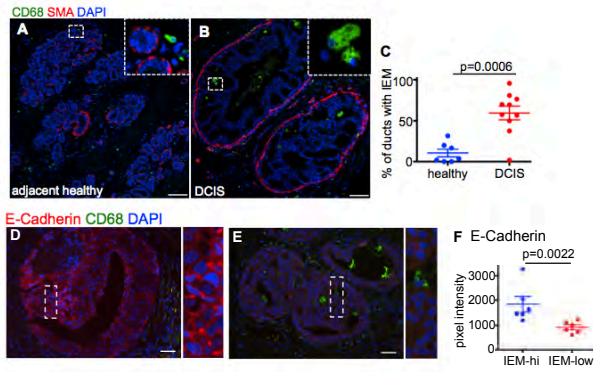

Figure 4. Intra-epithelial macrophage numbers in human DCIS lesions negatively correlate with E-Cadherin levels. Human adjacent healthy (**A**) and DCIS tissue (**B**) was stained against CD68 (macrophages) and smooth muscle actin (SMA). Bar: 75μm. Plot shows mean plus SEM of the percentage of ducts intra-epithelial macrophages (IEM) from 7 healthy and 10 DCIS patients; each dot represents one patient (**C**). Sections from human DCIS tissue were stained against CD68 (macrophages) and E-Cadherin (**D,E**). E-Cadherin pixel intensity was quantified in regions of individual cell junctions and medians for individual patients were quantified. Plot (**F**) depicts mean E-Cadherin intensity throughout DCIS lesions of individual patients with low or high intra-epithelial macrophage (IEM) numbers (total patient number N=12). All bars 25μm.

Conclusion: We successfully established the isolation of HER2+ cells from primary and secondary sites and were able to isolate RNA from isolated cells. This will allow us to identify factors in early vs. late DTCs that are responsible for MΦ recruitment (See below). We further identified that association of DTCs with MΦs is not sufficient to induce proliferation but the tissue context and macrophage subtype seem to be crucial as well. Specifically, while lung resident MΦs foster proliferation, BM resident MΦs seem to induce DTC dormancy due to the expression of high TGFβ2 levels. This might explain why in the bone even highly aggressive DTCs are not able to form metastases: upregulation of MΦs recruitment factors and subsequent recruitment of bone resident MΦs would only result in a more stable state of dormancy in the bone microenvironment.

Plans for the coming year: We will receive complete RNAseq data soon and perform bioinformatics analysis to compare the expression profiles of early versus late HER2+ cancer cells to identify possible factors upregulated in early vs. late HER2+ cancer cells that are involved in macrophage recruitment. This will then complete SA1.2

SA1.3. Objective: To correlate early dissemination markers in primary breast tumors (DCIS and invasive lesions) with DTC presence in BM.

Results*:* In FY1 we had performed a pilot study to test whether the presence of macrophages in DCIS lesions could predict dissemination. We received de-identified paraffin embedded DCIS sections from patients that had undergone a bone marrow biopsy to determine their DTC status from Tanja Fehm, University Clinic Duesseldorf, Germany. Using high levels for E-Cadherin and low numbers of intra-epithelial macrophages as a positive predictive criterion, we correctly predicted 7 out of 10 patients being positive for the presence of DTCs, resulting in a positive predictive value of 70%. While due to the small sample size, these results were not significant these preliminary data seemed promising. These data were reported last year. We are awaiting for new samples from the Fehm team to continue our analysis. We did however explore additional variables in this year, which tested whether the presence of macrophages in DCIS lesions from humans also correlated with an EMT-like phenotype and the loss of e-cadherin junctions.

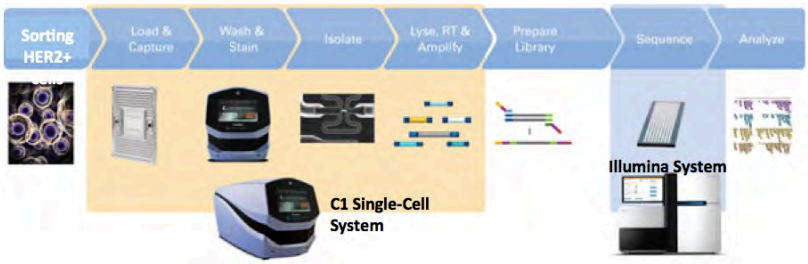

Figure 5. Flow chart of the protocol to obtain single-cell RNASeq using C1 Single-Cell and Illumina Systems. This pipeline was applied for single cell analysis from early cancer cells from premalignant lesions and tumor cells derived from primary tumors. By performing single cell RNA-seq from all stages and sites we will be able to better capture the heterogeneity and noise of the system.

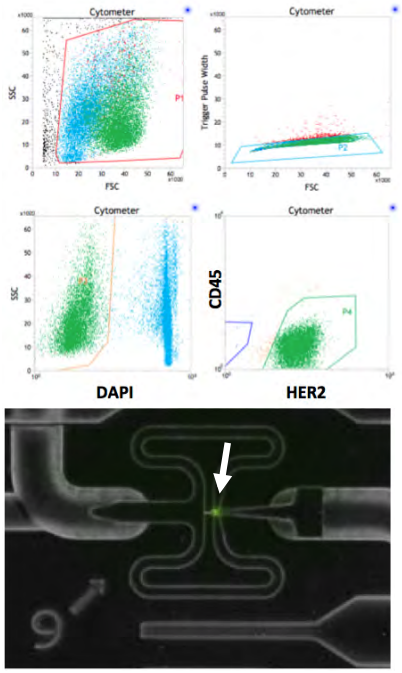

Figure 6. *Top,* Sorting of MMTV-Neu cells using HER2 immunofluorescence as a selection marker for subsequent loading into the C1 chips and machine. *Bottom*, Image of a HER2+ cell (green) captured in a C1 chip well before processing for RNA extraction.

Published data showed that more than 10% of patients with DCIS had detectable DCCs in their bone marrow (BM), but no histologic markers, which include invasive fronts and receptor status were indicative of the presence of DCCs [6]. To test whether macrophages could also infiltrate early lesions in humans, we compared macrophages in healthy human breast tissue vs. tissue from DCIS lesions as a model of early stage breast cancer lesions. Macrophages were identified as CD68+/CD45+ and cytokeratin 8/18 negative cells (**Fig.3A,B**). In breast tissue from healthy donors, macrophages were localized in the stroma in the vicinity of mammary ducts but remained outside of the ducts, which were delimited by an intact myoepithelial layer of cells (**Fig.4A**). In contrast, even in DCIS lesions that displayed an apparently intact myoepithelial layer, there was a statistically significant increase in the frequency of macrophages found inside the aberrant ductal epithelial structure in between cancer cells (**Fig.4B,C**). The association of intra-epithelial macrophages with reduced E-Cadherin levels was confirmed in human DCIS samples (N=12). This was independent of HER2 status and appeared in different patterns. Patients with high macrophage numbers within lesions showed overall lower E-Cadherin levels as measured by quantitative image analysis **(Fig.4D-F**). Additionally, within the same patient, individual lesions with high macrophage numbers had lower E-Cadherin levels (**Fig.3C-E**). This reveals an inter- and intra-tumor heterogeneity and suggests that some regions of DCIS lesions might be more prone to contain cancer cells able to undergo early dissemination. In previous studies the lab of Dr. Condeelis had identified that P-TMEM structures are indicative of metastasis in patients with invasive breast cancer[7]. In collaboration with the Condeelis lab we were now able to demonstrate that P-TMEM structures can also be found in MMTV-Her2 mouse pre-invasive lesions equivalent to DCIS and that their number might correspond with early dissemination (**see SA1.1 and collaborators progress report**).

Conclusion: Both the identification of intra-epithelial macrophage numbers with E-Cadherin levels and the formation of P-TMEM structures in pre-invasive lesions seem to be a promising tool to predict early dissemination. We postulate that combining TMEM detection of early cancer cells with macrophages around

the vasculature and E-Cadherin levels will provide a powerful tool for the prediction of early dissemination in DCIS patients.

Plans for the next year: The group of Tanja Fehm is currently extending their clinical study to collect more DCIS material from patients with matching DTC status and we are awaiting to receive more samples, to extend these data. In FY3 we are aiming to perform stainings of E-Cadherin and intra-epithelial macrophages as performed in FY1 and staining of P-TMEM structures as established in FY2 in serial sections of the extended data set. We are expecting to a) increase the accuracy of our predictive value by combining these two approaches and b) receive a better positive predictive value due to the increased sample size to be able to make a statistical statement about the quality of our predictive markers.

SA2. To test the role of S-TMEM in regulating early DTC dormancy.

Objective: Objectives: 1)- test whether early DTCs assemble S-TMEM for dormancy escape and 2)- expression profile early and late lung DTCs. In this first year majority of the effort was dedicated to Aim 1, which is very advanced in progress. In addition to the effort that went towards aim we focused most of the effort in Aim 2 towards optimizing the methods to obtain an early vs. late DTCs. In Y3, having optimized the detection of TMEM in the MMTV-Neu model, we are now going to focus o detecting S-TMEM in the secondary organs.

2.1 *To test whether early DTCs form S-TMEM and if these influence escape from dormancy.*

Results: Our aim proposed that the formation of a S-TMEM is required for the escape from dormancy and that early DTCs might be less efficient to form a S-TMEM. Our data in **Appendix 1** clearly supports the notion that for prolonged periods DTCs remain in a dormant state. Our past year's report supported the function for macrophages during early dissemination. Thus, in the next year the detection of S-TMEM in lungs and bone marrow will be executed.

Plans for the coming year: Once we confirm by histology the presence of the TMEM structure in lungs and bone marrow we will initiate the imaging of lungs of MMTV-PyMT-ECFP-c-fms-GFP mice while inhibiting p38 signaling as proposed.

2.2 Molecular profiling of early DTCs. In order to recover early and late DTCs in target organs and identify the gene programs distinguishing their behavior we are developing the optimization protocols described for the isolation of single cells from MMTV-Neu-CFP mice. We also need to know what the gene signatures are fro the tissue of origin so we need to optimize single cell analysis for all sites. As indicated we experienced problems due to leakiness of the MMTV promoter in target organs (see SA1.2). To overcome this problem we optimized a FACS protocol specific for the Her2 oncogene expressed in the MMTV-Her2 model. Given the low abundance of some of these DTCs we decided to incorporate singe cell RNA-seq into our pipeline in order to take advantage of any cell we can recover. Given the dramatic evolutionary differences between these two populations we are comparing, single cell analysis should reveal differences if we are able to compile the analysis of a few dozen cells. **Figure 5** shows the pipeline from cell sorting to RNA-seq we have utilized. Significant effort went into optimizing the cell suspension conditions to load the C1 Fluidigm chips that allowed trapping single cells and producing RNA from them. We used this system and the sorting protocol shown in **Figure 6**. This protocol yielded interpretable and alignable RNAseq data for 9 single cells from early lesions and 4 cells from primary tumor (**Table I**). These are currently being analyzed and as we add on new single cells they will be analyzed jointly to identify the signatures and the potential macrophage recruiting factors.

ID – single Cell	Total Reads	Mapped	Genes Detected	Transcripts Detected
MG14_S7	4748934	2813650	1588	2353
MG25_S8	579288	485168	2223	3317
MG26_S11	1427604	656324	735	1093
MG32_S9	882702	743310	1993	2928
MG33_S10	1870430	1091808	1083	1606
MG38_S12	930082	740698	1476	2213
MG39_S13	3095362	1913650	1420	2164
MG43_S15	1090996	585438	1270	1876
MG51_S16	587796	512026	2253	3380
PT26_S4	616958	224058	2121	3146
PT27_S1	827186	671482	526	770
PT32_S2	711652	558490	845	1249
PT51_S3	558992	457644	2421	3572

Table I. Library preparation using single cell RNAseq raw alignment data from pre-malignant MMTV-Neu tissue (MG) or from primary tumors (PT).

Plans for the next year: We plan to 1) continue to use the antibody based sorting approach to detect HER2 DTCs and then proceed with the original plan of profiling these cells. We plan to continue using the C1 RNA-seq system to obtain the signatures. We also plan to perform laser capture micro-dissection of the metastasis in mice that carry only early lesions or that were injected with early lesion developed mammospheres. This will also allow testing the expression profile and genetics of these lesions and compare them with spontaneously emerging metastasis in the autochthonous colony and with the single cell expression profiles. We anticipate that in Y3 we will be able to obtain a signature of early-disseminated cancer cells. This will allow monitoring the presence of these early DCCs over time in mouse tissue and monitor perhaps their presence in patient samples such as DCCs in bone marrow aspirates or circulating cancer cells.

Key Research Accomplishment

Specific Aim 1

- Macrophages enter pre-invasive lesions before any overt tumors can be detected and induce a WNT-dependent EMT.
- Depletion of macrophages in MMTV-HER2 mice before overt tumor detection drastically reduces early dissemination and diminishes the onset of metastasis even when macrophage depletion was stopped when tumors became invasive.
- Resident CCR2+/CD206+/VCAM-/Tie2+ macrophages are attracted into early lesions by CCL2 produced by early HER2+ cancer cells in an NFkB-dependent manner.
- In collaboration with the John Condeelis lab, we found that intra-epithelial macrophages inside early lesions in MMTV-HER2 mice are often associated with the vasculature and thus resemble P-TMEM structures.
- Using *in vitro* and *in vivo* approaches, we found that while addition of lung resident MΦs 4T1 breast cancer cells promote proliferation, BM resident macrophages have an adverse growth-inhibitory effect, indicating that S-TMEM formation might have organ specific effects.
- We analyzed more DCIS lesions (N=12) and found that the association of intra-epithelial macrophages with reduced E-Cadherin levels was significant. (these findings are reported in Linde et al. 2016 – Appendix 2).
- Succsessfuly performed intravital imaging and provided video evidence of intravasation dueing early stages of cancer progression when P-TMEM is forming in these tissues. (Reported by the partnering PI and in Harper et al., 2016 – Appendix 1).

Specific Aim 2

- We optimized the FACS sorting of early HER2+ cancer cells as well as disseminated cancer cells from late stages from lungs (ongoing efforts for SA1 and 2).
- Optimized the usage and isolation of single cells using the C1 Fluidigm system.
- Optimized the RNA extraction and library creation for single cell RNA-seq and successfully obtained RNA-seq data from ~14 single cells frommearly and late stages of progression using the FACS protocol for HER2.
- Identified gain of TWIST and loss of E-cadherin expression as a potential important regulator mechanism for early dissemination and DTC dormancy in lung (Harper et al., 2016 – Appendix 1)

Reportable Outcomes:
Publications relevant to this project:

Publications:

1. Linde N, Fluegen G, Aguirre-Ghiso JA. The Relationship Between Dormant Cancer Cells and Their Microenvironment. *Adv Cancer Res. 2016* ;132:45-71. doi: 10.1016/bs.acr.2016.07.002. Epub 2016 Aug 25. PMID:27613129.

2. Klionsky DJ, Abdelmohsen K, Abe A, Abedin MJ, Abeliovich H, Acevedo Arozena A, Adachi H, Adams CM, Adams PD, Adeli K, Adhihetty PJ, Adler SG, Agam G, Agarwal R, Aghi MK, Agnello M, Agostinis P, Aguilar PV, Aguirre-Ghiso, et al., Guidelines for the use and interpretation of assays for monitoring autophagy. *Autophagy*. 2016 Jan 2;12(1):1-222. No abstract available. PMID: 26799652

Manuscripts Accepted:

1. Kathryn Harper, Maria Soledad Sosa, Hedayatollah Hosseini, Alvaro Avivar Valderas, Chandandaneep Nagi, Roger Davis, Christoph Klein, David Entenberg, John Condeelis, Eduardo F. Farias and Julio A. Aguirre-Ghiso#. "Identification of an ErbB2+ early disseminating pre-malignant cancer cell sub-population with metastatic potential". * *Both authors contributed equally*. # Corresponding authors. Accepted in ***Nature.***

2. Hedayatollah Hosseini, Kathryn Harper, Maria Soledad Sosa, Lahiri Kanth Nanduri, Christian Werno, Carolin Ehrl, Matthias Maneck, Milan Obradovic, Nina Patwary, Gundula Haunschild, Christian Reimelt, Florian Weber, Josef Schroeder, Julio Aguirre-Ghiso, Piero Musiani, Andreas Hartkopf, Florin-Andrei Taran, Tanja Fehm, Gunter Meister, Christoph A. Klein. "Her2 and progesterone signaling cooperate for early dissemination of breast cancer cells". Accepted in ***Nature.***

3.

Manuscripts Submitted:

1. Nina Linde, Arthur Mortha, Eduardo Farias, Maria Soledad Sosa, Kathryn Harper, Ethan Tardio, Miriam Merad, and Julio A. Aguirre-Ghiso. Macrophages orchestrate early dissemination of HER2+ cancer cells.– *Manuscript under revision in* ***Nature Communications****.*

Oral presentations:

- **2015: Speaker, TMEN Steering Committee Meeting,** 21-23 January 2015. Seattle, WA
- **2015: Keynote Speaker – Porto Cancer and Stem Cells meeting, IPATIMUP,** Porto, Portugal.
- **2015: Invites speaker – FASEB SRC on TGFβ signaling,** Snowmass CO, USA.
- **2015: Invited Speaker – University of Colorado Cancer Center,** Denver CO, USA.
- **2015: Invited Speaker – University of Kentuky,** Lexington**,** KY, USA.
- **2015: Speaker – Samuel Waxman Cancer Research Foundation Annual Symposium**, New York, NY, USA.
- **2015: Invited Speaker - CNIO Metastasis Meeting, Madrid, Spain.**
- **2015: Invited Speaker - Abbvie –** Chicago, IL – USA
- **2015: Invited Speaker - AACR Tumor Metastasis Meeting,** Austin TX – USA
- **2016: Invited Speaker - TMEN Steering Committee Meeting**. OSHU, Portland OR.
- **2016: Invited Speaker – Distinguished Seminar Series – Wistar Institute,** Philadelphia, PA.
- **2016: Invited Speaker – Distinguished Seminar Series – Albert Einstein College of Medicine,** Bronx, NY.

- **2016: Invited Speaker – Biological Sciences Department Seminar Series, University of Southern California,** Los Angeles, CA

Posters
NA

Awards
NA

CONCLUSION

SUMMARY OF FINDINGS:
Progress in our second year of funding has been highly significant as we demonstrated that early pre-invasive breast cancer lesions contain P-TMEM structures and provided evidence for the role of P-TMEM associated macrophages in early dissemination and subsequent metastasis formation. We showed that this was driven by the induction of an EMT due to macrophage-derived Wnt. We further revealed the signaling pathway recruiting macrophages and characterized P-TMEM associated macrophages in detail. This was complemented by the first video documentation os intravasation and local invasion in early lesions performed in collaboration with the partnering PI, Dr. John Condeelis (See Harper et al 2016 – Appendix 1 and the partnering PI progress report). We also found that there was a significant association of intra-epithelial macrophages with low E-Cadherin levels in DCIS patients. We further demonstrate that macrophages as S-TMEM components are able to induce DTC proliferation but this depended on the macrophage subtype: while lung resident macrophages drive proliferation, BM resident macrophages rather inhibit proliferation and possibly even induce dormancy. Additionally, we successfully isolated early and late cancer cells both from the primary and the secondary target organ site and submitted these samples for RNAseq analysis. We also used an evidence based approach and identified TWIST as a potential regulator of early DTC dormancy and that the loss of E-cadherin expression is also linked to early DTC dormancy. This will allow us to investigate the expression profile of early and late cancer cells and specifically how these might act to establish an S-TMEM in funding year 3. Overall, our findings support our hypothesis that early dissemination contributes to metastasis but also to a dormant DTC population that may be reactivated from dormancy by macrophages in the lung while DTCs in the bone might escape a reactivation from dormancy through BM resident macrophages. Our identification of the origins of DTCs may help to understand their biology and how to suppress dissemination and to avoid metastasis formation.

SIGNIFICANCE:
Our work is revealing an unexpected contribution of early DTCs to dormancy and metastasis in cooperation with macrophages. Our work challenges the current model of linear metastasis formation and argues that a better understanding of disseminated disease is required and might allow for novel therapies that target dormant DTCs and prevent metastasis formation. Our work is highly relevant as it provides insight into early dissemination during stages that have commonly been considered as pre-invasive and thus harmless. Yet, recent studies have caused great confusion on how to treat women with stage 0 breast cancer. A recent study published in JAMA Oncology adds to this confusion as it shows that while breast cancer deaths from DCIS metastasis are ~3% of the whole population, 50% (thousands of women each year) die of metastasis in the absence of an invasive breast cancer recurrence and the choice of therapy did not affect survival. This suggests that the DTCs remain untouched by therapies and that a subpopulation of women with stage 0 breast cancer carry early disseminated cancer cells that can have deadly consequences. We therefore need better tools to identify those stage 0 patients at high risk of developing late metastatic relapses without overtreating the majority of women who have harmless variants of DCIS. We believe that our work provides significant progress towards identifying markers to differentiate high risk and low risk cases of early breast cancer stages. We will conclude these studies in funding year 3 by analyzing the expression profiles or early and late cancer cells that we will receive soon. We will then test those markers that we identified in funding year 1 and 2 and those that we will identify soon in collaboration with Tanja Fehm from the University Clinic Dusseldorf, Germany who is currently extending her clinical study to receive samples from more DCIS patients with known DTC status.

References:

1. Harney, A.S. *et al.* Real-Time Imaging Reveals Local, Transient Vascular Permeability, and Tumor Cell Intravasation Stimulated by TIE2hi Macrophage-Derived VEGFA. *Cancer discovery* **5**, 932-943 (2015).
2. Husemann, Y. *et al.* Systemic spread is an early step in breast cancer. *Cancer Cell* **13**, 58-68 (2008).
3. Sosa, M.S., Bragado, P. & Aguirre-Ghiso, J.A. Mechanisms of disseminated cancer cell dormancy: an awakening field. *Nature reviews. Cancer* **14**, 611-622 (2014).
4. Bragado, P. *et al.* TGF-beta2 dictates disseminated tumour cell fate in target organs through TGF-beta-RIII and p38alpha/beta signalling. *Nat Cell Biol* **15**, 1351-1361 (2013).
5. Aguirre-Ghiso, J.A., Bragado, P. & Sosa, M.S. Metastasis awakening: targeting dormant cancer. *Nat Med* **19**, 276-277 (2013).
6. Banys, M. *et al.* Hematogenous and lymphatic tumor cell dissemination may be detected in patients diagnosed with ductal carcinoma in situ of the breast. *Breast cancer research and treatment* **131**, 801-808 (2012).
7. Rohan, T.E. *et al.* Tumor microenvironment of metastasis and risk of distant metastasis of breast cancer. *J Natl Cancer Inst* **106** (2014).

Appendices:

Appendix 1: Kathryn Harper, Maria Soledad Sosa, Hedayatollah Hosseini, Alvaro Avivar Valderas, Chandandaneep Nagi, Roger Davis, Christoph Klein, David Entenberg, John Condeelis, Eduardo F. Farias and Julio A. Aguirre-Ghiso#. "Identification of an ErbB2+ early disseminating pre-malignant cancer cell sub-population with metastatic potential". ** Both authors contributed equally*. # Corresponding authors. Accepted in ***Nature. (See attached manuscript in following pages)***

Appendix 2: Nina Linde, Arthur Mortha, Eduardo Farias, Maria Soledad Sosa, Kathryn Harper, Ethan Tardio, Miriam Merad, and Julio A. Aguirre-Ghiso. Macrophages orchestrate early dissemination of HER2+ cancer cells.– *Manuscript under revision in* ***Nature Communications****.* ***(See attached manuscript in following pages)***

Mechanism of early dissemination and metastasis during early stages of Her2+ mammary cancer.

Kathryn L. Harper[1#], Maria Soledad Sosa[1#*], David Entenberg[4], Julie F. Cheung[1], Rita Nobre[1], Alvaro Avivar-Valderas[1], Chandandaneep Nagi[1], Hedayatollah Hosseini[2], Nomeda Girnius[3], Roger J. Davis[3], Eduardo F. Farias[1], John Condeelis[4], Christoph Klein[2], and Julio A. Aguirre-Ghiso[1*]

[1]Division of Hematology and Oncology, Department of Medicine, Department of Otolaryngology, Department of Oncological Sciences, Tisch Cancer Institute, Black Family Stem Cell Institute, Mount Sinai School of Medicine, New York, NY 10029, USA. [2]Experimental Medicine and Therapy Research Faculty of Medicine University of Regensburg, 93053 Regensburg, Germany. [3]Howard Hughes Medical Institute, University of Massachusetts Medical School, MA 01605, USA. [4]Department of Anatomy and Structural Biology, Integrated Imaging Program, Gruss Lipper Biophotonics Center, Albert Einstein College of Medicine, 1300 Morris Park Ave, Bronx, NY 10461, USA.

[*]*Correspondence to:* Maria Soledad Sosa and Julio A. Aguirre-Ghiso,

E-mails: maria.sosa@mssm.edu, julio.aguirre-ghiso@mssm.edu

# Denotes equal contribution.

Running title: Signaling pathways regulating early dissemination

ABSTRACT

The mechanisms that generate early-disseminated cancer cells (eDCC) during pre-malignant stages of cancer are poorly understood. Here we show that in early lesions, before any overt tumor masses are detected, there is a sub-population of Her2^{+}/P-p38^{lo}/ATF2^{lo}/TWIST^{hi}/E-cadherin^{lo} early cancer cells that are invasive and disseminate to target organs. Intra-vital imaging and organoid studies of early lesions revealed that Her2+ eDCC precursors locally invaded, intravasated and lodged in target organs. Her2 induced in eDCCs a Wnt-dependent EMT-like program but without complete loss of epithelial luminal phenotype. Further, Her2 or Wnt inhibition reversed the eDCC phenotype by restoring p38 activation and E-cadherin junctions. Surprisingly, although the majority of eDCCs are TWIST^{hi}/E-cadherin^{lo} and temporarily non-proliferative, they can eventually initiate metastasis. Our work reveals that, before stimulating growth, Her2 aberrantly activates an invasive program similar to mammary ductal branching that leads to early dissemination and metastasis. These findings provide insight into the mechanisms that give origin to eDCCs and their potential contribution to systemic cancer heterogeneity, dormancy and metastasis.

INTRODUCTION

Metastasis is the leading cause of cancer related deaths and these lesions can develop after prolonged periods of latency, possibly due to the existence of quiescent/dormant disseminated cancer cells (DCC)[1,2]. In addition to the genetic heterogeneity of DCCs, which has been appreciated for long[3,4], active and dormant DCCs may contribute to the phenotypic heterogeneity of metastasis initiating cells, the timing of metastasis and therapy failure [2,5]. These and other studies[3,4,6-8] showed that bone marrow residual DCCs detected before the manifestation of breast cancer metastasis contain fewer genetic abnormalities than primary tumors or than DCCs from patients with detectable metastases. These findings argued that dissemination might be occurring since early stages of tumor

evolution when lesions such as DCIS are detected[5,6,9]. Husemann et al.[5] found that activated Her2, which is commonly upregulated in DCIS at higher frequency than the gene amplification is detected in invasive cancers, was found to drive early dissemination but the mechanisms remained unknown. These authors also defined “early DCCs” (eDCCs) as those originating at times when the transgenic mice had no visible or palpable tumours or when patients displayed smallest invasive tumours or in situ lesions only[5].

Early dissemination was also documented in models of pancreatic cancer[10] and melanoma[11] arguing for its existence in other cancers. Another relevant scenario for early dissemination may be cancer of unknown primary, which is a frequent cancer diagnosis [12,13] where cancer cells might acquire disseminating capacity early, form metastases but fail to grow at the primary site. These concepts and findings have been highly debated because it was not clear how almost normal-like DCCs might complete the metastatic cascade long before accumulating genetic alterations commonly associated with malignancy. However, modeling pre-malignant disease in Her2 and PyMT transgenic mice provided a tractable model to ask these questions[5].

Anoikis resistance is a trait of metastatic cells that promotes survival upon interactions with varying extracellular matrices and loss of adhesion in circulation[14]. Interestingly, anoikis resistance is activated at early stages of Her2-driven mammary cancer by inhibiting the p38 kinase, known to also suppress breast tumorigenesis[15-17]. This process is also accompanied by ERK1/2 activation, which positively regulates motility and invasion [18,19]. Importantly, inactivating mutations in the p38 activator MKK4[20,21] and amplification of the p38 phosphatase PPM1D [16,22] are also frequent in breast cancer, suggesting that different mechanisms might allow for inactivation of p38–induced anoikis among other processes. We addressed the question of whether loss of p38 signaling and acquisition of anoikis resistance in the context of enhanced Her2 signaling in incipient cancers might be also accompanied by the acquisition of invasive programs that enable dissemination to distant organs. We further asked whether such traits could spawn innocuous DCCs or DCCs with metastatic potential.

Here we reveal that upregulation of Her2, before causing a frank stimulation of cancer cell proliferation, results in the activation of Wnt signaling, which contributes to p38 inhibition and an epithelium to mesenchyme (EMT)-like response. This culminates in Her2-dependent stimulation of intravasation and early dissemination to target organs where eDCCs maintain a TWIST^{hi}/E-cadherin^{lo} profile linked to a non-proliferative stem-like state that eventually leads to lung metastasis by reversing to a TWIST^{lo}/E-cadherin^{hi} profile. These findings are corroborated by the analysis of Hosseini et al., (see accompanying paper) and together reveal a previously unrecognized molecular mechanism for Her2-driven early dissemination that originates from deregulated survival and morphogenesis programs observed during mammary ductal tree development [17,23,24].

RESULTS

Her2^{+} Early Cancer Cells display p38 pathway inhibition and loss of E-cadherin/β-catenin junctions.

We previously showed in the FvB-derived MMTV-Her2 (wt) model (**S-Fig1A**), that Her2 upregulation induced anoikis resistance by inhibiting p38 signaling[17]. We now explored whether the concomitant loss of p38 signaling and upregulation of Her2 in early cancer cells might activate a disseminating phenotype. To this end we analyzed early lesions (EL) during stages where mammary gland whole mounts and exhaustive histological analysis revealed normal ductal architecture, hyperplasias and mammary intraepithelial neoplasias[25], but no primary tumor masses (**S-Fig1A-C)**. Her2 to overexpression in DCIS has been linked to E-cadherin downregulaiton and progression to invasive cancer[26]. Further, p38 can maintain E-cadherin expression[27]. Thus, we measured the correlation between levels of Her2^{+} and E-cadherin in EL of MMTV-Her2 mice. We found that >85% of Her2^{+} cells were E-cad^{lo} (**Fig. 1A**). Detection of P-p38 and P-ATF2 (a reliable p38 activity readout[17]) and E-cadherin (epithelial marker) in Her2+ and Her2-T+ EL tissues (**Fig. 1B, S-Fig. 1D)** revealed that E-Cad^{hi} early cancer cells were more frequently (>60%) P-ATF2^{hi} (**Fig. 1B and S-**

Fig1D). In each duct 60-70% of all EL cells were positive for membrane β-catenin (**Fig1C**). However, when considering Her2+ cells, only 30% displayed membrane localization for β-catenin (**S-Fig1E**). Thus, Her2 expression was associated with a loss of membrane β-catenin in both MMTV-Her2 and Balb-NeuT models (**Fig1C** and **S-Fig1E**) (membrane localized β-catenin, is considered to be in the *inactive* form). Overall, these results suggest that $Her2^{+}$ cells display loss of E-cadherin/β-catenin based junctions and are $P\text{-}ATF2^{lo}$ (**Fig. 1A, B, C, S-Fig. 1D-E**).

Overt MMTV-Her2 tumors showed low levels of E-cadherin, P-p38 and P-ATF2, while maintaining high P-ERK1/2 levels (**S-Fig. 2A, B and C**), suggesting that a $Her2^{+}/P\text{-}ATF2^{lo}/E\text{-}cad^{lo}$ profile is present in EL and also in primary tumors. When correlating P-ATF2 levels with E-cadherin junction levels with Her2 status in human DCIS lesions, we found that only $Her2^{negative}$ lesions (n=5) retained both high P-ATF2 levels and organized E-Cadherin junctions (**S-Fig. 2D-E**). In contrast, $Her2^{+}$ DCIS lesions (n=5) were low for P-ATF2 and E-cadherin signals (**S-Fig. 2D-E**). We also found that the $Her2^{+}/P\text{-}p38/P\text{-}ATF2^{lo}$ profile was present in larger $Her2^{+}$ breast carcinomas (n=20) where only $Her2^{negative}$ tumors (n=10) showed very strong nuclear staining for P-p38 and P-ATF2 compared to Her2+ lesions (n=10) (**S-Fig2F)**. We conclude that in early human and mouse cancer cells Her2 upregulation is associated with low E-cadherin, P-p38 and P-ATF2 levels. We further conclude that this profile persists in larger proliferative primary tumors in the MMTV-Her2 model and human tissues.

$Her2^{+}$ / $E\text{-}cad^{lo}$ / $P\text{-}p38^{lo}$ Early Cancer Cells Display an Invasive Phenotype.

The Her2+ DCIS samples and MMTV-Her2 lesions displayed loss of E-cadherin/β-catenin junctions and low P-ATF2 levels, suggesting reduced p38 signaling and possibly a role for p38 in preventing an invasive phenotype (**S-Fig2A-E**). Thus, we hypothesized that a $Her2^{+}/E\text{-}Cad^{lo}/P\text{-}ATF2^{lo}$ profile may foster invasive capacity. To this end we used MCF10A-Her2 overexpressing cells as a human 3D organoid model of EL cells because like early MMTV-Her2 lesions they show increased survival in the luminal space, misshapen architecture and occasional single cell invasion from the

organoids (**S-Fig.3A-B**). Her2 activation inhibited p38 signaling and E-cadherin junctions, because treatment of Her2-MCF10A cells or of MMTV-Her2 organoids with lapatinib or with siRNAs targeting Her2 (in MCF10A-Her2), restored E-cadherin junctions and P-ATF2 levels (**Fig1D-E and S-Fig3C**); the lapatinib effect was measured as downstream inhibition of P-S6 ribosomal protein (**Fig1E**). EGFR, (a target of lapatinib), was also involved in p38 signaling inhibition in Her2 overexpressing cells because inhibition of EGFR kinase activity with AG1478 led to inhibition of phosphorylation of the downstream target AKT and also to the restoration of E-cadherin junctions and increased the percentage of cells with high P-ATF2 levels (**Fig. 1D-E**, **S-Fig3C)**. Similar upregulation of P-ATF2 was seen when organoids derived from EL MMTV-Her2 mammary epithelial cells were treated with a pan-PI3K inhibitor (GDC-0941) or AKT inhibitor (MK2266) (**Fig. 1D-E and S-Fig. 3C**); inhibition of PI3K and AKT was monitored by detecting phosphorylation of S6 ribosomal protein, a downstream target of the pathway. Because JNK can also phosphorylate ATF2 we tested whether p38 inhibition eliminated the increase in P-ATF2 levels upon Lapatinib treatment (**S-Fig4F**). IF analysis revealed that MCF10A-Her2 cells displayed basal nuclear accumulation of P-ATF2 levels that was completely eliminated by a 24hrs treatment with 5 μM SB203580 (**S-Fig4F**). As in previous experiments (**Fig1D**) Lapatinib stimulated nuclear accumulation of P-ATF2 and this signal was reduced to basal levels in control cells by the same dose and time treatment with SB203580 (**S-Fig4F**). We conclude that a combined Her2/EGFR (HER1) signaling through PI3K and AKT regulates p38 inhibition in EL cells (**Fig 1D-E, S-Fig. 3C, S-Fig4F and Fig7 for pathway summary**). Based on our previous results in organoids and *in vivo* showing that P-ATF2 is almost entirely dependent on p38 activity in mammary epithelial cells[17] and the data in **S-Fig3C** and **S-Fig4F**, we conclude that the vast majority of P-ATF2 signal upon HER2/EGFR inhibition is dependent on p38α/β.

Her2-expressing MCF10A or early MMTV-Her2 misshapen organoids showed outward invasion of single cells rich in f-actin decorated projections, which are associated with cell migration[28,29], loss of E-cadherin and focalized loss of the basement membrane ECM molecule[30]

laminin-V deposition (**Fig1F and S-Fig3B and D**). The f-actin cytoskeleton of invading cells was in the cell-cell contacts indicating that these were not cells that had remained randomly solitary and incapable of forming organoids (**Fig1F and S-Fig3B and D**). The single cell invasion from organoids was confirmed by time-lapse confocal spinning disc microscopy (**Supplemental Movie1**), which revealed single cells invading into the Matrigel matrix out from the main body of the organoids (**Supplemental Movie1, top panels**); these invasive cells were further highlighted using a software filter of Image J (**Supplemental Movie1, bottom panels**). Downregulation of E-cadherin signal was also observed in $Her2^{+}$ invading MMTV-Her2 early cancer cells detected in histological sections (**Fig1G**). Interestingly, ~80% of invading $E\text{-}caderin^{lo}$ cells were $Her2^{+}$ and $CK8/18^{+}$, suggesting that downregulation of E-cadherin does not associate with a complete loss of epithelial identity; only ~20% of CK8/18+ invading cells were negative for Her2 (**S-Fig3E**).

We next tested whether forcing a Her2+/$P\text{-}p38^{lo}$ profile using the p38α/β inhibitor SB203580 on Her2+ cells would stimulate invasion. In 3D cultures, SB203580 stimulated an invasive phenotype of MMTV-Her2 cells and MCF10A-Her2 cells **(Fig1F and S-Fig3D**). Inhibition of p38α/β in MMTV-Her2 organoids resulted in a degradation of laminin-V basement membrane (diffuse green signal) and in enhanced f-actin protrusive structures into the 3D Matrigel (**Fig1F**). Invasion was frequently a single cell process and only occasionally we observed what appeared to be collective invasion and only after p38α/β inhibition (**Fig1F and S-Fig3D**). We conclude that $Her2^{+}/E\text{-}cad^{lo}/\beta\text{-}cat^{lo}/P\text{-}p38^{lo}$ early cancer cells display an invasive phenotype without loss of CK8/18 expression.

High-resolution intravital imaging reveals that p38 signaling antagonizes Her2+ early cancer cell intravasation and dissemination.

The previous results suggested that $Her2^{+}$ EL cancer cells are invasive undergo an epithelium to mesenchyme transition (EMT)-like response. However, these data, which were mostly inferred from static images. To fully confirm that the invasive capacity of Her2+ EL cells is functional *in vivo*

we used high-resolution intra-vital imaging[31] of MMTV-Her2-CFP transgenic mice to unambiguously record at single-cell level resolution the invasive capacity of early $Her2^+$ invasive cancer cells (**Fig2**). We designed a mammary imaging window to accommodate the depth and lax consistency of the mammary fat pad tissue. 2-photon imaging of regions of the ductal tree in vehicle treated Her2-CFP mice where the vasculature is revealed by i.v. delivered dextran-rhodamine[31] showed infrequent early cancer cell invasion at 10 weeks when the ducts still display mostly normal ductal architecture (**Fig2A, left – Supplemental Movie 2)**. However, at 15 and 18 weeks, when early lesions are observed, local invasive CFP+ cells were imaged even in an area that captures a very small fraction of the transgenic mammary tree (**Fig2A middle and right - Supplemental Movies 3 and 4**). We also detected at this time CFP+ cell translocation and invasion into the stroma (**Fig2A, right - Supplemental Movies 3 and 4**). Double staining for Her2 and CFP in tissue sections revealed that the vast majority of CFP positive cells were (>90%) Her2 positive regardless of their location (**S-Fig3F**). Thus, CFP reports faithfully for Her2 overexpressing cells.

Forcing a $Her2^+$/P-$p38^{lo}$ profile using a p38α/β inhibitor revealed an enhancement of the motile and invasive phenotype observed in basal conditions (**Fig2A-D**). Now CFP+ cells showed the formation of cell protrusions, intra-lesion migration and local invasion and intravasation (**Fig2B, C and D and Supplemental Movie 5, 6 and 7**). Unlike in 3D cultures (**Fig1F** bottom bright field and **S-Fig3D**), we did not observe collective cell migration *in vivo*. High-resolution imaging and 3D reconstruction of the invasion and intravasation events showed unambiguously how individual cells invaded outwards from the ductal pre-malignant lesions and invaded through the stroma (**Fig2B'-C and Supplemental Movies 7**) entering the lumen of blood vessels that is revealed by the overlay of the CFP signal an the dextran-rhodamine signal that only occupies the luminal space (**Fig2C and D and Supplemental Movie 7 and 8**).

We confirmed the intravasation documented in the movies by measuring CK8/18+ eCCCs in peripheral blood, in Her2+/CK8/18+ eDCCs in BM and Her2+ eDCCs in lungs of EL MMTV-Her2 mice

(**Fig2E-G and S-Fig3G).** We found that Her2+/CK8/18+ eDCCs are detected in the blood, BM and lungs of 100% of 14-18 weeks old mice, when only early lesions and no tumor masses are present (**Fig2E-G and S-Fig3G**). Her2 was detected using two independent antibodies (mouse and rabbit) and control IgG antibodies by IF. Both antibodies revealed similar patterns of Her2 staining absent when using the pre-immune IgG (**S-Fig. 4A-D**).

Systemic inhibition of p38α/β for 2 weeks revealed that SB203580 treatment significantly increased the numbers of eCCCs detected using CK8/18 detection (**Fig2H**). Using CK8/18 and Her2 detection we also detected an increase in the total number of CK8/18+/Her2^{+} eDCCs in the BM (**Fig2I**) and detection of Her2 also revealed an increase Her2^{+} eDCC in lungs after systemic p38α/β inhibition (**Fig2J**). The median number of eDCCs in the BM compartment is equivalent to ~20.2 eDCCs/ 10^6 BM host cells in control groups and ~46 eDCCs/10^6 BM host cells in SB203580 treated animals. The imaging of EL showing intravasation followed by the detection of circulating and disseminated cancer cells confirms that CK8/18+ early Her2^{+} cancer cells successfully disseminate and this process can be further stimulated by forcing a p38^{lo} profile.

Mechanism of Her2+ early dissemination requires p38 inhibition to enhance an EMT-like program.

The above results suggested that successful dissemination occurs in Her2+ EL cells that downregulate p38 signaling and E-cadherin junctions. We further explored this hypothesis and found that treatment of MCF10A-Her2 organoids with SB203580 or siRNAs targeting p38α caused a loss of E-cadherin junctions (**Fig3A-B**). A similar effect was found in early MMTV-Her2 organoids (**Fig3C-D**). We also found that both genetic and pharmacological inhibition of p38 signaling resulted in a trend to reduce total membrane localized inactive β-catenin and increased active-β-catenin (unphosphorylated β-catenin detected with a conformation-specific antibody[32]) (**Fig3A-D and S-Fig4E**); in MMTV-Her2 organoids p38 inhibition also resulted in increased cytosolic β-catenin signal (**Fig3C** right panels).

Despite the apparent decrease in β-catenin membrane localization we could not detect nuclear β-catenin by IF in MCF10A-Her2 or MMTV-Her2 organoids (**Fig3A, C, B**). The same IF protocol detected nuclear β-catenin in COMMA-1D mammary cells arguing that this assays is below the detection limit for these models (not shown). To further confirm the functional nuclear translocation of β-catenin we used *AXIN2* mRNA (a canonical target of β-catenin[33]) as readout of β-catenin transcriptional activity. Inhibition of p38α/β in MCF10A-Her2 cells resulted in the upregulation of *AXIN2* mRNA (**Fig3F**) and *SNAIL* and *TWIST* were also upregulated when MCF10A-Her2 3D organoids treated with siRNAs targeting *p38α* or *ATF2* (**Fig3G**). These data further support that p38α and ATF2 block the transcriptional activity of β-catenin.

Importantly, systemic inhibition of p38α/β for 2 weeks in MMTV-Her2 mice at early stages induced a strong loss of E-cadherin junctions in the vast majority of early cancer cells (**Fig4A and** IgG controls in **S-Fig4G**). *In vivo* this occurred concomitantly with the translocation of β-catenin from the membrane to the nucleus, which was now detected using the IHC protocols (**Fig4B and S-Fig4G**). The accumulation of nuclear β-catenin upon p38α/β inhibition correlated with a strong induction of *TWIST* in the same tissue (**Fig4C**). These data confirm that successful dissemination occurs in Her2+ EL cells that downregulate p38 signaling and E-cadherin junctions and display β-catenin activation.

To test whether p38 inhibition alone was sufficient to induce E-cadherin and β-catenin junction loss we compared E-cadherin and β-catenin localization in wild type FvB mice treated with or without SB203580 or wild type MKK3+/+|MKK6+/+ and MKK3−/−|MKK6+/− C57B mice (MKK3 and MKK6 activate all p38 isoforms). We found that in normal wild type tissues or in *wt* MCF10A cells, inhibition of the MKK3/MKK6-p38 pathway genetically or pharmacologically caused a loss of E-cadherin junctions (**Fig4D and S-Fig4H-I**), but not loss of membrane β-catenin (**S-Fig4J**). Inhibition of p38 did not alter the distribution of CK8/18 luminal cells and α-smooth muscle actin positive myoepithelial cells (**S-Fig4J**). We conclude that SB203580 recapitulates the genetic ablation of the MKK3/MKK6-

p38 pathway and its effect on E-Cadherin junction formation. Our data also suggest that in the absence of Her2 expression, p38 inhibition was insufficient to change β-catenin localization (**Fig4B and S-Fig4J**).

Activation of the EMT-like program in Her2^{+} early cancer cells requires Wnt signaling.

The possibility that Her2+ EL cells might activate an EMT-like response led us to measure the expression of 86 EMT-related genes in control (DMSO) and SB203580 treated wt MCF10A and MCF10A-Her2 organoids. Her2 expression or p38 inhibition alone induced a shared 14-gene EMT signature from the 86 tested genes (**Fig5A**), suggesting that both kinases operate antagonistically on the same pathway. The signature, (confirmed by subsequent qPCR (**S-Fig5A-B**), included non-canonical *WNT* ligands (WNT5a/b, WNT11) and a WNT receptor (*FRZD7*), canonical EMT transcription factors (TFs) (*TWIST, SNAIL, SLUG*) and *ERBB3* and was further upregulated by p38 inhibition in Her2-MCF10A cells (**Fig5A**). In agreement with a decrease in E-cadherin junction formation, *E-cadherin* mRNA was also downregulated by p38 inhibition using a p38α/β inhibitor or siRNA to p38α in Her2-MCF10A organoids (**Fig5B**). These data confirm that successful early dissemination occurs in Her2+ EL cells that downregulate p38 signaling induce an EMT-like response that correlated with Wnt ligands upregulation.

TWIST can induce pluripotency programs [34,35] but depending on the level of expression and timing it can also lead along with other genes to a migratory and non-proliferative phenotype [35,36] that may explain the dormancy of eDCCs[37]. We used IF to quantify the proportion of EL cells expressing the TWIST protein and whether its expression changed in overt primary tumors. **S-Fig5C** shows that TWIST was readily detected as a nuclear cluster signal using IF in both EL and PT cells. During early stages ~60% of the ductal cells were Her2+/TWIST+, ~15% were Her2+/TWIST- and ~10% were either Her2-/TWIST+ or double negative. The latter two groups likely represent normal MECs. In PT we found a 20% increase in the Her2+ cells expressing TWIST and a similar proportion of

Her2+/TWIST- cells. The other two populations are absent because the PT is largely Her2+ and there are no normal MECs. We conclude that TWIST is expressed in the majority of EL cells and that with progression to PT this proportion increases by ~20%, suggesting no major changes in the proportion of TWIST expressing in EL or PT lesions.

We next tested if Wnt ligands (**Fig5A and S-Fig5A and B**) were functionally linked to Her2-driven EMT. When Her2-MCF10A cells were treated with SB203580 the *AXIN2* mRNA was induced and this response was almost completely eliminated in MCF10A-Her2 cells expressing the Wnt-ligand antagonist sFRP (canonical and non-canonical Wnt ligand inhibitor) (**Fig5C, S-Fig5D**). Recombinant soluble Wnt3a ([38] and methods) also stimulated expression of *Axin2* in Her2-MCF10A cells, and this induction was significantly inhibited by expression of a constitutively active p38α kinase (p38αD176A + F327S mutant) cDNA[17] (**Fig5D**). We conclude that Her2^{+}/p38^{lo} pre-malignant cells rely on possibly both canonical and non-canonical Wnt ligands, to induce an EMT-like program.

Next, Her2-MCF10A and sFRP expressing Her2-MCF10A cells were treated with or without SB203580 (**Fig5E-G, S-Fig5D**). Loss of E-cadherin junctions and membrane-localized β-catenin after p38α/β inhibition was reversed in sFRP expressing cells (**Fig5F**). Importantly, the invasion observed in Her2^{+}/P-p38^{lo} organoids after p38 inhibition (**Fig1**) was blocked by sFRP (**Fig5E**). Further, the canonical Wnt inhibitor DKK1, also reversed the E-cadherin loss induced by p38 inhibition in MMTV-Her2 primary organoids (**Fig 5G**). Our data led us to suggest that *via* Wnt signaling, Her2 activation reduces p38α/β activity to activate a partial EMT response that while not causing complete loss of epithelial markers, drives early dissemination.

Her2+ eDCCs are commonly E-cadherin^{lo}, TWIST^{hi} and initiate spontaneous metastasis after a dormancy phase.

Our results suggest that Her2+ EL cells undergo a Wnt-dependent partial EMT (**Fig3-5**) that is sufficient to propel dissemination and lodging in target organs (**Fig2**). We next sought to determine

what is the phenotype and behavior of EL cancer cells in lungs and whether these eDCCs could initiate metastasis. We detected P-Rb (phosphorylated retinoblastoma protein) and P-Ser10 histone-H3 levels, which mark G1-exit and G2/M transition, respectively in lung Her2+ single DCCs (1-5 cell clusters) during EL stages when only eDCCs are found (**Fig6A**). The vast majority of lung solitary eDCCs (1-5 cells) were negative or weakly stained for P-Rb compared to growing micro and macro-metastases in mice carrying primary tumors (**Fig6A, B and D**). This was also the case for P-Ser10 histone-H3 that showed a larger proportion of non-cycling eDCCs in the lung (**Fig6D**). Quantification of E-Cadherin expression showed that the vast majority of Her2+ eDCCs (1-5 cell clusters) in lungs were negative for E-cadherin (**Fig6E**).

Disseminated cancer cells detected in animals bearing overt tumors were named DCCs because we cannot distinguish their exclusive EL origin from those originating from the overt primary tumor. We also measured P-Rb in DCCs present in lungs where solitary DCCs, micro- (6-50 Her2+ cells) and macro-metastasis (>50 Her2+ cells) are detectable (**Fig6 A, B and D**). Animals with overt tumors that were P-Rb^{strong} (**S-Fig5E**) and lungs bearing proliferative (P-Rb^{strong}) micro- and macro-metastases (**Fig6B**) still had numerous quiescent P-Rb^{negative} Her2+ DCCs (**Fig6A and D**). We conclude that eDCCs are primarily P-Rb/P-H3^{negative} and that even in animals bearing metastases >60% of single or small groups of DCCs (less than 5 cells), are non-proliferative. However, Her2+ DCCs detected in animals bearing overt late primary tumors were positive for E-cadherin in ~48% of the population (**Fig6E**), suggesting that reactivation might be linked to an MET as proposed by others[35].

We also found that close to 100% of the solitary (1-5 cell clusters) Her2+ eDCCs were high for TWIST (**S-Fig5F**). In contrast, only 30% of solitary DCCs detected in later stages of progression when animals carried overt primary tumors were positive for Her2 and high for TWIST, also consisitent with a subpopulation of cells restoring E-cadherin expression (**Fig6E**) and reversing the EMT-like response. In macro-metastases (anything larger than 6 cell clusters), now only 40% of the

cells were Her2+/TWIST+. We conclude that proliferation-negative eDCCs express almost in totality TWIST. In contrast, more than half of the DCCs in animals bearing overt primary tumors appear to downregulate TWIST expression.

Inhibition of p38 stimulated early dissemination by stimulating the expression of EMT genes including TWIST (**Fig3G, 4C and 5A**). We reasoned that if the high TWIST expression is due to an inhibition of p38 activation, then dormant eDCCs might be insensitive to p38 inhibitors that can reactivate dormant DCCs in other models of late DCC dormancy[39]. Accordingly, a treatment of MMTV-HER2 mice with p38 inhibitors during EL stages for 2 weeks, while stimulating dissemination from primary sites (**Fig2**), did not simulate the dormant eDCCs to start proliferating in the lungs as measured by P-Rb staining (**S-Fig5G**). However, if the p38 inhibition is done for 2 weeks during the time the tumor is overt (PT stage) now DCCs respond to the p38 inhibitor and the proportion of P-Rb+ cells increases (**S-Fig5G**). These data suggest that the non-proliferative state of $TWIST^{hi}$ eDCCs is independent of p38α/β activation. However, DCCs in animals with overt tumors regain sensitivity to p38α/β inhibition as observed in other models[39]. These last experiments highlight important differences and the dynamic phenotypes of DCCs during progression that need further analysis.

To directly test tumor and metastasis initiating capacity of pure EL cancer cells we prepared sphere cultures from EL MMTV-Her2 cells or tumorspheres from overt MMTV-Her2 tumors (**S-Fig5H**). The efficiency of mammo- or tumor-spheres to generate secondary spheres was higher for EL than PT cancer cells (**S-Fig5I**). However, after orthotopic injection into nude mouse mammary fat pads, 100% of tumorspheres (~300/site; from overt tumors) efficiently formed primary tumors within 4-12 weeks (**Fig 6H, S-Fig5H)**. However, Her2+ mammospheres (~300/site; from early lesions) did not produce obvious palpable tumors when monitored for 1, 3 and 12 months; in three animals Her2+ mammospheres formed small nodules at 2 months but these entered stasis (**Fig 6H**). The tumorigenic capacity of PT tumorspheres orver EL mammaorpheres correlated with enhanced P-ERK1/2 and P-RPS6 levels that were higher in PT than EL spheres indicating enhanced mitogenic

and translation initiation signaling in the former spheres (**S-Fig5J**). Surprisingly, while showing weak or no tumorigenic capacity, animals injected with EL Her2+ mammospheres developed lung metastases detected at 3 or 12 months (macro- and micro-metastases) (**Fig. 6F, G, H**). Micrometastases displayed cortical Her2+ staining and P-Rb^{strong} signal, confirming that these cells are derived from EL MMTV-Her2 cells and can eventually proliferate (**Fig6C and D**). Macro-metastases arising spontaneously in MMTV-Her2 mice bearing autochthonous tumors were also Her2+ and the majority was P-RB^{positive} (**Fig6B, D** and control staining in **S-Fig4B-C**). A similar percentage of P-Rb^{positive} tumor cells were found in macro-metastases derived from EL MMTV-Her2 mammospheres (**Fig6D).** Tumors derived from Her2+ tumorspheres produced detectable Her2+ DCCs (**Fig6G**) and also macrometastasis but with lower incidence (16%) than when mice were injected with mammospheres (**Fig6F-H**).

To determine whether the ability of EL cells to form metastasis was due to enhanced dissemination from primary and/or enhanced colony formation capacity in lugs we performed additional experiments. When mammospheres or tumorspheres (as opposed to single cells) were re-implanted in 3D matrices and imaged over time we found that mammospheres derived from EL cells were vastly superior (> 10 fold) at invading into the surrounding 3D ECM, compared to PT tumorspheres that remained globular and weakly invasive. Thus, in contrast to PT derived cells that proliferate orthotopically EL cells rapidly acquire a motile and invasive phenotype in the mammary fat pad (**S-Fig5J**). These data are in agreement with the invasive phenotype of EL organoids observed in **Fig3F** and also with data in **Figure 2** showing the efficient invasion, intravasation and dissemination of EL cells. We also delivered single EL and PT cells suspensions (not spheres) i.v. and scored the incidence and number of lung experimental metastasis (**S-Fig5K**). These results showed that experimental metastasis incidence was 100% in both groups and while EL cancer cells showed a trend to produce more metastatic nodules this difference was not significant when compared to PT cells. Our data suggest that Her2+ EL cells that downregulate p38 signaling and activate an EMT-like

response, while largely non-tumorigenic in orthotopic sites, successfully activate invasive programs that allow for efficient dissemination and metastasis formation. The latter does not seem to depend only on the ability to colonize lungs (**Fig6F-H and S-Fig5K**).

DISCUSSION

Our findings provide molecular and functional mechanisms of early dissemination by identifying a subpopulation of early cancer cells with disseminating capacity as Her2^{+}/CK8/18^{+}/Wnt^{hi}/P-p38^{lo}/ TWIST^{hi}/E-cad^{lo} (**Fig. 7**). We further show that these early cancer cells are more invasive than PT-derived cells, van generate secondary spheres more efficiently, can intravasate and lodge in secondary organs (**Fig. 7**). Remarkably, eDCCs originating from these early lesions show metastasis-initiating capacity in both spontaneous and experimental metastasis assays (**Fig. 7 and S-Fig5K**), which is not associated with a primary tumor forming capacity or with an obvious advantage in lung seeding and expansion potential in these organs. The tumorigenicity differences do, as expected, correlate with enhanced ERK1/2 activation and enhanced translation intiation as measured by RPS6 phosphorylation, a common readout of the AKT, mTOR pathway[40]. These results support the notion that EL cancer cells are not in a growth mode yet, but are highly efficient at disseminating, carry stem-cell like properties and this efficiency provides an overall increase in subsequent metastasis potential compared to PT-derived cells. Our data also reveal a new sequence in the gene expression programs that Her2 signaling executes early in cancer progression. We find that before detecting any obvious proliferation in early lesions[17], Her2 activates Wnt-driven programs of motility and invasion (**Fig. 7**) along with enhanced survival[17], also observed during branching morphogenesis[23]. Interestingly, Wnt and TGFβ signaling in conjunction with progesterone receptor-B (PgR) favored side branching [23]. With Hosseini et al., we also found that PgR and Wnt4 signaling are enriched in the pre-malignant tissues that spawned eDCCs. Hosseini et al., also showed that wild type ducts that were still undergoing morphogenesis showed a PgR^{hi}

profile. How Her2 and Wnt crosstalk to inhibit p38 is not clear, but Her2, EGFR, PI3K and AKT inhibition restored P-ATF2 levels. While we cannot rule out a contriubution of JNK signaling to ATF2 phosphorylation, our published data and the result reported here strongly argue that p38α/β signaling plays a majoritarian role in ATF2 phosphorylation and this is functionally linked to the early dissemination phenotype.

In both our and the Hosseini et al., studies, EL cells disseminated spontaneously from autochthonous early lesions in the MMTV-Her2 models (FvB-Neu and Balb-Neu) models, from fat pad injected mammospheres or from transplanted pre-malignant mammary tissue (Hosseini et al). Hüsemann et al[5]. also showed that early dissemination occurs in the MMTV-PyMT mouse model and other studies documented early dissemination in pancreatic cancer[10] and melanoma[11] models. These data suggest that the process is not a rarity of the Her2 models and that other cancer types can display oncogene-driven early dissemination before frank overt growth. We found that the majority of Her2+ eDCCs, once in lungs, are predominantly negative for P-Rb and P-Ser10-histone H3, both proliferation markers that allow capturing cells in G1-S and G2/M transitions. These eDCCs are also in their majority E-cadherin^{lo} and TWIST^{hi} suggesting that it may hold the phenoptype of eDCCs in a partial EMT for long periods. Importantly, this phenotype associated with a non-proliferatve phenoptype as proposed by others[35,37]. For example, Prrx1-driven mesenchymal gene programs may prevent eDCCs from forming metastasis[36,37,41]. Although additional data is needed, these data suggest that eDCCs may enter a unique state of dormancy (**Fig. 7** and see below). As seen from mammospheres injected into the fat pad of nude mice, eDCCs eventually were able to form Her2+ metastasis in the absence of overt primary tumors. The exact reasons for this divergence in phenotypes between the primary site and lung are still unclear. However, our 3D organogenesis and experimental metastasis experiments suggest that EL cancer cells are mostly committed to cell movement rather than growth (low activation of ERK and mTOR pathways), which results in very efficient dissemination and once in lungs the cells can eventually grow into metastasis efficiently

albeit after different dormancy phases. The switch controlling the timing of reactivation remains unknown but changes in TWIST and E-cadherin expression may play a role as DCCs found in animals with primary tumors and metastasis had reduced expression of this transcription factor in 70% of cases and upregulation of E-cadherin in about 50% of DCCs. Why EL cancer cells lack strong tumorigenic capacity in the primary site is still unclear but it could be linked to the reduced ERK1/2 and mTOR signaling we detected and/or to the mammary fat pad being primarily permissive for the activation of invasion programs observed during mammary morphogenesis [23,42].

The majority (~98%) of eDCCs in lungs, which were also single cells or <5 cell clusters, were Her2+/TWIST^{hi} but E-cadherin^{lo}. However, eDCCs still expressed CK8/18+, suggesting that a partial EMT program is sufficient for early dissemination and metastasis formation. The partial nature of the EMT program in eDCCs may allow cells to interconvert between dormant and proliferative states as transient *TWIST*-induced EMT allows for stem-cell program activation[43] and a strong EMT and mesenchymal phenptype may strongly block metastasis[43,44]. Cancer cell invasion can also proceed when collective invasion is activated in CK14+/p63+ basal mammary epithelial cells without evidence of EMT [45] and this lack of requirement of a full EMT program is supported by recent studies[35,44,46]. We argue that when Her2 upregulation is combined with p38 inhibition, at least a 14-gene EMT gene module is activated and linked to early dissemination, eDCC dormancy and subsequent metastasis.

Our work also reveals a new role for the tumor suppressive p38α/β kinases[15,22,50-52] and ATF2[53] in antagonizing Her2 signaling early in progression. However, how p38 executes these functions is not clear. The tumor suppressor ATF2 [53], is a likely candidate in preventing an EMT as it can block β-catenin activity [54] and our data showed that *ATF2* RNAi upregulated EMT TFs, while a p38α active mutant blocked *AXIN2* induction by Wnt3a. Non-canonical Wnt ligands were also induced in Her2+/P-p38/P-ATF2^{lo} cells suggesting a potential role in early dissemination. eDCC displayed low p38 activation suggesting that their dormant state might be different from the mechanisms observed previously by us and others[39,55]. Accordingly, we found that eDCCs were not stimulated to

phosphorylate Rb upon systemic treatment with p38α/β inhibitors, which can stimulate expansion of DCCs in HNSCC and prostate cancer models[39,56]. DCCs present at late stages of progression, when animals carry overt tumors, now responded with Rb phosphorylation to p38 inhibition. The mechanism behind this switch awaits further analysis. However, the results suggest that along with TWIST regulation, eDCCs may be different from DCCs that have accumulated up to the time of overt tumor growth. These mechanisms are important as Hosseini et al.,using genetic lineage analysis, showed that a large proportion of metastasis are derived from eDCC ancestors.

Our intra-vital imaging revealed that the process of dissemination is not an exclusive property of invasive overt tumors [57-59]. Local invasion and intravasation was observed for single cancer cells *in vivo* and we did not observe collective migration as observed in 3D systems, including ours ([45] and **Fig2**). CCC or DCC clusters in blood or bone marrow were extremely rare and even the cell clusters (>5 cells) in lungs were negative for proliferation markers (**Fig6A**), suggesting that there is no immediate proliferative advantage for these clusters.

An important question, is in which ways if any, eDCCs contribute to metastasis? One scenario is cancer of unknown primary cancer. This diagnosis in which metastases present without ever finding a primary lesion, accounts for 3-5% of all malignancies and ~4.2% of all solid cancer cases/year, of which 50% are adenocarcinomas[12,13, 60]. Further, 50% of DCIS patients that developed metastasis did so without ever developing any local recurrence[61]. Could these metastases originate from eDCCs? Early dissemination might have contributed to the development of 7 prostate cancer metastases resected 17 years after radical prostatectomy[62]. These metastases showed evolutionary traits that originated from a small low-grade primary tumor subpopulation of cells and not to the more prevalent “aggressive” tumor regions[62].

Our work provides novel insight into how certain oncogenes may initiate dissemination programs before aggressive proliferation is triggered and how a tumor suppressor pathway such as p38, might have previously unrecognized metastasis suppressive function by blocking Her2-driven

early dissemination. These findings expand our understanding of how oncogene and tumor-suppressive pathways operate in early stages of cancer progression and they may improve our understanding on the origins of DCC heterogeneity and how to target it to prevent and treat metastasis.

EXPERIMENTAL PROCEDURES.

See **Supplemental Experimental Procedures** for additional procedures

Cells and cell culture. MCF10A-Her2 cells expressing sFRP were generated using sFRP lentiviral vectors. Wnt3a and DKK1 conditioned media was prepared from Wnt3a expressing L-cells and Dkk1 expressing 293T cells. Vectors and sFRP plasmids were a kind gift from Dr. Stuart Aaronson, ISMMS, New York, NY. Conditioned media was prepared from cells cultured with serum free medium (DMEM + 1%P/S) for 24 hours and then concentrated using Vivaspin 20 Centrifugal Concentrating tubes (Sartorius, VS2021) at 3000g up to 3 hours until desired concentration (10x) was reached.

Mammospheres and tumorspheres assays. Animal procedures were approved by the Institutional Animal Care and Use Committee (IACUC) of Icahn School of Medicine at Mount Sinai protocol 08-0366. MMTV-Her2 mice were sacrificed using CO_2 at age 14-18wk or when overt tumors had formed (PT). For mammosphere preparations, all 5 pairs of glands in mice were checked for the presence of any visible small lesions or palpable tumors when processed for early cancer cell and none were found. Even when other mammary glands were inspected microscopically in whole mounts we could not detect small tumors. Whole mammary glands or tumors were digested in Collagenase/BSA at 37°C for 45-60min. Red blood cell lysis buffer was used to remove blood cells from cultures and cells were then plated for 10-15min in DMEM+10%FBS in 35mm dishes at 37°C to for fibroblast removal. Cells were then incubated in PBS-EDTA 2mM for 15min at 37°C and passed through a 25 gauge needle. Cell suspensions were then filtered through a 70μM filter before counting. Cells were seeded in 6-well ultra low adhesion plates at a density >5.0x10^5 cells per well in 1mL mammosphere media (DMEM/F12 (Gibco 11320-082), 1:50 B27 (Invitrogen 17504-044), EGF (Peprotech AF-100-15-A), 1:100 Pen/Strep). Approximately 300 spheres were injected per site. Suspension cultures were spun at 300rpm for 4min and then suspended in 150ul PBS++/300 spheres. Matrigel (Corning 356231) was

then added in a 1:1 ratio. Spheres were injected into the two 4^{th} inguinal gland fat pad using a 27-gauge needle.

3D mammary primary epithelial cell organoid cultures. MMTV-Her2 mice were sacrificed using CO_2 at age 14-18wk and MECs were isolated using the same protocol used for mammosphere preparation.). Similar to mammosphere preparations, all 5 pairs of glands in mice were checked for the presence of any visible or palpable tumors when processed for early cancer cell and none were found even in whole mounts prepared from mammary glands from the same mouse processed for mammoprsphere preparation. 5.0X10^4 MECs were seeded in 400ul Assay Medium (DMEM/F12, 5% HS, 1% P/S and EGF plus 2% Matrigel) in 8-well chamber slides with 40ul of Matrigel. Organoids formed at an efficiency of around 30 organoids/$1.0x10^4$ MECs plated. Cultures were treated every 24 hours with 5uM DMSO/SB203580 and 500ng/ml DKK1 for 48 hours following organoids formation and fixed for immunofluorescence (IF) with 4%PFA or 10% Formalin with phosphatase and protease inhibitors. In some cases spheres growing in suspension conditions were seeded in assay media plus 2% of Matrigel directly in 40 ul of Matrigel and 3 days later the number of invasive spheres was counted.

Patient samples. Paraffin embedded sections from DCIS and invasive breast cancer patient tumors were obtained from the Cancer Biorepository at Icahn School of Medicine at Mount Sinai, New York, NY. Samples were de-identified and obtained with Institutional Review Board approval, which indicated that this work does not meet the definition of human subject research according to the 45 CFR 46 and the Office of Human Subject Research. IF and immunohistochemistry (IHC) analysis was done using samples from 10 DCIS and 20 invasive breast cancer patients. Invasive breast cancer samples included Luminal A, B and Her2 positive subtypes.

Circulating Cancer Cells (CCCs) and Disseminated Cancer Cells (DCCs) detection. 16 week-old MMTV-Her2 mice were treated with SB203580 (10 mg/kg) or DMSO for 2 weeks and blood was drawn by cardiac puncture following IACUC protocols. CCCs were purified using negative lineage cell-depletion kit (Cat 130-090-858, Milteny) fixed and stained with anti-CK8/18 antibody in cytospin preparations. Bone marrow cells from 4 long bones were flushed out Minimum Essential Medium Eagle (MEME) (Sigma, MO, USA) using 26-G needle and 1 ml syringe. Tumor cells were enriched by Ficoll-Paque plus (GE Healthcare) density gradient separation and filtered through 30uM nylon mesh to remove large aggregates. Cells were fixed with 3% PFA for 20 min on ice and cytospin preparations were carried out by centrifugation of bone marrow cells at 500 rpm for 3 min using poly-L-lysine-coated slides (Sigma, MO, USA). DCCs were stained with anti-CK8/18 or anti-Her2 antibodies in cytospin preparations were analyzed. We screened 0.5-2.0x10^6 BM cells, which represents 20% of the total BM cells obtained from 2 tibiae and 2 femurs per mouse after Ficoll gradient separation and then normalized to 1x10^6 BM cells. Similar to mammosphere preparations, all 5 pairs of glands in mice were checked for the presence of any visible or palpable tumors when processed for early cancer cell and none were found as described above.

Intra-vital microscopy. Intravital imaging was performed using a custom-built two-laser multiphoton microscope following previously reported imaging protocols[31]. All procedures were conducted in accordance with the National Institutes of Health regulations and approved by the Albert Einstein College of Medicine animal use committee. More detailed description of two-photon imaging can be found in Supplemental Experimental Procedures. For computational rendering of the movies in Supplemental movie S5 and S8, the signals within the segmented vessel and the manually outlined cell were separately extracted into a sequence of tiff images and then imported into Imaris. A colocalization algorithm was performed on the two signals to identify overlapping pixels. Intensity

based surface reconstructions of the vessel (red), tumor cell (cyan) and colocalization signal (yellow) were created and then animated.

Statistical Analysis. Statistical Analysis was done using Prism Software. Differences were considered significant if *P* values was <0.05. For all cell cultures, one tailed *student t-tests* were performed. For mouse experiments one tailed *Mann-Whitney* tests were used.

AUTHORS CONTRIBUTIONS. KH: designed, optimized and performed experiments, analyzed data and co-wrote the manuscript, MSS: designed and optimized experimental approach, performed experiments, designed and executed intravital imaging experiments, provided guidance and oversight, analyzed data and co-wrote the manuscript, DE: designed and executed intravital imaging, analyzed data, performed 3D rendering of movies and co-wrote the manuscript. HH: designed and performed experiments and analyzed data, AAV: performed experiments, CN: provided human histological samples and provided histopathological analysis. J.F.C: managed MMTV-Neu and MMTV-Neu-CFP mouse colonies. R.N. optimized and performed experiments and analyzed data. N.G. maintained the MKK3/MKK6 wild-type and KO mice and provided tissue sections under the supervision of R.J.D, who provided mouse mammary gland samples. CK: designed experiments, analyzed data and co-wrote the manuscript, JC: designed intra-vital experiments, analyzed data and co-wrote the manuscript, EFF: provided expertise in the MMTV-Her2 model, deigned experiments and analyzed data, JAA-G: designed and optimized experimental approach, provided general guidance and oversight, collected microscopy data, analyzed data and co-wrote the manuscript.

Acknowledgements. We thank the Aguirre-Ghiso, Klein and Condeelis labs for useful discussions. We thank Drs. Ramon Parsons and Poulikos Polulikakos for sharing PI3K and AKT inhibitors, respectively. We also thank Dr. Stuart Aaronson for sharing the Wnt3a, sFRP and DKK1 reagents

and Huei-Chi Wen for efforts during the initial stages of this project. Grant Support: R.J.D. is an Investigator of the Howard Hughes Medical Institute. Samuel Waxman Cancer Research Foundation Tumor Dormancy Program to J.A.A-G. and E.F.F., NIH/NCI (CA109182) to J.A.A-G., NCI - Tumor Microenvironment Network (CA163131) to J.A.A-G and J.C., NIH/NCI F31 CA183185 to K.H., DoD-BCRP Breakthrough Award (BC132674) to J.A.A-G and J.C., DoD-BCRP Grant (BC112380) to M.S.S. J.A.A-G is also supported by an NCI Cancer Center P30 grant CA196521. Spinning disk confocal microscopy was performed in the Microscopy CORE at the Icahn School of Medicine at Mount Sinai, supported with funding from NIH Shared Instrumentation Grant (1S10RR024745-01A1).

REFERENCES:

1 Klein, C. A. Framework models of tumor dormancy from patient-derived observations. *Current opinion in genetics & development* (2010).
2 Sosa, M. S., Bragado, P. & Aguirre-Ghiso, J. A. Mechanisms of disseminated cancer cell dormancy: an awakening field. *Nature reviews. Cancer* **14**, 611-622, doi:10.1038/nrc3793 (2014).
3 Klein, C. A. *et al.* Comparative genomic hybridization, loss of heterozygosity, and DNA sequence analysis of single cells. *Proc Natl Acad Sci U S A* **96**, 4494-4499 (1999).
4 Klein, C. A. *et al.* Genetic heterogeneity of single disseminated tumour cells in minimal residual cancer. *Lancet* **360**, 683-689, doi:10.1016/S0140-6736(02)09838-0 (2002).
5 Husemann, Y. *et al.* Systemic spread is an early step in breast cancer. *Cancer Cell* **13**, 58-68 (2008).
6 Schardt, J. A. *et al.* Genomic analysis of single cytokeratin-positive cells from bone marrow reveals early mutational events in breast cancer. *Cancer Cell* **8**, 227-239 (2005).
7 Schmidt-Kittler, O. *et al.* From latent disseminated cells to overt metastasis: genetic analysis of systemic breast cancer progression. *Proc Natl Acad Sci U S A* **100**, 7737-7742 (2003).
8 Riethmuller, G. & Klein, C. A. Early cancer cell dissemination and late metastatic relapse: clinical reflections and biological approaches to the dormancy problem in patients. *Seminars in cancer biology* **11**, 307-311 (2001).
9 Sanger, N. *et al.* Disseminated tumor cells in the bone marrow of patients with ductal carcinoma in situ. *Int J Cancer* **129**, 2522-2526, doi:10.1002/ijc.25895 (2011).
10 Rhim, A. D. *et al.* EMT and dissemination precede pancreatic tumor formation. *Cell* **148**, 349-361, doi:10.1016/j.cell.2011.11.025 (2012).
11 Eyles, J. *et al.* Tumor cells disseminate early, but immunosurveillance limits metastatic outgrowth, in a mouse model of melanoma. *The Journal of clinical investigation* **120**, 2030-2039 (2010).
12 Pavlidis, N., Briasoulis, E., Hainsworth, J. & Greco, F. A. Diagnostic and therapeutic management of cancer of an unknown primary. *European journal of cancer* **39**, 1990-2005 (2003).
13 Pavlidis, N. & Fizazi, K. Carcinoma of unknown primary (CUP). *Critical reviews in oncology/hematology* **69**, 271-278, doi:10.1016/j.critrevonc.2008.09.005 (2009).

14 del Barco Barrantes, I. & Nebreda, A. R. Roles of p38 MAPKs in invasion and metastasis. *Biochem Soc Trans* **40**, 79-84, doi:10.1042/BST20110676 (2012).
15 Ventura, J. J. *et al.* p38alpha MAP kinase is essential in lung stem and progenitor cell proliferation and differentiation. *Nature genetics* **39**, 750-758 (2007).
16 Bulavin, D. V. *et al.* Amplification of PPM1D in human tumors abrogates p53 tumor-suppressor activity. *Nature genetics* **31**, 210-215 (2002).
17 Wen, H. C. *et al.* p38alpha Signaling Induces Anoikis and Lumen Formation During Mammary Morphogenesis. *Science signaling* **4**, ra34, doi:10.1126/scisignal.2001684 (2011).
18 Pearson, G. W. & Hunter, T. Real-time imaging reveals that noninvasive mammary epithelial acini can contain motile cells. *The Journal of cell biology* **179**, 1555-1567 (2007).
19 Klemke, R. L. *et al.* Regulation of cell motility by mitogen-activated protein kinase. *The Journal of cell biology* **137**, 481-492 (1997).
20 Su, G. H., Song, J. J., Repasky, E. A., Schutte, M. & Kern, S. E. Mutation rate of MAP2K4/MKK4 in breast carcinoma. *Human mutation* **19**, 81, doi:10.1002/humu.9002 (2002).
21 Teng, D. H. *et al.* Human mitogen-activated protein kinase kinase 4 as a candidate tumor suppressor. *Cancer Res* **57**, 4177-4182 (1997).
22 Bulavin, D. V. *et al.* Inactivation of the Wip1 phosphatase inhibits mammary tumorigenesis through p38 MAPK-mediated activation of the p16(Ink4a)-p19(Arf) pathway. *Nature genetics* **36**, 343-350 (2004).
23 Brisken, C. *et al.* Essential function of Wnt-4 in mammary gland development downstream of progesterone signaling. *Genes Dev* **14**, 650-654 (2000).
24 Nelson, C. M., Vanduijn, M. M., Inman, J. L., Fletcher, D. A. & Bissell, M. J. Tissue geometry determines sites of mammary branching morphogenesis in organotypic cultures. *Science* **314**, 298-300, doi:10.1126/science.1131000 (2006).
25 Cardiff, R. D. Validity of mouse mammary tumour models for human breast cancer: comparative pathology. *Microscopy research and technique* **52**, 224-230, doi:10.1002/1097-0029(20010115)52:2<224::AID-JEMT1007>3.0.CO;2-A (2001).
26 Lu, J. *et al.* 14-3-3zeta Cooperates with ErbB2 to promote ductal carcinoma in situ progression to invasive breast cancer by inducing epithelial-mesenchymal transition. *Cancer Cell* **16**, 195-207 (2009).
27 Strippoli, R. *et al.* p38 maintains E-cadherin expression by modulating TAK1-NF-kappa B during epithelial-to-mesenchymal transition. *Journal of cell science* **123**, 4321-4331 (2010).
28 Oser, M. & Condeelis, J. The cofilin activity cycle in lamellipodia and invadopodia. *Journal of cellular biochemistry* **108**, 1252-1262, doi:10.1002/jcb.22372 (2009).
29 van Rheenen, J. *et al.* EGF-induced PIP2 hydrolysis releases and activates cofilin locally in carcinoma cells. *The Journal of cell biology* **179**, 1247-1259, doi:10.1083/jcb.200706206 (2007).
30 Debnath, J., Muthuswamy, S. K. & Brugge, J. S. Morphogenesis and oncogenesis of MCF-10A mammary epithelial acini grown in three-dimensional basement membrane cultures. *Methods* **30**, 256-268 (2003).
31 Entenberg, D. *et al.* Setup and use of a two-laser multiphoton microscope for multichannel intravital fluorescence imaging. *Nature protocols* **6**, 1500-1520, doi:10.1038/nprot.2011.376 (2011).
32 Malladi, S. *et al.* Metastatic Latency and Immune Evasion through Autocrine Inhibition of WNT. *Cell* **165**, 45-60, doi:10.1016/j.cell.2016.02.025 (2016).
33 Leung, J. Y. *et al.* Activation of AXIN2 expression by beta-catenin-T cell factor. A feedback repressor pathway regulating Wnt signaling. *The Journal of biological chemistry* **277**, 21657-21665, doi:10.1074/jbc.M200139200 (2002).

34 Taube, J. H. *et al.* Core epithelial-to-mesenchymal transition interactome gene-expression signature is associated with claudin-low and metaplastic breast cancer subtypes. *Proc Natl Acad Sci U S A* **107**, 15449-15454, doi:10.1073/pnas.1004900107 (2010).
35 Nieto, M. A., Huang, R. Y., Jackson, R. A. & Thiery, J. P. Emt: 2016. *Cell* **166**, 21-45, doi:10.1016/j.cell.2016.06.028 (2016).
36 Ocana, O. H. *et al.* Metastatic colonization requires the repression of the epithelial-mesenchymal transition inducer Prrx1. *Cancer Cell* **22**, 709-724, doi:10.1016/j.ccr.2012.10.012 (2012).
37 Brabletz, T. To differentiate or not--routes towards metastasis. *Nature reviews. Cancer* **12**, 425-436, doi:10.1038/nrc3265 (2012).
38 Grumolato, L. *et al.* Canonical and noncanonical Wnts use a common mechanism to activate completely unrelated coreceptors. *Genes Dev* **24**, 2517-2530, doi:10.1101/gad.1957710 (2010).
39 Bragado, P. *et al.* TGF-beta2 dictates disseminated tumour cell fate in target organs through TGF-beta-RIII and p38alpha/beta signalling. *Nat Cell Biol* **15**, 1351-1361, doi:10.1038/ncb2861 (2013).
40 Debnath, J., Walker, S. J. & Brugge, J. S. Akt activation disrupts mammary acinar architecture and enhances proliferation in an mTOR-dependent manner. *The Journal of cell biology* **163**, 315-326 (2003).
41 Nieto, M. A. Epithelial plasticity: a common theme in embryonic and cancer cells. *Science* **342**, 1234850, doi:10.1126/science.1234850 (2013).
42 Micalizzi, D. S., Farabaugh, S. M. & Ford, H. L. Epithelial-mesenchymal transition in cancer: parallels between normal development and tumor progression. *Journal of mammary gland biology and neoplasia* **15**, 117-134 (2010).
43 Schmidt, J. M. *et al.* Stem-cell-like properties and epithelial plasticity arise as stable traits after transient Twist1 activation. *Cell reports* **10**, 131-139, doi:10.1016/j.celrep.2014.12.032 (2015).
44 Fischer, K. R. *et al.* Epithelial-to-mesenchymal transition is not required for lung metastasis but contributes to chemoresistance. *Nature* **527**, 472-476, doi:10.1038/nature15748 (2015).
45 Cheung, K. J., Gabrielson, E., Werb, Z. & Ewald, A. J. Collective invasion in breast cancer requires a conserved basal epithelial program. *Cell* **155**, 1639-1651, doi:10.1016/j.cell.2013.11.029 (2013).
46 Shamir, E. R. *et al.* Twist1-induced dissemination preserves epithelial identity and requires E-cadherin. *The Journal of cell biology* **204**, 839-856, doi:10.1083/jcb.201306088 (2014).
47 Liu, Y. J. *et al.* Confinement and low adhesion induce fast amoeboid migration of slow mesenchymal cells. *Cell* **160**, 659-672, doi:10.1016/j.cell.2015.01.007 (2015).
48 Harney, A. S. *et al.* Real-Time Imaging Reveals Local, Transient Vascular Permeability, and Tumor Cell Intravasation Stimulated by TIE2hi Macrophage-Derived VEGFA. *Cancer discovery* **5**, 932-943, doi:10.1158/2159-8290.CD-15-0012 (2015).
49 Bravo-Cordero, J. J., Hodgson, L. & Condeelis, J. Directed cell invasion and migration during metastasis. *Current opinion in cell biology*, doi:10.1016/j.ceb.2011.12.004 (2011).
50 Avivar-Valderas, A., Wen, H. C. & Aguirre-Ghiso, J. A. Stress signaling and the shaping of the mammary tissue in development and cancer. *Oncogene*, doi:10.1038/onc.2013.554 (2014).
51 Dolado, I. *et al.* p38alpha MAP kinase as a sensor of reactive oxygen species in tumorigenesis. *Cancer Cell* **11**, 191-205 (2007).
52 Hui, L. *et al.* p38alpha suppresses normal and cancer cell proliferation by antagonizing the JNK-c-Jun pathway. *Nature genetics* **39**, 741-749 (2007).
53 Gozdecka, M. *et al.* JNK suppresses tumor formation via a gene-expression program mediated by ATF2. *Cell reports* **9**, 1361-1374, doi:10.1016/j.celrep.2014.10.043 (2014).
54 Bhoumik, A. *et al.* Suppressor role of activating transcription factor 2 (ATF2) in skin cancer. *Proc Natl Acad Sci U S A* **105**, 1674-1679 (2008).

55 Kobayashi, A. *et al.* Bone morphogenetic protein 7 in dormancy and metastasis of prostate cancer stem-like cells in bone. *The Journal of experimental medicine* **208**, 2641-2655, doi:10.1084/jem.20110840 (2011).
56 Marlow, R. *et al.* A novel model of dormancy for bone metastatic breast cancer cells. *Cancer Res* **73**, 6886-6899, doi:10.1158/0008-5472.CAN-13-0991 (2013).
57 Dovas, A. *et al.* Visualization of actin polymerization in invasive structures of macrophages and carcinoma cells using photoconvertible beta-actin-Dendra2 fusion proteins. *PloS one* **6**, e16485, doi:10.1371/journal.pone.0016485 (2011).
58 Oser, M. *et al.* Cortactin regulates cofilin and N-WASp activities to control the stages of invadopodium assembly and maturation. *The Journal of cell biology* **186**, 571-587, doi:10.1083/jcb.200812176 (2009).
59 Lorenz, M., Yamaguchi, H., Wang, Y., Singer, R. H. & Condeelis, J. Imaging sites of N-wasp activity in lamellipodia and invadopodia of carcinoma cells. *Current biology : CB* **14**, 697-703, doi:10.1016/j.cub.2004.04.008 (2004).
60 Pavlidis, N., Peccatori, F., Lofts, F. & Greco, A. F. Cancer of unknown primary during pregnancy: an exceptionally rare coexistence. *Anticancer research* **35**, 575-579 (2015).
61 Narod, S. A., Iqbal, J., Giannakeas, V., Sopik, V. & Sun, P. Breast Cancer Mortality After a Diagnosis of Ductal Carcinoma In Situ. *JAMA oncology* **1**, 888-896, doi:10.1001/jamaoncol.2015.2510 (2015).
62 Haffner, M. C. *et al.* Tracking the clonal origin of lethal prostate cancer. *The Journal of clinical investigation* **123**, 4918-4922, doi:10.1172/JCI70354 (2013).
63 Brisken, C. *et al.* A paracrine role for the epithelial progesterone receptor in mammary gland development. *Proc Natl Acad Sci U S A* **95**, 5076-5081 (1998).

FIGURE LEGENDS:

Figure 1. E-cadherin, Her2 and p38 expression and function in early cancer cells. (A) MMTV-Her2 EL sections co-stained for E-cadherin (green), Her2 (red) and DAPI (blue). Arrowheads indicate $Her2^{HI}$/$E\text{-}cad^{LO}$ cells and arrows indicate $Her2^{LO}$/$E\text{-}cad^{HI}$ cells. Bottom panel: detail of intra-ductal heterogeneity of E-cadherin and Her2 expression. Inset C' in bottom panel shows detailed image of boxed region. (Scale bar=10 μM inset, 25 μM panels). Right Graph = percentage of $Her2^{HI}$ cells that were E-$cadherin^{LO\ or\ HI}$ (n=20 ducts, 2 mice). **(B)** Representative images of $E\text{-}cad^{hi}$/$p\text{-}ATF2^{hi}$ (TOP) and $E\text{-}cad^{LO}$/$p\text{-}ATF2^{LO}$ (BOTTOM) ducts in MMTV-Her2 EL (scale bar=25μM). Scale bar=10μM. Arrowhead=$P\text{-}ATF2^{HI}$/$E\text{-}cad^{HI}$ cells. Arrow=$P\text{-}ATF2^{LO}$/$E\text{-}cad^{LO}$ cells (scale bars=10 μM). **(C)** Early stage MMTV-Her2 (age 14-18 week – left panel) and MMTV-Her2-T (Balb-NeuT age 15 week – right panel) EL sections stained for Her2 and β-catenin. Arrows= $Her2^{+}$/β-$catenin^{MEM\text{-}LO}$ EL cells; arrowheads = $Her2^{-}$/β-$catenin^{MEM\text{-}HI}$ MECs (Scale bars=25 μM). Digital dye separation Leica module used on the images. Upper graph: Quantification of the % of cells/duct with β-$catenin^{MEM}$ is shown in the graph for both MMTV-Her2 and MMTV-Her2-T models. (n=5-10 ducts). Lower panel: Quantification of the percentage of cells with membrane-associated β-catenin ($BCAT^{MEM}$) which were $HER2^{-}$ or $HER2^{+}$ for FvB MMTV-HER2 and Balb MMTV-HER2-T sections (Her2 and Her2-T). Mean±SEM; MMTV-HER2 30 ducts, 3 mice; MMTV-HER2-T 10 ducts 1 mouse; *=$p<0.05$. **(D)** Detection of E-cadherin and P-ATF2 in MCF10A-Her2 cells treated with or without Lapatinib (100nM), EGFR inhibitor AG1478 (5uM) and siRNA targeting Her2 (40nM) for 24 hrs; E-cadherin (GREEN) and pATF2 (RED). Images: treatment with Lapatinib; additional treatment images in S. Fig4B. Graph: % of P-ATF2+ cells for each treatment showing mean and SEM. ***=$p<0.001$, **=$p<0.01$ (n= 3 experimental replicates, 10 images/treatment). **(E)** Left panel: MCF-10A-Her2 cells were treated for 24 hrs with the EGFR inhibitor AG1478 (1 uM). Western blots for P-AKT and AKT antigens are shown. Right panel: MCF-10A-Her2 cells were treated for 24 hrs with the AKT inhibitor MK2266 (5 uM), PI3K inhibitor GDC-0941 (1uM) and HER2/EGFR inhibitor Lapatinib (1uM). Western blots for P-

S6 and β-tubulin antigens are shown. Bottom panel: control for Her2 knock down in MCF10A-Her2 cells. **(F)** MMTV-Her2 EL organoids treated for 48hr with DMSO (top panels) or 5μM of the p38α/β inhibitor SB203580 (bottom panels). BF=bright field images. D' and D''=Z zoomed regions on the right show invasive cells only in SB203580-treated organoids. **(E)** MMTV-Her2 organoids were stained for F-actin (red), Laminin V (green) and DAPI (blue). Arrowheads = invasive cells; arrow = intact laminin-V layer in DMSO controls. Bottom Graph = Quantification of the number of organoids with invasion in DMSO and SB203580 groups. (DMSO=11; SB203580=9). Scale bars=25μM. **(G)** MMTV-Her2 EL sections co-stained for E-cadherin (GREEN), Her2 (RED) and DAPI (BLUE). Arrows indicate $Her2^{+}/E\text{-}cad^{LO}$ invading cells. Quantification of the % $E\text{-}cad^{lo}$ invading cells in both MCF10A-Her2 organoids or in MMTV-Her2 EL sections is shown in the graph (n= 20 organoids, n=54-63 cells/mammary gland section, 2 mice).

Figure 2. Intra-vital imaging of intravasation and systemic detection of $Her2^{hi}/Pp38^{lo}$ eDCCs. **(A)** Stills from intra-vital movies of 10 (left, S-Movie 2), 15 (middle, S-Movie 3) and 18 (right, S-Movie 4) weeks old EL in MMTV-Her2-CFP mice, scale bars= 38, 5 and 56 μm, respectively. Blue-white signal = CFP+ cells RED signal= rhodamine-dextran injected vasculature. Dotted ellipses define a duct. Right panel inset: direction of movement of an eDCC at 5 consecutive time points (2 min each panel). Dotted arrow= direction of movement, scale bar= 7.8 μm. **(B)** Stills from S-Movie 5 (**B)** and S-Movie 6 (**B'**) of an EL in an MMTV-Her2-CFP mouse treated with SB203580 for 2 weeks, scale bar= 25.5 μm. **B'** high power high resolution intra-vital still from a movie of the area boxed in B' showing active breaching of MMTV-Her2-CFP cells from the ductal structure into the stroma and interacting with blood vessels (red) (S-Movie 6), scale bar= 5.2 μm. **(C)** Frames of a 3D computer generated reconstruction of the movie in **B'**; bottom panel is a rotated projection to show invasion (yellow) of early cancer cells (CFP) into blood vessels (red) (S-Movie 7). Scale bar=6.6 μm. **(D)** Still from S-movie 8 of an EL cell in MMTV-Her2-CFP mice treated with SB203580 for 4 weeks. A single cell (in

blue) is followed (arrows) as it intravasates (cell in yellow inside the red blood vessel, S-Movie 8). **(E)** Circulating cancer cells (CCCs) were detected in cytospin preparations for CK8/18 (green) and nuclei with DAPI (blue) after ficoll gradient and negative selection. Scale bar=10μM. **(F)** Detection of eDCCs in lung sections from MMTV-Her2 mice by IHC for Her2 (rabbit Ab, calbiochem OP15L anti-Her2 antibody) (scale bar=25μM). Right panels, augmented images from additional sections. Red arrowheads = Her2+ DTCs; red hourglass= host Her2- cells (scale bar=10μM). Staining controls are in **S-Fig4B**. **(G)** eDCCs in the bone marrow of MMTV-Her2 mice detected in cytospin preparations of whole bone marrow samples after ficoll gradient and staining for CK8/18 (green), Her2 (red) and nuclei with DAPI (blue). CK8/18+, Her2+ or +/+ were considered eDCCs. Right panels: individual channel signals. Left panel: merged channels on the right detecting a BM CK8/18+/Her2+ DCC (arrow) next to a CK8/18-/Her2- bone marrow cell (hourglass). Scale bar=10μM. (**H**) CCCs detected as CK8/18+ as in **Fig 2E** in blood of MMTV-Her2 mice (age 14-18wk) treated for two weeks with DMSO (C) or the p38α/β inhibitor SB203580 (n=5 mice/group). **(I)** eDCCs detected as CK8/18+ as in **Fig 2G** in BM of MMTV-Her2 mice treated as in **H** (n=5 mice/group). **(J)** eDCCs detected in the lung of MMTV-Her2 mice carrying early lesions only as in **F** and treated as in **H**. Graph= % of Her2+ DCCs/field is each group (n=30 fields, 3 mice/treatment). *p<0.05, **p<0.01, ***p<0.001.

Figure 3. EMT markers in Her2+ early cancer cells. (A) Organoids from MCF10A-Her2 treated for 6 days with SB203580 were stained for E-cadherin (green) and β-catenin (red) or DAPI (blue); MCF10A-Her2 n=20 organoids/treatment. **(B)** MCF10A-Her2 organoids were treated as in **A** but with siRNAs targeting p38α as well as a non-targeting control (siCTL) and stained as in A; MCF10A-Her2 n=20 organoids/treatment. **(C)** EL MMTV-Her2 organoids were treated for 48 hrs with SB203580 following organoid formation and stained for β-catenin (green) or DAPI (blue); right gray scale panels are MMTV-Her2 organoid zoomed in images showing membrane- and cytosolic-localized β-catenin. MMTV-Her2 n=10 organoids/treatment) scale bars=25μM. **(D)** MMTV-Her2 organoids were treated as

in **B** and stained for E-cadherin or with an antibody recognizing the active conformation of β-catenin (see methods). Righ graph=Quantification of organoids, which were strongly stained with this antibody (n=10 organoids/treatment). Scale bars=25μM. MMTV-Her2 E-cadherin=30 organoids/treatment, b-catenin=10 organoids/treatment. **(E)** Quantification of the data in A, B and D. Graph= quantification of % of E-cad^{HI} in MCF10A-Her2 and MMTV-Her2 organoids. **(F)** AXIN2 mRNA expression in MCF10A-Her2 monolayer cultures treated for 24 hours with DMSO control (C) or SB203580 (5μM). Technical triplicate determinations were normalized to GAPDH and fold change (FC) over control was determined for five biological replicates. **(G)** mRNA levels for *Snail* and *Twist* normalized to GAPDH in MCF10A-Her2 3D cultures treated with siRNA targeting p38α isoform or ATF2 from Day 6-12. Values represent FC over control in three biological replicates.

Figure 4. E-cadherin and β-catenin regulation by p38 in early lesions (A-B). Sections of EL in MMTV-Her2 mice treated for 2 weeks with the p38α/β inhibitor SB203580 (age 16-18 weeks, 10mg/kg, i.p. every 48hr) stained for E-cadherin (**A**) and β-catenin (**B**). (Scale bars=20 μM). in A, top and bottom rows show 40x and 100x magnifications respectively. In B, top row shows a 100x magnification and the bottom row a digital zoom of the top row. Arrows= membrane localized E-cadherin (A, left column) or β-catenin (B, left column) or nuclear b-catenin (B, right column) in boxed area (B, top right) (Scale bar=10 μM). Quantification of the average % of E-cad^{HI} ducts in DMSO (B, bottom graph) and SB203580 treated mice and % of nuclear β-catenin events/duct is shown in the B bottom graph (n=30-40 ducts for both antigens). **(C)** *Twist* mRNA levels in MMTV-Her2 EL (age 14-18wk) treated for 2 weeks with vehicle or SB203580 (10mg/kg, i.p every 48hr). Fold change over control (DMSO) is shown with values normalized to GAPDH (n=3 mice/treatment). **(D)** IHC for E-cadherin in C57 (wt) and MKK3$^{+/-}$/MKK6$^{-/-}$ mice [17] or FvB mice treated 2 weeks SB203580 (bottom panel, 10mg/kg, i.p every 48hr). Quantification for F is in S-Fig.5C.

Figure 5. Her2 and p38 regulate a Wnt-driven EMT-like program in early cancer cells. (A) Expression of EMT-related genes in MCF10A and MCF10A-Her2 organoids treated for 6 days with or without the p38α/β inhibitor SB203580 (5μM). A 14-gene EMT signature (right gene list) was generated from genes upregulated > 2 fold over three trials and plotted using Gene-E. Green columns = control values set to 1 and fold change over control is shown in red. **(B)** Q-PCR measurement of *E-Cadherin* mRNA levels in MCF10A-Her2 organoids treated for 6 days with SB203580 (5μM) or si-p38α (20nM). Fold change over control is shown biological triplicates. DMSO was the control for SB203580 samples and, scrambled siRNA the control for sip38α **(C)** *Axin2* mRNA levels measured in MCF10A-Her2 and MCF10A-Her2-sFRP cells treated with or without SB203580 (5uM) for 24hr. Fold change over control is shown with error bars representing SEM for six biological replicates. **(D)** *Axin2* mRNA levels measured in MCF10A 2D cultures transfected with pcDNA3 (empty vector) and CAp38α (D176A/F372S, constitutively active mutant) plasmids and then treated with or without Wnt3a for 24 hrs. Fold change over control is shown for three biological replicates. **(E)** Invasion from MCF10A-Her2 and MCF10A-Her2-sFRP organoids treated for 6 das with DMSO or the p38α/β inhibitor SB203580 (5 μM). Grapgh = # of organoids with outward invading cells; n=20 organoids/treatment, 2 biological replicates. **(F)** E-cadherin and β-catenin junction expression in MCF10A-Her2 and MCF10A-Her2-sFRP organoids treated for 6 days with SB203580 (5uM). First and second rows from top show IF staining for E-cadherin (green) and the third and fourth rows show β-catenin (red). Insets in the β-catenin images in the fifth row (F1-F4) show boxed regions above with detail of the disruption of β-catenin junctions. Bottom graph shows percentage of E-cadherin^{HI} (green bars, left axis) and β-catenin^{MEM} (red bars, right axis) organoids (error bars represent SEM; n=20 organoids/treatment, 2 biological replicates); scale bars=25μM, n.s.=not significant, *=p<0.05. **(G)** Early MMTV-Her2 organoids were treated for 2 days with SB203580 (5μM) as well as 500ng/ml DKK1 conditioned media following organoid formation. E-cadherin (red). Panel bottom numbers= %

of E-cadherin^{HI} organoids (mean± SEM; n=10 organoids/treatment, 2 biological replicates *p<0.05). scale bars=25μM.

Figure 6. Tumorigenic and metastatic potential of Her2+ early cancer cells. (A) IF detection of Her2 (red or yellow), p-Rb (green - to mark proliferating cells) and DAPI (blue) for nuclei in eDCCs and DCCs in lung sections from MMTV-Her2 mice with early lesions (14-18 wks. age, eDCC left column) and mice with overt primary tumors (>25 wks. age, DCC right column). Specificity controls in **S-Fig 4A-C**. **(B)** Spontaneous macro-metastases sections stained for Her2 (red) and p-Rb (green) in MMTV-Her2 mice carrying autochthonous overt tumors. Scale bars=10μM. **(C)** Micro-metastasis generated from EL (early lesion) mammospheres experiment (explained in **Fig. 6F-H**) showing Her2 (red), p-Rb (green) and DAPI (blue). Scale bars=10μM. **(D)** Left graph: % of P-Rb or P-Ser10-histone-H3 positive (red) and negative (blue) Her2+ solitary cancer cells quantified in mice with early lesions (eDCC) or overt tumors (DCC) (n>200cells). Single eDCCs or DCCs were considered when 1-3 Her2+ cancer cells were found solitary or in a cluster (2-3 Her2+cells). Right graph: the % of p-Rb positive or negative cells within spontaneous macro-metastases (n=5 metastasis) in Her2 mice carrying overt autochthonous primary tumors or in metastases derived from MMTV-Her2 mammospheres from EL (early lesions) injected in the fat pad (n=11 micro, n=4 macro metastasis scored). Micro-metastases= clusters from 3-20 cells. Macro-metastases= clusters >20 cells. Values = mean % p-Rb + cells with error bars representing ± SEM. *=p<0.05. **(E)** Detection of Her2 (red), E-cadherin (green) and DAPI (blue) in eDCCs in lung sections from MMTV-Her2 mice (age 16-20 wks.) carrying EL only; 98 ± 0.57% of Her2+ DTCs were **E-cadherin negative** (n≥100 DTCs, 3 mice) or in lung sections from MMTV-Her2 mice (age 33 wks.) carrying overt primary tumors; 48.2 ± 5.4% of Her2+ DTCs were **E-cadherin positive** (n≥100 DTCs, 2 mice) Scale bar=5 μM, *=p<0.05. **(F)** H&E staining of lung macro-metastasis found in nude mice injected with MMTV-Her2 mammospheres obtained from early lesions and injected in the mammary fat pad (left and middle panels scale bars=

200 μm, right panel bar=100μm). **(G)** Her2+ DCCs detection in mice injected with tumorspheres (left and middle panels scale bars= 200 μm, right panel bar=100μm). Arrows = Her2+ DCCs *= Her2- cells. **(H)** Table= tumorigenic and metastatic incidence of early lesion (EL) or overt primary tumor (PT) spheres prepared from MMTV-Her2 mice as outlined in **S-Fig 5E**. Incidence was measured at 1, 3 and 12 months. The 12 months time point was not assessed for the tumorsphere group.

Figure 7. Cartoon depicting the mechanisms of early dissemination by Her2+ EL cells. From left to right: (**A)** early Her2+ EL cancer cells (RED) turn on Wnt signaling, inhibit p38 activation and E-cadherin junction formation allowing for a $TWIST^{HI}$ EMT-like and invasion program; p38 and E-cadherin function are to inhibit the Wnt and β-catenin-driven EMT-like program and invasion - gray inhibitory symbols. (**B**) $Her2^{+}/p38^{LO}/TWIST^{HI}/E\text{-}cad^{LO}$ EL cancer cells can intravasate and disseminate. **(C)** In lungs >85% of eDCCs (RED) were $Her2+/E\text{-}cad^{LO}$/pRb/$P\text{-}H3^{LO}$ suggesting a large population of dormant cells. The majority of eDCCs are also $TWIST^{HI}/E\text{-}cad^{LO}$. Nevertheless, eDCCs can initiate metastasis (**Fig6**), which is correlated with the acquisition of a $TWIST^{LO}/E\text{-}cad^{HI}$ phenotype. In the BM, eDCCs were Her2+/CK8/18+ and remain dormant for the duration of the experiments, as bone lesions are never observed.

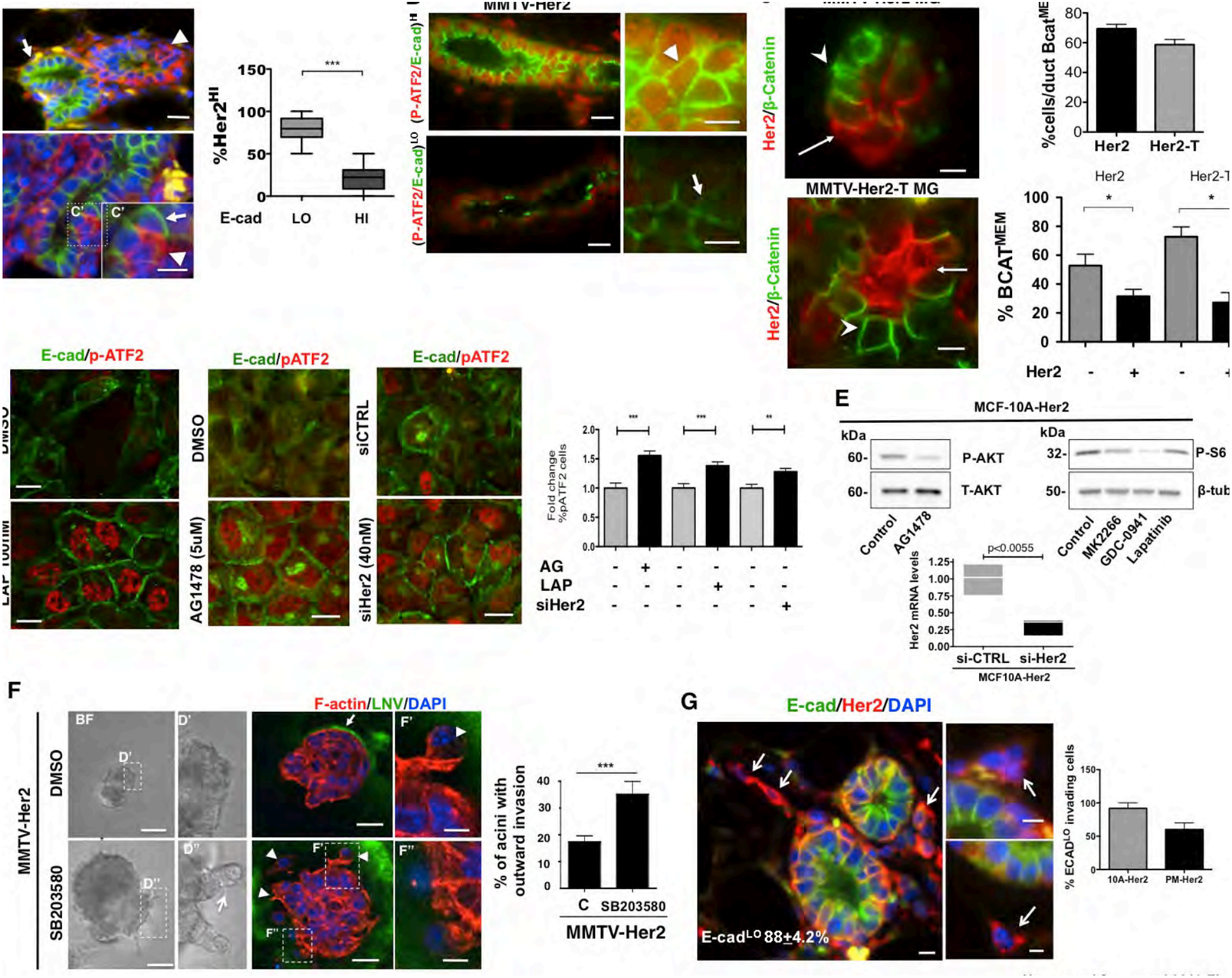
C'
C'
%Her2HI
150
100
50
0
***
E-cad
LO
HI
MMTV-Her2
(P-ATF2/E-cad)HI
(P-ATF2/E-cad)LO
Her2/β-Catenin
MMTV-Her2-T MG
%cells/duct BcatME
80
60
40
20
0
Her2
Her2-T
% BCATMEM
Her2
Her2-T
*
*
100
80
60
40
20
0
Her2 - + - +
E-cad/p-ATF2
E-cad/pATF2
E-cad/pATF2
DMSO
DMSO
siCTRL
AG1478 (5uM)
siHer2 (40nM)
Fold change %pATF2 cells
***
***
**
2.0
1.5
1.0
0.5
0.0
AG - + - - - -
LAP - - - + - -
siHer2 - - - - - +
E
MCF-10A-Her2
kDa
60-
60-
P-AKT
T-AKT
kDa
32-
50-
P-S6
β-tub
Control
AG1478
Control
MK2266
GDC-0941
Lapatinib
p<0.0055
Her2 mRNA levels
1.25
1.00
0.75
0.50
0.25
0.00
si-CTRL
si-Her2
MCF10A-Her2
F
MMTV-Her2
DMSO
SB203580
BF
D'
D''
F-actin/LNV/DAPI
F'
F''
% of acini with outward invasion
***
40
30
20
10
0
C
SB203580
MMTV-Her2
G
E-cad/Her2/DAPI
E-cadLO 88±4.2%
% ECADLO invading cells
150
100
50
0
10A-Her2
PM-Her2

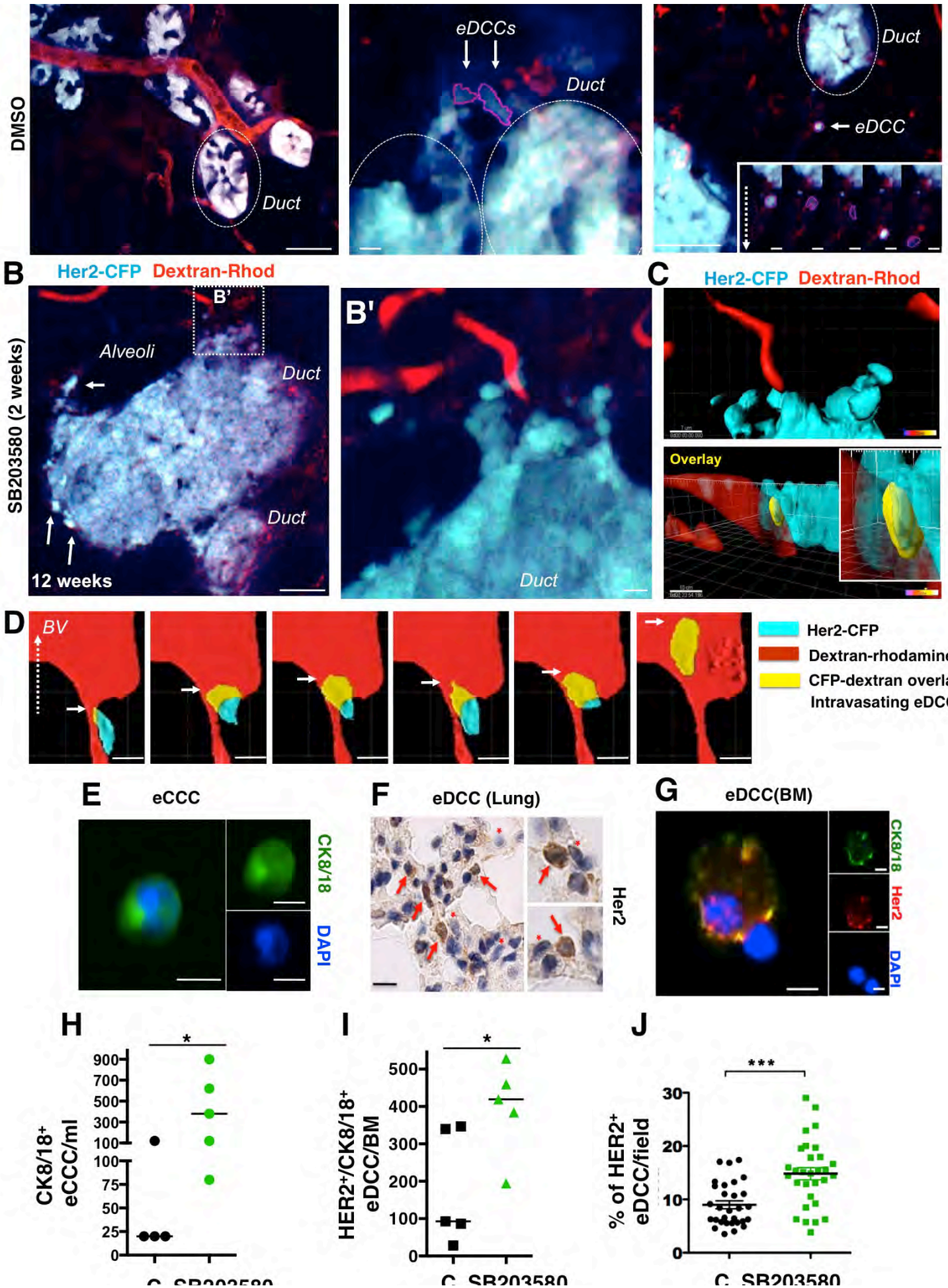
DMSO
Duct
eDCCs
Duct
Duct
eDCC
B
Her2-CFP Dextran-Rhod
SB203580 (2 weeks)
B'
Alveoli
Duct
Duct
12 weeks
B'
Duct
C
Her2-CFP Dextran-Rhod
Overlay
D
BV
Her2-CFP
Dextran-rhodamine
CFP-dextran overlay
Intravasating eDCC
E
eCCC
CK8/18
DAPI
F
eDCC (Lung)
Her2
G
eDCC(BM)
CK8/18
Her2
DAPI
H
CK8/18+ eCCC/ml
900
700
500
300
100
100
75
50
25
0
*
C
SB203580
I
HER2+/CK8/18+ eDCC/BM
500
400
300
200
100
0
*
C
SB203580
J
% of HER2+ eDCC/field
30
20
10
0
***
C
SB203580

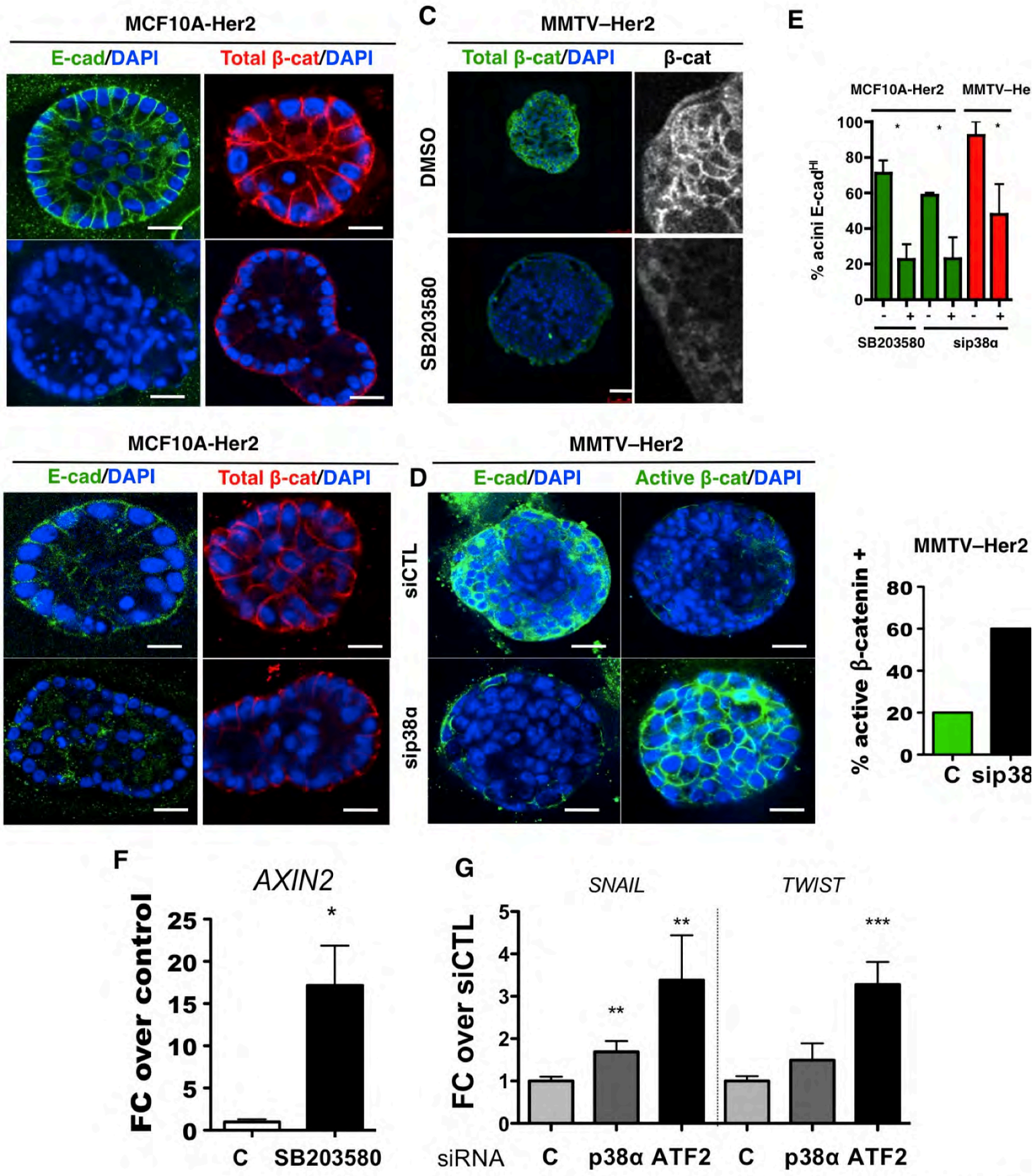

Harper and Sosa et al 2016-Figu

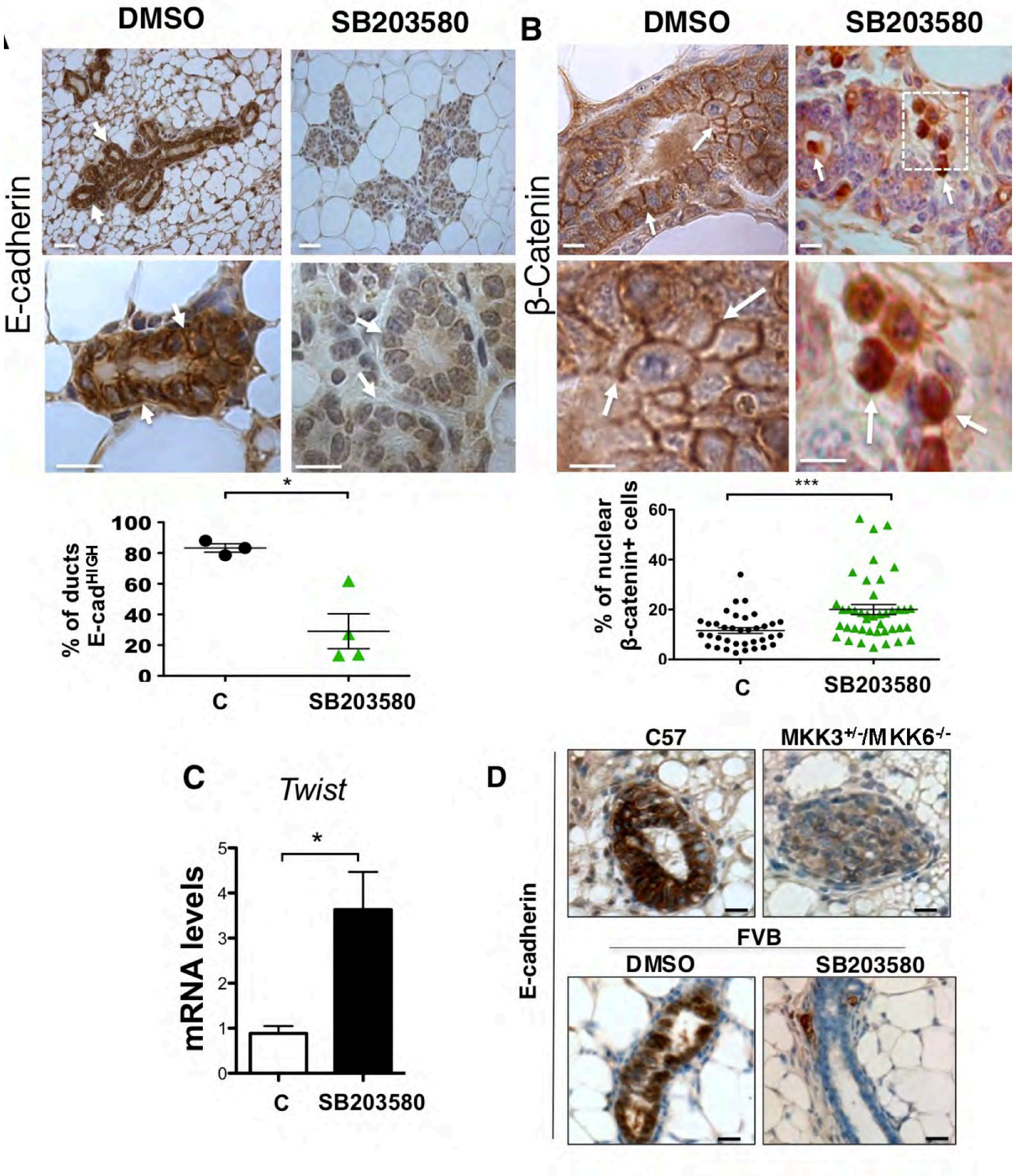

Harper and Sosa et al 2016-Figure 4

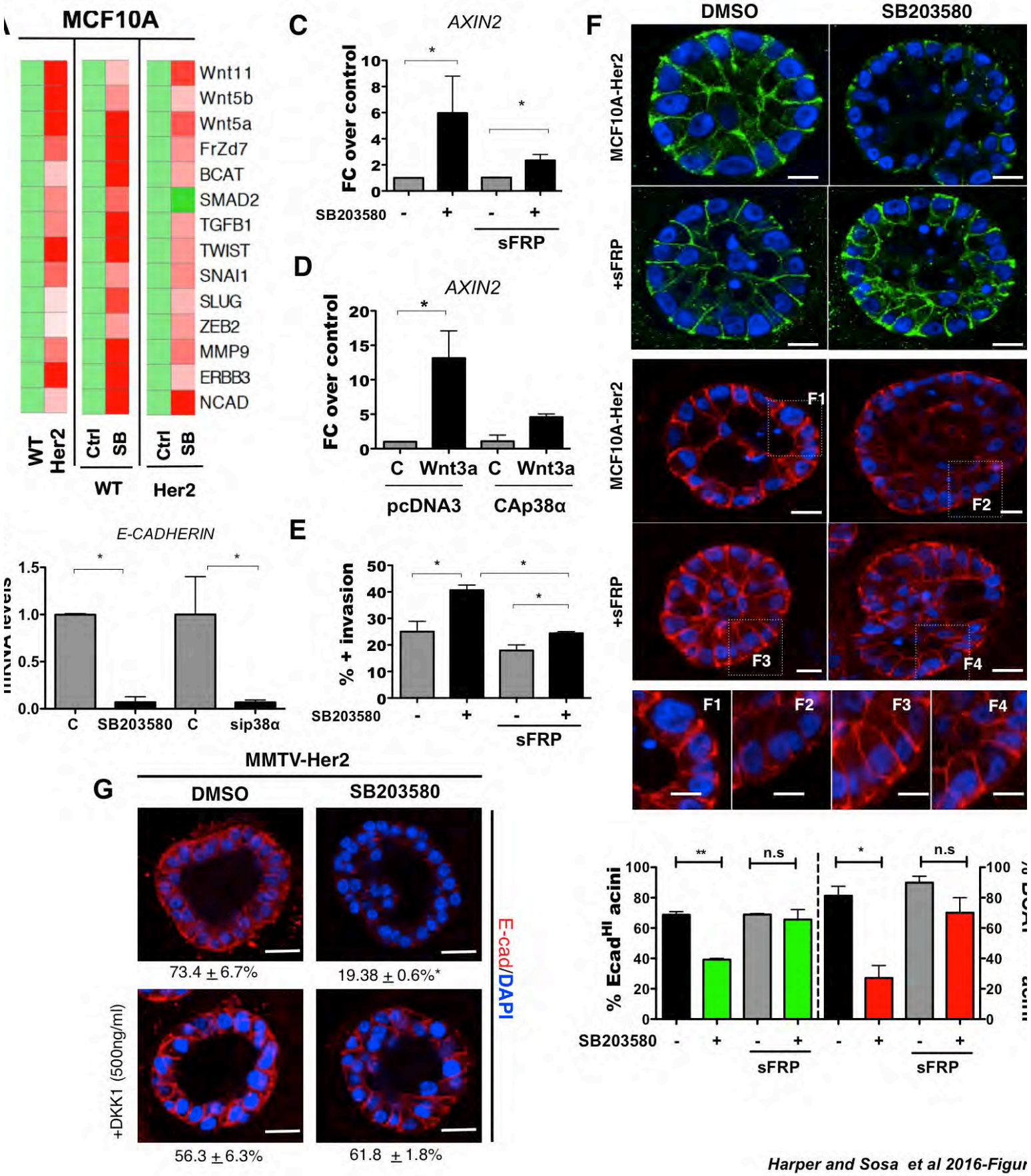

Harper and Sosa et al 2016-Figu

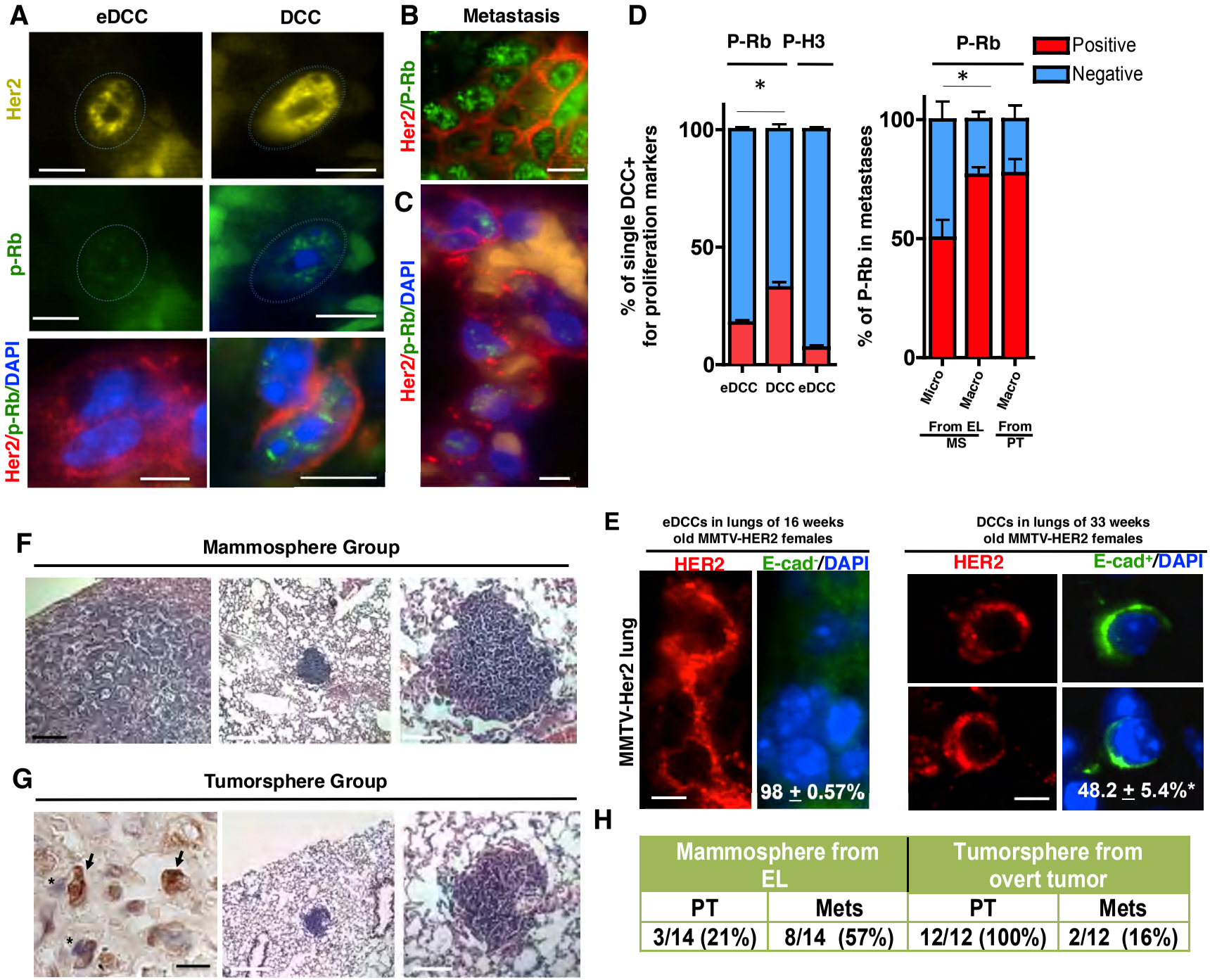

H

Mammosphere from EL		Tumorsphere from overt tumor	
PT	Mets	PT	Mets
3/14 (21%)	8/14 (57%)	12/12 (100%)	2/12 (16%)

Harper and Sosa et al 2016-Figure 6

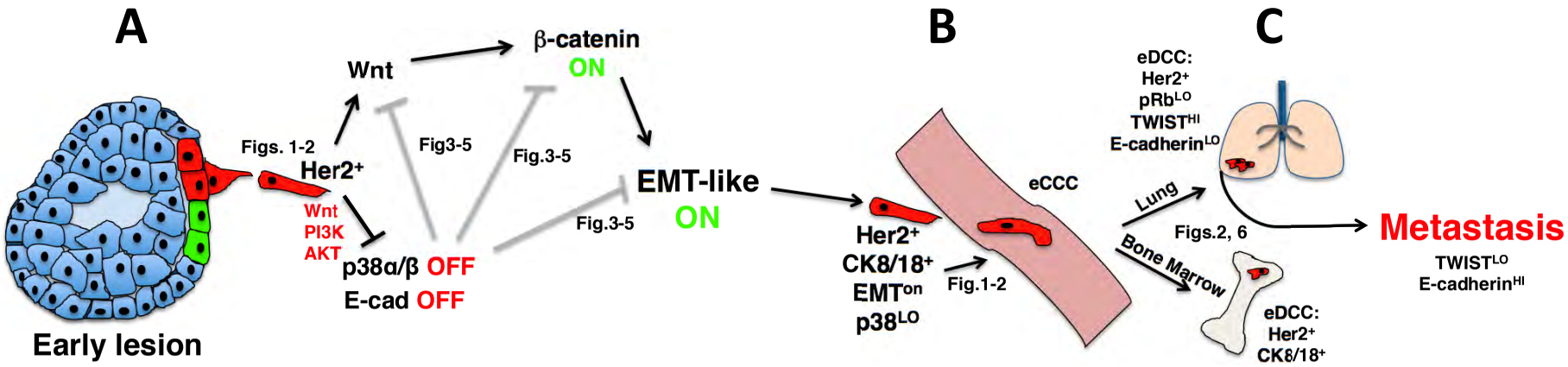

Harper and Sosa et al 2016-Figure 7

Macrophages orchestrate early dissemination and metastasis of HER2+ cancer cells.

Nina Linde[1], Arthur Mortha[2], Adeeb Rahman[3], Eduardo Farias[1], Maria Soledad Sosa[1], Kathryn Harper[1], Ethan Tardio[1], Miriam Merad[2,3], and Julio A. Aguirre-Ghiso[1,4].

[1]Division of Hematology and Oncology, Department of Medicine, Department of Otolaryngology, Tisch Cancer Institute, Black Family Stem Cell Institute, Icahn School of Medicine at Mount Sinai, New York, NY, USA.

[2]Department of Oncological Sciences, The Immunology Institute, Tisch Cancer Institute, Icahn School of Medicine at Mount Sinai, New York, NY, USA

[3]Human Immune Monitoring Core, Icahn School of Medicine at Mount Sinai, New York, NY, USA

[4]Correspondence: julio.aguirre-ghiso@mssm.edu

Abstract

Cancer cell dissemination can occur during very early stages of breast cancer but the mechanisms controlling this process and how they contribute to metastasis are unclear. Here we show that MMTV-HER2 early cancer lesions contain an invasive subpopulation of HER2+/E-cadherin-lo cancer cells that depend on macrophages for dissemination. Macrophages produced Wnt-1 and induced loss of E-cadherin and dissemination of early HER2+ cancer cells. Depletion of macrophages before overt tumor detection drastically reduced early dissemination and diminished the onset of metastasis even when macrophage depletion was stopped when tumors became invasive. Resident CCR2+/CD206+/VCAM-/Tie2+ macrophages were attracted into early lesions by CCL2 produced by early HER2+ cancer cells in an NFkB-dependent manner. Intra-epithelial macrophages and loss of E-cadherin junctions was also found in human DCIS, but not normal breast tissue. We reveal a previously unrecognized mechanism by which macrophages play a causal role in early dissemination impacting long-term metastasis development.

Introduction

The paradigm of cancer metastasis states that dissemination and metastasis occur when advanced aggressive tumors acquire invasive mechanisms. The finding that dissemination does not only occur from late stage invasive tumors has challenged this model [1]. Large cohort patient studies [2-5] and studies with spontaneous mouse tumor models [6] showed that dissemination also occurs during early stages of cancer when lesions are diagnosed by light microscopy as pre-malignant or pre-invasive. In addition, cancer of unknown primary is a relatively frequent event in solid cancers where metastases develop without the presence of an obvious primary tumor mass that evolved to become invasive [7].

The “early dissemination” definition was refined by Husemann et al. [6] when they showed that early disseminated cancer cells (DCCs) originate at times when lesions are only defined *in situ* by light microscopy (e.g. ductal carcinoma in situ (DCIS) in humans and mammary intraepithelial neoplasia in mice) but dissemination occurs and early DCCs show few genetic aberrations. In the MMTV-HER2 model, early DCCs are able to form lung metastases in the absence of invasive carcinoma [6]. This argues that in these models early DCCs are endowed with latent metastasis initiating capacity. Similarly, women treated for DCIS can develop metastases without ever developing any subsequent local invasive breast cancer [8-12]. This might indicate that, albeit at low frequency, early DCCs can unpredictably form metastases in patients. Early dissemination is not a rarity of breast cancer models (MMTV-HER2 and -PyMT models [6], as it also occurs in spontaneous mouse models of melanoma [13] and pancreatic cancer [14].

While in K-Ras-driven pancreatic cancer an EMT has been linked to early dissemination [14], its contribution to metastasis is unknown. Further, it remains poorly understood how dissemination occurs during pre-invasive stages of breast cancer when the epithelium-to-stroma barrier is intact. Early DCCs displayed only few genetic alterations [4,6], indicating that early dissemination might be driven by epigenetic and micro-environmental mechanisms that turn on programs of epithelial cell motility [15,16]. In fact, invasion of epithelial cells occurs physiologically during development.

The mammary epithelium forms postnatally during adolescence in a process called branching morphogenesis where rapidly dividing epithelial cells elongate the terminal end bud into the fat pad and bifurcate into the ductal tree. Macrophages are key regulators of branching morphogenesis during mammary gland development [17,18], arguing that normal mammary epithelial cells cooperate with these innate immune cells for invasive processes. These data led to the discovery of macrophages as powerful drivers of intravasation from invasive breast cancer tumors *via* the establishment of tumor microenvironments of metastasis [19]. This follows a streaming process where breast cancer cells recruit macrophages *via* production of colony stimulating factor 1 (CSF1) and then cancer cell motility is stimulated *via* macrophage-derived EGF [20]. Additionally, macrophages can induce an epithelial to mesenchymal transition (EMT) in malignant cells [21,22]. However, the role of macrophages in early spread of cancer remained unexoplored.

Here we show that the branching morphogenesis program is altered by the HER2 oncogene early in cancer development. Mammary tissue macrophages are recruited by HER2+ early cancer cells from the stroma into the epithelial layer of lesions

defined as mammary intraepithelial neoplasia in mice (similar to DCIS in humans) [23]. This process depends on HER2-NFkB-mediated induction of CCL2. CCR2+ intra-epithelial macrophages respond to CCL2, produce Wnt-1 and disrupt the myo-epithelial layer locally by downregulating E-cadherin junctions in a subpopulation of HER2+ cancer cells. Before tumors form, these events result in early dissemination microenvironments that propel active intravasation and dissemination to the lung that was efficiently blocked by macrophage depletion. Transient depletion of macrophages in mice before the formation of invasive tumors reduced lung metastatic burden. Importantly, this was the case when macrophage depletion had been stopped with formation of invasive tumors and mice were followed until they carried large overt invasive tumors. Our results suggest a previously unrecognized role for HER2-mediated recruitment of macrophages to favor dissemination of HER2+ tumor cells much earlier than growth is induced by the oncogene. Our work also reveals a role for early DCCs in supporting late metastasis development.

RESULTS

MACROPHAGES INFILTRATE THE EPITHELIAL COMPARTMENT OF EARLY HER2+ MAMMARY CANCER LESIONS.

We asked whether the HER2 oncogene might recruit macrophages to orchestrate early dissemination. We used MMTV-HER2 mice as a murine model of breast cancer since these show slow progression from early lesions such as hyperplasia and mammary intra-epithelial neoplasia (**Fig.1A,B**), the latter a similar lesion to DCIS [23], to invasive tumors (**Fig.1C**). We stained MMTV-HER2 mammary

gland sections for the murine macrophage marker F4/80 before we could detect any signs of invasive tumor masses in serial sections of mammary tissue or even enhanced proliferation in HER2+ early lesions [24]. Macrophages were located to the stroma outside of mammary ducts in healthy FVB wild type animals (**Fig.1D**). This was also true in young 14wk old MMTV-HER2 mice (**Fig.1E**). However, when MMTV-HER2 mice progressed over time but still showed no signs of tumor masses or enhanced proliferation [24], macrophages were often localized inside the luminal epithelial layer of early lesions as demonstrated by co-staining of F4/80 and cytokeratin 8/18 (**Fig. 1F**). We hypothesized that as macrophages enter the early lesions, they might disrupt the architecture of the duct. Close inspection of sections co-stained for smooth muscle actin and F4/80 showed that the myoepithelial cell layer was frequently disrupted at sites where macrophages were in immediate contact with the duct (**Fig. 1G-I**). Quantification of the abundance of intra-epithelial macrophages confirmed that the incidence of ducts with intra-epithelial macrophages correlated with HER2 upregulation and disease progression (**Fig. 1J**).

MACROPHAGES DISMANTLE E-CADHERIN JUNCTIONS IN EARLY HER2+ CANCER CELLS.

We hypothesized that HER2 might aberrantly activate a mechanism of invasion and motility involving macrophages in early lesions. We found that intra-epithelial macrophages were associated with a strong local downregulation of E-cadherin junctions *in vivo* in early lesion cells located directly adjacent to macrophages (1-2 cell diameter away) (**Fig.2A-C**). This was paralleled by a general downregulation of E-Cadherin mRNA in early lesions compared to wild type glands (**Fig.2D**). Additionally, β-

Catenin levels were increased in early lesions containing intra-epithelial macrophages as measured by dual color IHC (**Fig.2E-G**). A loss of E-Cadherin and translocation of β-Catenin to the nucleus could also be induced *in vitro* when Raw264.7 macrophages were added to Comma-1D healthy mammary epithelial cell monolayers used as a readout for epithelial junction formation (**Fig.2H-J**). The loss of E-cadherin junctions in epithelial cells adjacent to macrophages suggested that macrophages might produce cues that stimulate a loss of E-cadherin junctions as observed during the epithelium to mesenchyme transition (EMT). Macrophages can produce Wnt ligands [25-27] which are potent inducers of an EMT. We therefore tested the response of Raw264.7 macrophages or primary mammary tissue macrophages isolated from early lesions to conditioned media from healthy epithelial cells or from HER2+ early cancer cells. Only conditioned media derived from HER2+ cells induced an upregulation of Wnt-1 (**Fig.2K, L**); no changes were detected for Wnt-3, Wnt5a and Wnt7 (data not shown). The loss of E-Cadherin junctions in Comma-1D cells induced by Raw264.7 macrophages was reversed by addition of DKK1, an inhibitor of canonical Wnt signaling, to the co-cultures (**Fig.2M-P**). We conclude that downregulation of E-cadherin mRNA and junctions and β-catenin upregulation and nuclear translocation in early lesion cells results from HER2-dependent recruitment of Wnt-1 secreting macrophages into the early lesions.

MACROPHAGE DEPLETION PREVENTS AN E-CADHERIN AND β-CATENIN JUNCTION DISASSEMBLY AND EARLY DISSEMINATION.

Our data indicated that HER2 leads to macrophage mobilization into early lesions where they induce an EMT in early cancer cells. We next tested whether this process leads to early dissemination. CSF1R is expressed by most tissue resident macrophages

and is required for macrophages survival in tissues [28]. Thus, we injected MMTV-HER2 mice during early lesions with a blocking antibody to Csf-1 receptor (CSF1R) to eliminate macrophages from early lesions and then quantified circulating and disseminated early cancer cells in blood and target organs respectively (**Fig.3A**). CSF1R blockade led to efficient depletion of tissue resident $CD11b^{+}/F4/80^{+}/Gr1^{-}$ macrophages (**Supplementary Fig.1A**). Immunofluorescence staining for F4/80 in HER2+ early lesions confirmed a significant reduction in the number of intra-epithelial macrophages when CSF1R was blocked (**Supplementary Fig.1B**). We confirmed that at the end of the experiment, no tumor masses had formed, by inspecting whole mount stainings of mammary glands (**Supplementary Fig.1D,E**) and HE staining of serially sectioned mammary tissue (**Fig.3B,C**). Macrophage depletion was accompanied by a significant reduction in the number of hyperplastic ducts (**Supplementary Fig.1C**) and a tissue wide upregulation of E-Cadherin mRNA (**Fig.3D**) and E-Cadherin-based junctions (**Fig.3E-G**). We conclude that macrophages contribute to the loss of E-cadherin mRNA and junctions and disrupted mammary tissue architecture in early lesions.

The above changes correlated with the finding that CSF1R blockade significantly reduced the numbers of early circulating cancer cells (**Fig.3H**). Accordingly, CSF1R blockade also reduced early disseminated cancer cell (DCC) burden in target organs as measured by the detection of the transgene surface HER2 expressing early DCCs in the lungs (**Fig.3I-K**). We conclude that macrophages play a critical role in the ability of early cancer cells to acquire an invasive and disseminating phenotype. As indicated previously, these events of dissemination take place during a stage where no invasive

tumors are detectable and early lesions show similar proliferative capacity than normal resting mammary epithelium [24].

HER2-RECRUITED MACROPHAGES CONTROL EARLY DISSEMINATION AND CONTRIBUTE TO METACHRONOUS METASTASIS FORMATION.

We next tested whether macrophage-regulated early dissemination contributed to metastasis formation. To this end we blocked CSF1R only during early asymptomatic stages of cancer, starting at age week 18, and stopped as soon as tumors became palpable (size <3mm in diameter). We then waited until tumors reached 1 cm in diameter (4-6 weeks later) and quantified solitary DCCs and metastatic lesions in lungs (**Fig.4A)**. We found that the time to tumor detection was slightly delayed when macrophages were depleted during asymptomatic pre-malignant stages (**Fig.4B)**. However, once palpable tumors had formed, the progression to overt tumors was not affected (**Fig.4C**). Additionally, overt tumors showed no difference in macrophage content (**Fig.4D-F**) and vascularization (**Fig.4G-J**) at the end of the experiment between control and anti-CSF1R treated mice. This suggests that there is no impact on overt tumor growth in late tumors when macrophages were depleted during early stages. Additionally, flow analysis of lungs revealed that neither alveolar macrophage nor CD11b+/Gr1+ monocyte content was significantly affected (**Supplementary Fig.2A-E**) by the same treatment arguing against a systemic loss of all macrophages. However, CSF1R blockade during early stages significantly decreased solitary DCC burden in lungs (**Fig.4K**). CSF1R blockade during early stages also caused a statistically significant decrease in the number of metachronous metastases per mouse (**Fig.4M**),

196 which were defined as the number of metastatic lesions bigger than three cells (**Fig.4L**).
197 This inhibitory effect of DCC burden and metastasis was detected even after
198 macrophage depletion had been stopped in average for one month and animals had
199 carried fast-growing tumors. That the number of solitary DCCs, likely a mixture of DCCs
200 accumulated since the early stages was reduced by CSF1R blockade suggests that the
201 reduced influx of DCCs to lungs during early stages was not replaced by DCCs arriving
202 during the time of tumor detection to euthanasia when tumors were large. We conclude
203 that HER2+ early cancer cells recruit macrophages and that these play a seminal role in
204 early dissemination, allowing for the early DCCs to reach target organs and form
205 metastasis.
206
207 **HETEROGENEITY OF MYELOID CELLS IN EARLY MIN LESIONS.**
208 Our data suggests that macrophages play an active role in favoring early
209 dissemination and that early DCCs contribute to metachronous metastasis formation.
210 Remarkably, this occurs during early cancer stages in the absence of highly proliferative
211 tumor masses when the mammary tree mostly resembles that of a healthy gland. We
212 hypothesized that dissemination might be facilitated by tissue resident macrophages
213 involved in programs of branching morphogenesis during mammary gland development
214 [17,29]. We therefore compared the phenotype of macrophages present in wild type and
215 early lesion mammary glands. Mammary glands derived from FVB wild type mice and
216 MMTV-HER2 early lesion at 14 and 22 weeks were analyzed using CyTOF with a panel
217 of 17 hematopoietic cell markers and IdU as a proliferation marker (**Supplementary**
218 **Fig.3A**). Myelo-monocytic cells were identified as CD45+CD11b+F4/80+ cells lacking

lymphoid and granulocytic markers (**Supplementary Fig.3B**). viSNE plots [30] of myelo-monocytic cells (**Fig.5A**) showed that myelomonocytic numbers and patterns were similar between wild type glands and early lesions. viSNE analysis further revealed three putative populations, one of which could be identified as monocyte based on its high Ly6C levels (**Fig.5B**) and did not differ in numbers between these samples (**Fig.5D**). The remaining LY6C- macrophages could be distinguished into two populations according to the expression of CD206 (**Fig.5C**). The pre-dominant macrophage subtype present in both wild type glands and early lesions was $CD206^{hi}$ (**Fig.5E,F**). CD206-hi macrophages were also $Tie2^{hi}$, $CD11b^{hi}$ and VCAM-lo and did not show any signs of proliferation based on IdU incorporation (**Fig.5I,J; Supplementary Fig.3C,D**). This matches previous findings [31] that wild type resident mammary glands contained M2 polarized $CD11b^{hi,}$ $CD206^{hi}$ and $Tie2^{hi}$ macrophages termed mammary tissue macrophages (MTMs) whereas tumor-associated macrophages prevalent in invasive MMTV-PyMT tumors were $CD11b^{int}$, $CD206^{lo}$, $Tie2^{lo}$ and $VCAM^{hi}$. We found that these $CD206^{lo}$ TAMs were a minority in wild type glands or early lesions but indeed constituted the majority of myelomonocytic cells in overt invasive MMTV-HER2 tumors (**Fig.5G,H**). Since our global CyTOF analysis showed that the predominant macrophage population in HER2+ early lesions resembled MTMs, we wanted to correlate the macrophage status with their localization and performed *in situ* stainings to identify whether intra-epithelial macrophages in early lesions might be $CD206^{hi}$ MTMs as well. To this end we co-stained wild type glands, early lesions and overt tumors tissues against F4/80 and CD206 (**Fig.5K-M**). We found that stromal and intra-epithelial macrophages in both wild type glands and early lesions were $CD206^{hi}$ whereas tumor

associated macrophages in overt tumors were CD206^{lo} (**Fig.5N**). While tracing the exact origin and lineage of macrophage subtypes will require further scrutiny, our data suggest that intra-epithelial macrophages might be derived from resident mammary tissue macrophages and that expansion of monocyte derived tumor associated macrophages is a hallmark of overt tumor stages.

HER2+ EARLY CANCER CELLS PRODUCE CCL2 AND RECRUIT MACROPHAGES INTO MAMMARY DUCTS.

We next explored what signals might HER2 upregulation induce that might attract resident mammary tissue macrophages from the stroma into the ductal epithelium of HER2+ early lesions. In invasive breast cancer models, HER2 signaling activates NFkB, which transcriptionally induces CCL2, a potent macrophage chemotactic factor [32]. Accordingly, the p65 subunit of NFκB subunit was phosphorylated in mammospheres derived from HER2+ early cancer cells, and Lapatinib, a HER2 and EGFR inhibitor, inhibited its phosphorylation (**Fig.6A**). We then isolated RNA from mammospheres derived from either FVB wild type or MMTV-HER2 early MIN lesions as described [33] and performed quantitative real-time PCR analysis for cytokine mRNAs. We found that already at these early stages of progression, when enhanced proliferation is not yet detectable [24], HER2+ cancer cells upregulated expression of CCL2 but not CSF2, CSF1, IL1β, and IL6 (**Fig. 6B, Supplementary Fig.4A,B)**. Upregulation of CCL2 around HER2+ early cancer cells was also observed at the protein levels as revealed by immunofluorescence (**Fig.6C,D, Supplementary Fig.4C-E**). CCR2+ cells could be found close to CCL2+ early cancer cells (**Fig.6C insert**). Additionally, acinar-like

structures produced by early MMTV-HER2 cancer cells displayed a reduction in secreted and peri-organoid CCL2 production upon inhibition of HER2 or NFkB signaling with specific inhibitors [34] (**Fig.6E-G**). To confirm that CCL2 signaling was necessary and sufficient for HER2-dependent macrophage recruitment, HER2+ early cancer cells were grown as 3D acinar structures *in vitro* for 5 days. Cultures were then treated with Lapatinib, an IKKβ inhibitor [34] or an inhibitor of the CCL2 receptor CCR2 (RS504393) and macrophages isolated from mammary glands of MMTV-HER2 mice were added to the cultures. After 24 hours of co-culture, macrophages were associated with ~50% of all organoid structures in control samples (**Fig.6H**). In contrast, co-cultures treated with the inhibitors all showed significant reduction in macrophage association (**Fig.6I,J**). We next treated 20 week old MMTV-HER2 mice carrying only early lesions (no palpable or overt tumors) for 2 weeks with a CCR2 inhibitor (**Fig.6K,L**). We found that the number of intra-epithelial macrophages was significantly reduced when mice were treated systemically (**Fig.6M**). When the CCR2 inhibitor was administered locally into the fat pad to avoid systemic effects (**Fig.6N**), intra-epithelial macrophage content was reduced compared to contra-lateral control treated glands (**Fig.6O**), supporting that intra-epithelial macrophages are indeed derived from resident mammary gland macrophages instead of circulating monocyte derived macrophages. Additionally, mammary tissue macrophages can also be depleted by genetic ablation of CCR2 [31] arguing that we may be eliminating the same population during early mammary cancer stages. We conclude that HER2 signaling in cancer cells from early lesions activates NFkB to induce CCL2, which in turn mobilizes CCR2+ resident mammary macrophages from the stroma into these early lesions.

HIGH INTRA-EPITHELIAL MACROPHAGE NUMBERS IN PATIENT DCIS LESIONS CORRELATE WITH LOW E-CADHERIN LEVELS.

Published data showed that more than 10% of patients with DCIS had detectable DCCs in their bone marrow (BM), but no histologic markers, which include invasive fronts and receptor status were indicative of the presence of DCCs [3]. To test whether macrophages could also infiltrate early lesions in humans, we compared macrophages in healthy human breast tissue vs. tissue from DCIS lesions as a model of early stage breast cancer lesions. Macrophages were identified as CD68+/CD45+ and cytokeratin8/18 negative cells (**Supplementary Fig.5A,B**). In breast tissue from healthy donors, macrophages were localized in the stroma in the vicinity of mammary ducts but remained outside of the ducts, which were delimited by an intact myoepithelial layer of cells (**Fig.7A**). In contrast, even in DCIS lesions that displayed an apparently intact myoepithelial layer, there was a statistically significant increase in the frequency of macrophages found inside the aberrant ductal epithelial structure in between cancer cells (**Fig.7B,C**). The association of intra-epithelial macrophages with reduced E-Cadherin levels was confirmed in human DCIS samples (N=12). This was independent of HER2 status and appeared in different patterns. Patients with high macrophage numbers within lesions showed overall lower E-Cadherin levels as measured by quantitative image analysis **(Fig.7D-F**). Additionally, within the same patient, individual lesions with high macrophage numbers had lower E-Cadherin levels (**Supplementary Fig.5C-E**). This reveals an inter- and intra-tumor heterogeneity and suggests that some regions of DCIS lesions might be more prone to contain cancer cells able to undergo early dissemination.

Discussion

Following the assumption that dissemination occurs only during late invasive cancer stages, many studies have focused on investigating dissemination from invasive lesions. However, micro-invasion events were detected in patients' "pre-invasive" DCIS lesions using electron microscopy, but these events might go unnoticed by light microscopy [6]. Additionally, DCIS lesions were found to be vascularized [35], indicating that there might be a possibility for early cancer cell dissemination within the DCIS lesions. Our data reveal that macrophages enter the epithelium of early lesions in mice and human DCIS where they create early dissemination microenvironments. In mice this process can be initiated by the HER2 oncogene before growth stimulation is evident, revealing a novel function for the HER2 oncogene that could be targeted. The HER2 orchestrated early dissemination microenvironments contain early cancer cells that attract CCR2+ macrophages *via* CCL2 secretion that in turn secrete Wnt-1 to dismantle epithelial E-Cadherin junctions. The dissemination-promoting function of macrophages was proven when we found that depletion of macrophages in early HER2+ lesions using anti-CSF1R antibodies reversed the loss of E-cadherin in HER2+ lesions as well as intravasation and dissemination to lungs. Interestingly, Wnt signaling is linked to branching morphogenesis [36,37] and a subset of tumor-associated macrophages that drive invasive cancer dissemination also secrete Wnt ligands [27].

We found that the myelo-monocytic landscape of HER2+ early lesions at the time of early dissemination resembled that of healthy mammary glands and largely consisted of M2 polarized F4/80+/CD11b+/CD206+/Tie2+ macrophages. In contrast, overt tumors predominantly contained $CD11b^{int}/CD206^{lo}/Tie2^{lo}$/VCAM+ macrophages as described [31]

but these were the minority of macrophages in wild type and early lesion ducts. We corroborated these findings *in situ* by immunofluorescence staining, confirming that intra-epithelial macrophages and wild type resident macrophages are CD206+ whereas tumor associated macrophages are CD206^{lo}. Interestingly, the profile of resident and early lesion macrophages is characteristic for a subset of macrophages in invasive breast cancer lesions that are gatekeepers of intravasation doorways [19].

This raises the possibility that when HER2 is overexpressed in mammary epithelila cells, resident macrophages have the inherent potential to aberrantly fuel epithelial cell motility as is the case during physiologic mammary gland development [17,18,29]. While the barrier between stroma and epithelium prevents resident macrophages from disrupting the steady state epithelial architecture, oncogene-activated attraction of resident macrophages into the epithelium might result in disruption of normal tissue boundaries and early dissemination. However, further scrutiny and lineage tracing experiments are required to fully understand the origin of macrophages driving early and late dissemination.

We further found that when macrophages were depleted during early stages but allowed to rebound during invasive stages, lung metastatic burden was still reduced. This indicates that early DCCs contribute to lung metastasis formation, either directly or indirectly and surprisingly large tumors that persisted in mice for ~1.5 months were not able to compensate for the reduced dissemination during early stages. While the exact clinical implications of our findings need further analysis, a few scenarios of clinical relevance can be discussed. It is argued that because 13% of DCIS patients show disseminated disease and only 3% develop metastatic disease [8-12], early dissemination

357 is not a contributor to lethal metastatic cancer. However, approximately 50% of breast
358 cancer deaths after DCIS occurred in the absence of a detectable local invasive disease
359 and were not influenced by current treatments [10]. Further, cancer can manifest with
360 metastasis without a detectable primary even after careful inspection of the patients [38].
361 These clinical findings indicate that at least in a subgroup of patients, early DCCs may
362 develop lethal metastases [10] (**Fig.7G** scenario 1). Additionally, early DCCs may
363 cooperate with later arriving DCCs to form metastasis in patients that after DCIS
364 treatment go on to develop invasive lesions or in patients that had DCIS but only were
365 diagnosed later for invasive cancer (**Fig.7G** scenario 2). This resembles the concept of
366 the "pre-metastatic" niche described previously [39,40] where the pre-metastatic niche
367 could also be orchestrated by early DCCs. Next phase studies will address the genetic
368 identity of metastasis affected by macrophage depletion and determine the contribution
369 of early DCCs to the metastatic burden late in cancer progression.

370 Overall, our studies suggest that before propelling rapid growth, oncogenes such
371 as HER2 might turn on developmental programs of anoikis resistance [24], macrophage
372 recruitment and invasion that initiate dissemination much earlier than anticipated. We
373 provide critical new insight into the understanding of the natural history of metastatic
374 disease and we demonstrate that macrophages and early DCCs appear to play a
375 seminal role in metastatic breast cancer.

376

377 **Methods.**

378 **Cells and cell culture.** Raw264.7 cells expressing mCherry were generated using
379 mCherry lentiviral vectors and maintained in DMEM (Lonza) with 10% FBS and 1%

Pen/Strep. Comma-1D cells were maintained in DMEM-F12 medium containing 2%FBS, 1% Pen/Strep. For DKK1 stimulation, conditioned media was prepared from DKK1 expressing 293T cells and protein concentration was determined using a Bradford assay cells cultured with serum free medium (DMEM + 1%P/S) for 24 hours and then concentrated using Vivaspin 20 Centrifugal Concentrating tubes (Sartorius, VS2021) at 3000g up to 3 hours until desired concentration (10x) was reached. 0.5ug/ml DKK1 protein was used for stimulation. For co-culture experiments, Comma-1D cells were seeded on coverslips and after 12h, Raw-264.7-mCherry cells were added. Co-cultures were fixed in 2% formalin after 12h and then stained. All cell lines were routinely tested for mycoplasma.

Mouse experiments. All animal procedures were approved by the Institutional Animal Care and Use Committee (IACUC) of Icahn School of Medicine at Mount Sinai, protocols 08-0366 and 2014-0190. FVB/N-Tg(MMTVneu)202Mul/J or FVB wild type mice were purchased from Jackson laboratory and bred in-house. Animals were sacrificed using CO_2 at age 14, 20-22wk or when invasive tumors had reached a diameter of 1cm. For macrophage depletion, we administered 3mg of the CSF1R antibody clone ASF98 on day 1 and 1mg on day 7 and weekly thereafter by injection into the tail vein of 18wk old pre-malignant MMTV-Her2 mice. PBS was used as vehicle control. Treatment lasted 14 days or until tumors were first palpable (3mm diameter). ASF98 antibody was a generous gift of Dr. Miriam Merad. For CCR2 blockade, mice were either treated with 2mg/kg of RS504393 (Tocris Bioscience) or

vehicle control (DMSO) daily by i.p. injections for 14 days or by injection of 1mg/kg RS504393 into the fat pad for 5d.

Mammary Gland Whole Mounts. Mammary glands were excised, fixed in Carnoy's fixative and stained in carmine alum solution as described in http://mammary.nih.gov/tools/histological/Histology/index.html.

Microscopy. Formalin fixed and paraffin embedded samples were prepared and stained as described [41]. For immunohistochemistry, VectaStain Elite ABC Rabbit IgG and Mouse IgG (PK-6102) kits from Vector Laboratories were used for secondary antibodies. Secondary antibodies were left for one hour at room temperature. DAB and Vector Blue substrate kit (Vector Laboratories) were used for enzymatic substrate. Mounting was done using VECTASHIELD mounting media (Vector Laboratories). For CD206 stainings, cryosections were used. Tissue was fixed in 4% formalin over night, incubated in 30% sucrose/PBS over night and sectioned into 6mm sections. Staining of cryosection was done as described [42]. Antibodies used were: CD68 (Sigma, polyclonal), F4/80 (abcam CIA:3-1), Iba-1 (Wako polyclonal), Cytokeratin 8/18 (Progen, polyclonal), smooth muscle actin (Sigma IA4), CD206 (Biolegend C068C2), CCL2 (Novus 2D8), E-Cadherin (Becton Dickinson, polyclonal), beta catenin (cell signaling, polyclonal), Her2 (abcam, polyclonal), Endomucin (Santa Cruz 7C7). For costaining of F4/80 and CD206 (both raised in rat) a FITC-conjugated F4/80 antibody (Biolegend BM8) was used in combination with CD206 (Biolegend C068C2) in a sequential stain. Microscopic analysis was carried out with a Leica widefield microscope or with a Leica confocal microscope for 3D cultures. For quantification of immunofluorescence signal intensity with the Metamorph software, regions of interest were defined in original tiff files that

had been taken under the same exposure time and settings and the mean signal intensity was measured. Because the use of a directly conjugated F4/80 antibody resulted in lower signal intensity, we used Iba1 as a macrophage marker [19] to identify macrophages for CD206 signal intensity measurement instead.

Flow Cytometry. MMTV-HER2 mice were sacrificed using CO_2 at age 18-22wk (early pre-malignant cancer lesions) or when overt tumors had formed. Whole mammary glands or tumors were digested in Collagenase/BSA at 37°C for 30-45min. Red blood cell lysis buffer (Sigma) was used to remove blood cells. Cell suspensions were blocked with Fc-blocking reagent (eBioscience) and samples were surface stained in FACS buffer (PBS supplemented with 1% BSA and 2mM EDTA) for 20-30 min on ice using the following antibodies: CD45-PerCPCy5.5 (Biolegend 30-F11), CD11b-PeCy7 (eBioscience M1/70), CD11c-PE (eBioscience N418), Gr1-AF700 (eBioscience RB68C5), Tie2-biotin (eBioscience TEK4), F4/80-biotin (Biolegend BM8), CD206-APC (Biolegend C068C2), VCAM-FITC (eBioscience 429). DAPI was used to label dead cells. Multiparameter analysis was performed on a Fortessa (BD) and analyzed with FlowJo software (Tree Star). DAPI+ cells and doublets were excluded from all analysis. To sort mammary tissue macrophages, whole mammary glands from 14wk, 18-22wk (early pre-malignant cancer lesions) mammary glands or from invasive tumors were digested in Collagenase/BSA at 37°C for 30-45min. Mononuclear cells were enriched in a Percoll gradient and then macrophages were sorted as viable CD45+/Gr1-/CD11b+/F4/80+ cells.

CyTOF analysis. All mass cytometry reagents were purchased from Fluidigm Inc. (former DVS) unless otherwise noted. Mice were injected i.p. with 1mg IdU per mouse 16h prior to the experiment. Lymph nodes were removed and mammary glands were digested using the Miltenyi fatty tissue digestion kit. Cells were then washed with PBS containing 1% BSA and blocked with Fc-blocking reagent (eBioscience) to minimize non-specific antibody binding. Cells were stained with a panel of metal-labeled antibodies against 20 cell surface markers (Fig.5 supplement 1A) for 30 minutes on ice, and then washed. All antibodies were either purchased pre-conjugated to metal tags, or conjugated in-house using MaxPar X8 conjugation kits according to the manufacturer's instructions. After antibody staining, cells were incubated with cisplatin for 5 minutes at RT as a viability dye for dead cell exclusion. Cells were then fixed and permeabilized with a commercial fix/perm buffer (BD Biosciences) and stored in PBS containing 1.6% formaldehyde and a 1:4000 dilution of Ir nucleic acid intercalator to label all nucleated cells. Immediately prior to acquisition, cells were washed in PBS, and diH20 and resuspended in diH20 containing a 1/10 dilution of EQ 4 Element Calibration beads. After routine instrument tuning and optimization, the samples were acquired on a CyTOF2 Mass Cytometer in sequential 10min acquisitions at an acquisition rate of <500 events/s. The resulting FCS files were concatenated and normalized using a bead-based normalization algorithm in the CyTOF acquisition software and analyzed with Cytobank. FCS files were manually pre-gated on Ir193 DNA+ CD45+ events, excluding dead cells, doublets and DNA-negative debris. Myeloid derived cells were manually gated based on CD11c and CD11b expression and the gated myeloid populations were then analyzed using viSNE [30] based on all myeloid phenotypic markers. Putative cell

populations on the resulting viSNE map were manually gated based on the expression of canonical markers, while allowing for visualization of additional heterogeneity within and outside of the labeled population bubbles.

Mammospheres and 3D mammary primary epithelial cell cultures. Acini cultures were performed as described [33,43]. 5x10^4 eCCs were seeded in in 400ul Assay Medium in 8-well chamber slides coated with 40ul of Matrigel (Corning). Acini formed at an efficiency of around 30 acini/1*10^4 MECs plated. For macrophage co-cultures, primary tissue macrophages were added at a ratio of 500 per 1x10^4 eCCs seeded to 5d old acini cultures. For inhibitory treatments, 5d old acini cultures were treated for 24h with 1μM Lapatinib (LC Laboratories), 2uM IKK Inhibitor [34] (generous gift from Dr. Albert Baldwin), 1μM CCR2 inhibitor RS504393 (Tocris Bioscience) or DMSO as vehicle control. Cultures were then fixed for immunofluorescence (IF) with 4% PFA. Mammosphere cultures were prepared as described [33]. To prepare conditioned medium, 5d old mammosphere culture were plated in serum free DMEM medium and conditioned medium was harvested after 24h.

Immunoblotting, RT–PCR, and quantitative PCR (qPCR). Immunoblotting was performed as described previously [44,45]. Antibodies used were P-NF-kappa-B p65 (Cell Signaling polyclonal) and beta-tubulin (abcam, polyclonal). For expression analysis of FVB wild type mammary epithelial cells or MMTV-Her2 eCCs, epithelial cells were isolated and grown as mammospheres for 5d as described [33]. For expression analysis of Raw264.7 macrophages, cells were grown as monolayers in 6-well culture dishes

and treated with conditioned medium for 24h. RNA isolation was performed using Trizol (Life Technologies) or the RNeasy Kit (Qiagen) for MTMs. RT– and qPCR were performed as described [41]. All samples were normalized to GAPDH expression and $2^{-\text{delta delta Ct}}$ values were calculated as described [46]. Primers were purchased from IDT. Primer sequences were: Mouse- GAPDH forward primer 5'-AACTTTGGCATTGTGGAAGGGCTC-3'; GAPDH reverse primer 5'-TGGAAGAGTGGGAGTTGCTGTTGA-3. E-Cadherin forward primer 5'-CAAGGACAGCCTTCTTTTCG-3'; E-Cadherin reverse primer 5'-TGGACTTCAGCGTCACTTTG-3'. Wnt-1 forward primer 5'-CAGTGGAAGGTGCAGTTGCAG-3'; Wnt-1 reverse primer 5'-CAGTGGAAGGTGCAGTTGCAGC-3'. CSF1 forward primer 5'-CAACAGCTTTGCTAAGTGCTCTA-3'; CSF1 reverse primer 5'-CACTGCTAGGGGTGGCTTTA-3'. CCL2 forward primer 5'-GGCTGGAGAGCTACAAGAGG-3'; CCL2 reverse primer 5'-GGTCAGCACAGACCTCTCTC-3'.

Patient samples. Paraffin embedded sections from patients with DCIS were obtained from the Cancer Biorepository at Icahn School of Medicine at Mount Sinai, New York, NY and from Thomas Karn, University of Frankfurt, Germany. Samples were fully de-identified and obtained with Institutional Review Board approval, which indicated that this work does not meet the definition of human subject research according to the 45 CFR 46 and the Office of Human Subject Research.

Circulating Cancer Cells (CCCs) and Disseminated Cancer Cells (DCCs) detection. For CCC analysis, blood was drawn by cardiac puncture following IACUC protocols. CCCs were purified using negative lineage cell-depletion kit (Miltenyi), fixed with 3% PFA for 20 min on ice and cytospin preparations were carried out by centrifugation of blood cells at 500 rpm for 3 min using poly-L-lysine-coated slides (Sigma).

Statistical Analysis. Unless noted otherwise, all of the experiments presented in the manuscript were repeated at least 3 times with replicates of at least 3. Statistical Analysis was done using Graph Pad Prism Software. For all cell culture experiments (experiments with technical replicates), one-tailed *student t-tests* were performed. For mouse experiments, *Mann-Whitney* tests were used. Differences were considered significant if *P* values were ≤ 0.05.

References.

1 Turajlic, S. & Swanton, C. Metastasis as an evolutionary process. *Science* **352**, 169-175, doi:10.1126/science.aaf2784 (2016).

2 Braun, S. *et al.* A pooled analysis of bone marrow micrometastasis in breast cancer. *The New England journal of medicine* **353**, 793-802, doi:10.1056/NEJMoa050434 (2005).

3 Banys, M. *et al.* Hematogenous and lymphatic tumor cell dissemination may be detected in patients diagnosed with ductal carcinoma in situ of the breast. *Breast cancer research and treatment* **131**, 801-808, doi:10.1007/s10549-011-1478-2 (2012).

4 Schardt, J. A. *et al.* Genomic analysis of single cytokeratin-positive cells from bone marrow reveals early mutational events in breast cancer. *Cancer cell* **8**, 227-239, doi:10.1016/j.ccr.2005.08.003 (2005).

5 Sanger, N. *et al.* Disseminated tumor cells in the bone marrow of patients with ductal carcinoma in situ. *Int J Cancer* **129**, 2522-2526, doi:10.1002/ijc.25895 (2011).

6 Husemann, Y. *et al.* Systemic spread is an early step in breast cancer. *Cancer cell* **13**, 58-68, doi:10.1016/j.ccr.2007.12.003 (2008).

7 Pavlidis, N., Khaled, H. & Gaafar, R. A mini review on cancer of unknown primary site: A clinical puzzle for the oncologists. *Journal of advanced research* **6**, 375-382, doi:10.1016/j.jare.2014.11.007 (2015).
8 Cutuli, B. *et al.* Ductal carcinoma in situ of the breast results of conservative and radical treatments in 716 patients. *Eur J Cancer* **37**, 2365-2372 (2001).
9 Donker, M. *et al.* Breast-conserving treatment with or without radiotherapy in ductal carcinoma In Situ: 15-year recurrence rates and outcome after a recurrence, from the EORTC 10853 randomized phase III trial. *Journal of clinical oncology : official journal of the American Society of Clinical Oncology* **31**, 4054-4059, doi:10.1200/JCO.2013.49.5077 (2013).
10 Narod, S. A., Iqbal, J., Giannakeas, V., Sopik, V. & Sun, P. Breast Cancer Mortality After a Diagnosis of Ductal Carcinoma In Situ. *JAMA oncology*, doi:10.1001/jamaoncol.2015.2510 (2015).
11 Warnberg, F., Bergh, J., Zack, M. & Holmberg, L. Risk factors for subsequent invasive breast cancer and breast cancer death after ductal carcinoma in situ: a population-based case-control study in Sweden. *Cancer epidemiology, biomarkers & prevention : a publication of the American Association for Cancer Research, cosponsored by the American Society of Preventive Oncology* **10**, 495-499 (2001).
12 Warnberg, F. *et al.* Effect of radiotherapy after breast-conserving surgery for ductal carcinoma in situ: 20 years follow-up in the randomized SweDCIS Trial. *Journal of clinical oncology : official journal of the American Society of Clinical Oncology* **32**, 3613-3618, doi:10.1200/JCO.2014.56.2595 (2014).
13 Eyles, J. *et al.* Tumor cells disseminate early, but immunosurveillance limits metastatic outgrowth, in a mouse model of melanoma. *The Journal of clinical investigation* **120**, 2030-2039, doi:10.1172/JCI42002 (2010).
14 Rhim, A. D. *et al.* EMT and dissemination precede pancreatic tumor formation. *Cell* **148**, 349-361, doi:10.1016/j.cell.2011.11.025 (2012).
15 Liu, Y. J. *et al.* Confinement and low adhesion induce fast amoeboid migration of slow mesenchymal cells. *Cell* **160**, 659-672, doi:10.1016/j.cell.2015.01.007 (2015).
16 Nguyen-Ngoc, K. V. *et al.* ECM microenvironment regulates collective migration and local dissemination in normal and malignant mammary epithelium. *Proc Natl Acad Sci U S A* **109**, E2595-2604, doi:10.1073/pnas.1212834109 (2012).
17 Van Nguyen, A. & Pollard, J. W. Colony stimulating factor-1 is required to recruit macrophages into the mammary gland to facilitate mammary ductal outgrowth. *Developmental biology* **247**, 11-25, doi:10.1006/dbio.2002.0669 (2002).
18 Gouon-Evans, V., Rothenberg, M. E. & Pollard, J. W. Postnatal mammary gland development requires macrophages and eosinophils. *Development* **127**, 2269-2282 (2000).
19 Harney, A. S. *et al.* Real-Time Imaging Reveals Local, Transient Vascular Permeability, and Tumor Cell Intravasation Stimulated by TIE2hi Macrophage-Derived VEGFA. *Cancer discovery*, doi:10.1158/2159-8290.CD-15-0012 (2015).
20 Wyckoff, J. *et al.* A paracrine loop between tumor cells and macrophages is required for tumor cell migration in mammary tumors. *Cancer research* **64**, 7022-7029, doi:10.1158/0008-5472.CAN-04-1449 (2004).

21 Liu, C. Y. *et al.* M2-polarized tumor-associated macrophages promoted epithelial-mesenchymal transition in pancreatic cancer cells, partially through TLR4/IL-10 signaling pathway. *Laboratory investigation; a journal of technical methods and pathology* **93**, 844-854, doi:10.1038/labinvest.2013.69 (2013).

22 Bonde, A. K., Tischler, V., Kumar, S., Soltermann, A. & Schwendener, R. A. Intratumoral macrophages contribute to epithelial-mesenchymal transition in solid tumors. *BMC cancer* **12**, 35, doi:10.1186/1471-2407-12-35 (2012).

23 Cardiff, R. D. Validity of mouse mammary tumour models for human breast cancer: comparative pathology. *Microscopy research and technique* **52**, 224-230, doi:10.1002/1097-0029(20010115)52:2<224::AID-JEMT1007>3.0.CO;2-A (2001).

24 Wen, H. C. *et al.* p38alpha Signaling Induces Anoikis and Lumen Formation During Mammary Morphogenesis. *Science signaling* **4**, ra34, doi:10.1126/scisignal.2001684 (2011).

25 Wang, S. *et al.* Wnt1 positively regulates CD36 expression via TCF4 and PPAR-gamma in macrophages. *Cellular physiology and biochemistry : international journal of experimental cellular physiology, biochemistry, and pharmacology* **35**, 1289-1302, doi:10.1159/000373951 (2015).

26 Cosin-Roger, J. *et al.* M2 macrophages activate WNT signaling pathway in epithelial cells: relevance in ulcerative colitis. *PloS one* **8**, e78128, doi:10.1371/journal.pone.0078128 (2013).

27 Ojalvo, L. S., Whittaker, C. A., Condeelis, J. S. & Pollard, J. W. Gene expression analysis of macrophages that facilitate tumor invasion supports a role for Wnt-signaling in mediating their activity in primary mammary tumors. *J Immunol* **184**, 702-712, doi:10.4049/jimmunol.0902360 (2010).

28 Stanley, E. R., Cifone, M., Heard, P. M. & Defendi, V. Factors regulating macrophage production and growth: identity of colony-stimulating factor and macrophage growth factor. *The Journal of experimental medicine* **143**, 631-647 (1976).

29 Gouon-Evans, V., Lin, E. Y. & Pollard, J. W. Requirement of macrophages and eosinophils and their cytokines/chemokines for mammary gland development. *Breast cancer research : BCR* **4**, 155-164 (2002).

30 Amir el, A. D. *et al.* viSNE enables visualization of high dimensional single-cell data and reveals phenotypic heterogeneity of leukemia. *Nature biotechnology* **31**, 545-552, doi:10.1038/nbt.2594 (2013).

31 Franklin, R. A. *et al.* The cellular and molecular origin of tumor-associated macrophages. *Science* **344**, 921-925, doi:10.1126/science.1252510 (2014).

32 Cogswell, P. C., Guttridge, D. C., Funkhouser, W. K. & Baldwin, A. S., Jr. Selective activation of NF-kappa B subunits in human breast cancer: potential roles for NF-kappa B2/p52 and for Bcl-3. *Oncogene* **19**, 1123-1131, doi:10.1038/sj.onc.1203412 (2000).

33 Cohn, E., Ossowski, L., Bertran, S., Marzan, C. & Farias, E. F. RARalpha1 control of mammary gland ductal morphogenesis and wnt1-tumorigenesis. *Breast cancer research : BCR* **12**, R79, doi:10.1186/bcr2724 (2010).

34 Basseres, D. S., Ebbs, A., Cogswell, P. C. & Baldwin, A. S. IKK is a therapeutic target in KRAS-Induced lung cancer with disrupted p53 activity. *Genes & cancer* **5**, 41-55 (2014).
35 Cocker, R., Oktay, M. H., Sunkara, J. L. & Koss, L. G. Mechanisms of progression of ductal carcinoma in situ of the breast to invasive cancer. A hypothesis. *Medical hypotheses* **69**, 57-63, doi:10.1016/j.mehy.2006.11.042 (2007).
36 Brisken, C. *et al.* Essential function of Wnt-4 in mammary gland development downstream of progesterone signaling. *Genes & development* **14**, 650-654 (2000).
37 Robinson, G. W., Hennighausen, L. & Johnson, P. F. Side-branching in the mammary gland: the progesterone-Wnt connection. *Genes & development* **14**, 889-894 (2000).
38 Pavlidis, N. & Fizazi, K. Cancer of unknown primary (CUP). *Critical reviews in oncology/hematology* **54**, 243-250, doi:10.1016/j.critrevonc.2004.10.002 (2005).
39 Kaplan, R. N. *et al.* VEGFR1-positive haematopoietic bone marrow progenitors initiate the pre-metastatic niche. *Nature* **438**, 820-827, doi:10.1038/nature04186 (2005).
40 Peinado, H. *et al.* Melanoma exosomes educate bone marrow progenitor cells toward a pro-metastatic phenotype through MET. *Nature medicine* **18**, 883-891, doi:10.1038/nm.2753 (2012).
41 Bragado, P. *et al.* TGF-beta2 dictates disseminated tumour cell fate in target organs through TGF-beta-RIII and p38alpha/beta signalling. *Nature cell biology* **15**, 1351-1361, doi:10.1038/ncb2861 (2013).
42 Lederle, W. *et al.* Platelet-derived growth factor-B normalizes micromorphology and vessel function in vascular endothelial growth factor-A-induced squamous cell carcinomas. *The American journal of pathology* **176**, 981-994, doi:10.2353/ajpath.2010.080998 (2010).
43 Debnath, J., Muthuswamy, S. K. & Brugge, J. S. Morphogenesis and oncogenesis of MCF-10A mammary epithelial acini grown in three-dimensional basement membrane cultures. *Methods* **30**, 256-268 (2003).
44 Adam, A. P. *et al.* Computational identification of a p38SAPK-regulated transcription factor network required for tumor cell quiescence. *Cancer research* **69**, 5664-5672, doi:10.1158/0008-5472.CAN-08-3820 (2009).
45 Ranganathan, A. C., Zhang, L., Adam, A. P. & Aguirre-Ghiso, J. A. Functional coupling of p38-induced up-regulation of BiP and activation of RNA-dependent protein kinase-like endoplasmic reticulum kinase to drug resistance of dormant carcinoma cells. *Cancer research* **66**, 1702-1711, doi:10.1158/0008-5472.CAN-05-3092 (2006).
46 Livak, K. J. & Schmittgen, T. D. Analysis of relative gene expression data using real-time quantitative PCR and the 2(-Delta Delta C(T)) Method. *Methods* **25**, 402-408, doi:10.1006/meth.2001.1262 (2001).

Author Contributions.

N.L. designed and optimized experimental approach, performed *in vitro* and *in vivo* experiments, analyzed data and co-wrote the manuscript, A.M. and A.R. and the Human Immune Monitoring Core performed CyTOF experiments, E.F., M.S.S., E.T., and K.H. performed experiments, M.M. provided general guidance and oversight and co-wrote the manuscript, J.A.A.-G. designed and optimized experimental approach, provided general guidance and oversight, analyzed data and co-wrote the manuscript.

Acknowledgments.

We thank the Aguirre-Ghiso and the Merad labs for helpful discussion. We are grateful to A. Baldwin for providing the IKK inhibitor. We thank J. Ochando and the Flow Cytometry Core for technical support and assistance with cell sorting. N.L. was funded by DFG fellowship Li23561-1 and DoD-BrCRP BC133807 and J.A.A.-G. was funded by NIH/National Cancer Institute (CA109182, CA163131).

Author information.

The authors declare no competing financial interests.

Figure Legends.

Figure 1: Macrophages enter the ductal epithelial layer in early breast cancer lesions. HE stainings of mammary gland sections show progression from healthy mammary ducts in FVB wild type glands (**A**) to early lesions classified as hyperplasia and mammary intra-epithelial neoplasia (**B**) to invasive tumors (**C**) in the MMTV-HER2 mouse model. Mammary glands from FVB wild type (**D**) of pre-malignant MMTV-HER2 mice at age 14 (**E**) and 22 (**F**) weeks were stained against F4/80 (macrophages) and CK8/18 (epithelial cells) and against F4/80 and SMA (**E-G**). Bars 10μm. The mean plus SEM of the percentage of ducts containing IEM is shown; each dot represents one animals (**H**).

Figure 2: Intra-epithelial macrophages induce an EMT-like response in early cancer cells. 20wk old MMTV-HER2 mouse mammary glands were stained against E-Cadherin and F4/80. E-Cadherin localization was analyzed dependent on whether macrophages did not make direct contact to the duct (no M. or distant M.; **A**) or whether ducts contain intra-epithelial macrophages (IEM; **B**). The percentage of individual epithelial cells that showed disrupted E-Cadherin (arrow in B) was quantified (**C**). Plot shows means plus SEM; each dot represents one animal. E-Cadherin mRNA expression in whole mammary glands of FVB wild type (WT) or 20wk old MMTV-HER2 mice was determined by qPCR. Plot (**D**) shows means plus SEM; each dot represents one animal. 24wk old MMTV-HER2 mammary glands were stained against β-Catenin and Iba1, a macrophage marker (**E,F**). β-Catenin+ early cancer cells (blue arrows in F)

were more frequent in ducts containing intra-epithelial macrophages (black arrows in F) (**G**). Each dot represents one animal, plots show mean plus SEM. The mammary epithelial cell line Comma-1D was grown as a monolayer and Raw264.7 macrophages stably transfected with mCherry were added. After 12h, co-cultures were stained against E-Cadherin (**H**) or β-Catenin (**I**) and the signal intensity of β-Catenin signals inside individual nuclei was quantified (**J**). Boxplot shows range of nuclear β-catenin signal intensity in individual cells; independent experiments N=3. (**K,L**) Conditioned medium was harvested from primary cultures of wild type (WT) or pre-malignant MMTV-HER2 mammospheres and added to Raw264.7 macrophages or mammary tissue macrophages (MTMs) isolated from pre-malignant MMTV-HER2 mammary glands. Wnt-1 expression was determined by qPCR, plots show means plus SEM of three technical replicates; individual experiments N=3 for Raw264.7 and N=2 for MTMs. Comma-1D cells were grown as monolayers (**M**) and Raw-264.7-mCherry macrophages were added (**N**) and additionally treated with DKK1 (**O**). Co-cultures were harvested after 12h and stained against E-Cadherin. E-Cadherin signal intensity in whole section was quantified. Plot (**P**) shows mean plus SEM; each dot represents one microscopic field; independent experiments N=2.

Figure 3: Macrophage depletion during pre-malignant stages prevents early cancer cell dissemination. 20wk old pre-malignant MMTV-HER2 mice were treated with the anti CSF1R ASF98 antibody and animals were harvested after two weeks with no signs of invasive carcinoma (**A**). Analysis of HE staining of mammary gland sections confirmed the absence of invasive lesions (**B**). E-Cadherin expression in whole

mammary glands was determined by RealTime PCR of whole mammary gland lysates (**D**; mean plus SEM; each dot represents one individual mammary glands; N=2 experiments combined) and by immunofluorescent staining against E-Cadherin in mammary gland sections (**E,F**; bars 10μm). E-Cadherin signal intensity was measured in regions of cell junctions (**G**). Box plots depict values of individual regions for 3 animals each; N=2. Early circulating cancer cells (eCCCs) were quantified by harvesting peripheral blood and determining the amount of HER2 and CK8/18 positive eCCs per mL blood which then were normalized to the mean of controls. Plot (**H**) depicts normalized means plus SEM; each dot represents one animal; combined independent experiments N=2. Disseminated eCCs were quantified by staining lung sections against HER2 (**I,J**; bars 25μM) and quantifying the average of HER2+ cells per 100 randomly chosen microscopic fields (**K**). Plot (**K**) shows means + SEM where each dot represents one animal of 2 individual experiments combined.

Figure 4: Early disseminated cancer cells can contribute to metastasis formation. Macrophages were depleted from pre-malignant MMTV-HER2 mice by ASF98 treatment starting at week 18. Treatment was stopped when mice developed palpable tumors (1-3mm average) (**A**). Mice were left until tumors reached 1cm in diameter and then sacrificed. Time from beginning of treatment at age wk18 until development of palpable tumors (**B**) and from formation of palpable tumors until tumors were overt (**C**) is depicted as mean plus SEM where each dot represents one animal of two independent experiments combined. Macrophages in sections of overt tumors at the end of the experiment identified by staining against F4/80 (**D,E**) and quantified as

numbers of macrophages relative to tumor area (**F**). Vascularization of overt tumors was analyzed by staining against endomucin, an endothelial cell marker (**G,H**) and quantification of vascularized area (**I**). Plots show mean plus SEM where each dot represents one section of at least 3 animals combined. Solitary DCCs in lung sections and metastases defined as cell clusters bigger than 3 cells were quantified in lung sections stained against HER2 (**K**). For solitary cell analysis, the average of DCCs or metastases per 100 fields was counted; each dot represents one lung section (**J**). For metastasis analysis, the total number of metastases per lung sections was quantified and plotted (**L**). Number of mice N=6 (control) and N=4 (αCSF1R) animals combined; independent experiments N=2.

Figure 5: Phenotypic profiling of macrophages in early mammary cancer lesions. Whole mammary glands from FVB wild type mice or 14 and 22 week old pre-malignant MMTV-HER2 mice were analyzed by mass cytometry. viSNE plots were generated from myelo-monocytic cells (gating strategy **Fig.5 supplement 1B**) (**A**). Results from one representative animal is shown; number of animals per group N=5; individual experiments N=2. The three subpopulations were identified as Ly6C+ monocytes and CD206-hi and CD206-lo macrophages based on their expression levels of Ly6C (**B**) and CD206 (**C**). These three populations were then analyzed for their frequency amongst all myelomonocytic cells (**D-F**) Dot plots show mean plus SEM of 5 animals per group, each dot represents one animal. Heat plots for 3 individual animals per group with expression levels of selected markers Ly6C (**B**), CD206 (**C**), Tie2 (**I**) and IdU incorporation as a proliferation marker (**J**) were generated for CD206-lo and –hi

macrophages as identified in the viSNE plots. **G, H**: viSNE plot and quantification of myelomonocytic population in overt MMTV-HER2 tumors. Mammary glands from FVB wild type mice (**K**), MMTV-HER2 mice at 24wks (**L**) and overt MMTV-HER2 tumors (**M**) were stained against CD206 and F4/80 and CD206 signal intensity in F4/80+ macrophages was quantified. Plot (N) depicts mean plus EM, each dot represents one macrophages; 3 animals combined. Bars 10μm.

Figure 6: HER2 upregulation leads to activation of NFkB and CCL2 overexpression. Phosphorylation of the p65 subunit of NFkB was analyzed in Western Blots of whole cell lysates of mammospheres from 20wk old pre-malignant MMTV-HER2 mice (**A)**. One representative plot of three independent experiments is shown. (**B**) CCL2 expression in mammospheres derived from FVB wild type and pre-malignant MMTV-HER2 mammary glands was measured by real time PCR analysis. Plot shows means plus SEM where each dot represents one technical replicate; number of individual experiments N=3. (**C**) Mammary glands from FVB wild type, 14wk old and 22wk old MMTV-HER2 mice were stained against CCL2, HER2, and CCR2. CCL2 immunofluorescent signal intensity around the ductal epithelium was quantified (**D**). Plot shows mean plus SEM, each dot represents one duct. Bars 25μm. CCL2 was stained in acini cultures derived from pre-malignant MMTV-HER2 mammary glands that were grown for 5d and then treated with DMSO (vehicle control; **E**), 1μM Lapatinib (**F**) or 1μM IKK inhibitor compound A (**G**) for 24h. Acini derived from 20 week old pre-malignant MMTV-HER2 mammary glands were grown for 5d, then treated with DMSO (vehicle control), Lapatinib (1μM), IKK inhibitor compound A (1μM), or CCR2 inhibitor RS504393

(1μM) and macrophages isolated from 20wk old pre-malignant MMTV-HER2 mammary glands were added. After 24h, acini were stained against F4/80 and the percentage of acini associated with mammary gland macrophages in 3D co-cultures (exemplary image in **H**) compared to those not associated with macrophages (**I**) was determined (bar 25μm). Plot (**J**) shows means plus SEM; each dot represents one technical replicate; independent experiments N=2. 20wk old pre-malignant MMTV-HER2 mice were treated with a CCR2 inhibitior RS504393 (2mg/kg i.p. daily) for 2 weeks. Additionally, mice were treated locally by injecting 2mg/kg CCR2 inhibitor into the fat pad of one gland and vehicle control into the contra-lateral gland. Injections were performed daily for 5 days (**N**). Pre-malignant mammary glands were stained against E-Cadherin and F4/80 (**K,L** bars 25μm) and intra-epithelial macrophage (IEM) containing ducts were quantified (**M,O**). For local treatment, values were normalized to the IEM content of each contra-lateral control treated gland. Plot shows means plus SEM; each dot represents one animal.

Figure 7: Intra-epithelial macrophage numbers in human DCIS lesions negatively correlate with E-Cadherin levels. Human adjacent healthy (**A**) and DCIS tissue (**B**) was stained against CD68 (macrophages) and smooth muscle actin (SMA). Bar: 75μm. Plot shows mean plus SEM of the percentage of ducts intra-epithelial macrophages (IEM) from 7 healthy and 10 DCIS patients; each dot represents one patient (**C**). Sections from human DCIS tissue were stained against CD68 (macrophages) and E-Cadherin (**D,E**). E-Cadherin pixel intensity was quantified in regions of individual cell junctions and medians for individual patients were quantified. Plot (**F**) depicts mean E-Cadherin intensity throughout DCIS lesions of individual patients with low or high intra-

837 epithelial macrophage (IEM) numbers (total patient number N=12). All bars 25μm.
838 Scheme of macrophage (**G**) assisted early dissemination from pre-invasive lesions
839 where mammary tissue macrophages (MTM) are attracted into pre-invasive ducts by
840 early cancer cells (CC) via HER2 and NFkB mediated upregulation of CCL2. Intra-
841 epithelial macrophages secrete Wnt proteins and thereby induce an EMT that drives
842 early dissemination. Early disseminated cancer cells then contribute to metastasis
843 formation, either as a slow cycling seeds of metastasis (scenario 1) or by interacting
844 with the microenvironment to make it more permissive for the growth of more adapted
845 late cancer cells (scenario 2).
846
847

Supplementary Figure Legends.

Supplementary Fig.1. Depletion of mammary gland macrophages (F4/80+/CD11b+) after two weeks of treatment with a CSF1R antibody compared to vehicle control (**A**). Percentage of ducts with intra-epithelial macrophages (IEM; **B**) and hyperplastic ducts (**C**) was quantified in mammary gland sections after two weeks of CSF1R antibody or vehicle treatment. Whole mount staining of mammary glands after two weeks of CSF1R antibody or vehicle control treatment (**D,E**).

Supplementary Fig.2. Flow cytometry lung gating strategy were CD45+ viable cells were identified as F4/80+/Gr1+/CD11b+ and F4/80-/Gr1+/CD11b+ monocytes and F4/80+/Gr1-/CD11c^{hi} alveolar macrophages (**A,B**). Quantification of alveolar macrophage (**C**) and monocyte populations (**D**,**E**) in lungs of MMTV-HER2 mice that had been treated with a CSF1R antibody or vehicle control during pre-malignant stages and were then allowed to progress to over tumor stages.

Supplementary Fig.3. A: List of markers analyzed by mass cytometry (CyTOF). **B**: Gating scheme to create viSNE plots of macrophages and monocytes. DNA staining and Cisplatin was used to identify viable cells. **C**: Heatplot of CD11b in the three myelo-monocytic populations identified by visne plot (Fig.2A). N=3 animals per group; independent experiments: N=2. **D**: Heatplot of VCAM1 in the three myelo-monocytic populations identified by viSNE plot. N=2 animals per group; independent experiments N=2.

Supplementary Fig.4. A: Overview of qRT-PCR expression and immunofluorescent analysis results of selected cytokines in mammospheres derived from 20wk old MMTV-Her2 mammary glands that were not detectable (n.d.), did not change (n.c.) or did not chance significantly (n.s.) or were increased in relation to expression levels in FVB wild type mammary glands. **B**: qRT-PCR expression analysis of CSF2 expression in mammospheres derived from either FVB wild type or 20wk old MMTV-Her2 pre-malignant mice. Three independent experiments with triplicates were performed. **C-E**: Immunofluorescent staining of FVB wild type (C) and 22wk old MMTV-Her2 mammary glands (D) against CSF2 or with IgG control (E). Bars 25μM

Supplementary Fig.5. Human DCIS sections were stained against CD68 and CD45 (**A**) and CD68 and cytokeratin 8/18 (**B**). **B,C**: Two individual ducts in one DCIS lesion of the same patient with either high E-Cadherin and low intra-epithelial macrophage (IEM) levels (**C**) or low E-Cadherin levels and high IEM levels (**D**) within the same patient. **E**: Quantification of E-Cadherin signal intensity in the region of cell junctions within ducts of the same patients with either high or low numbers of IEMs.

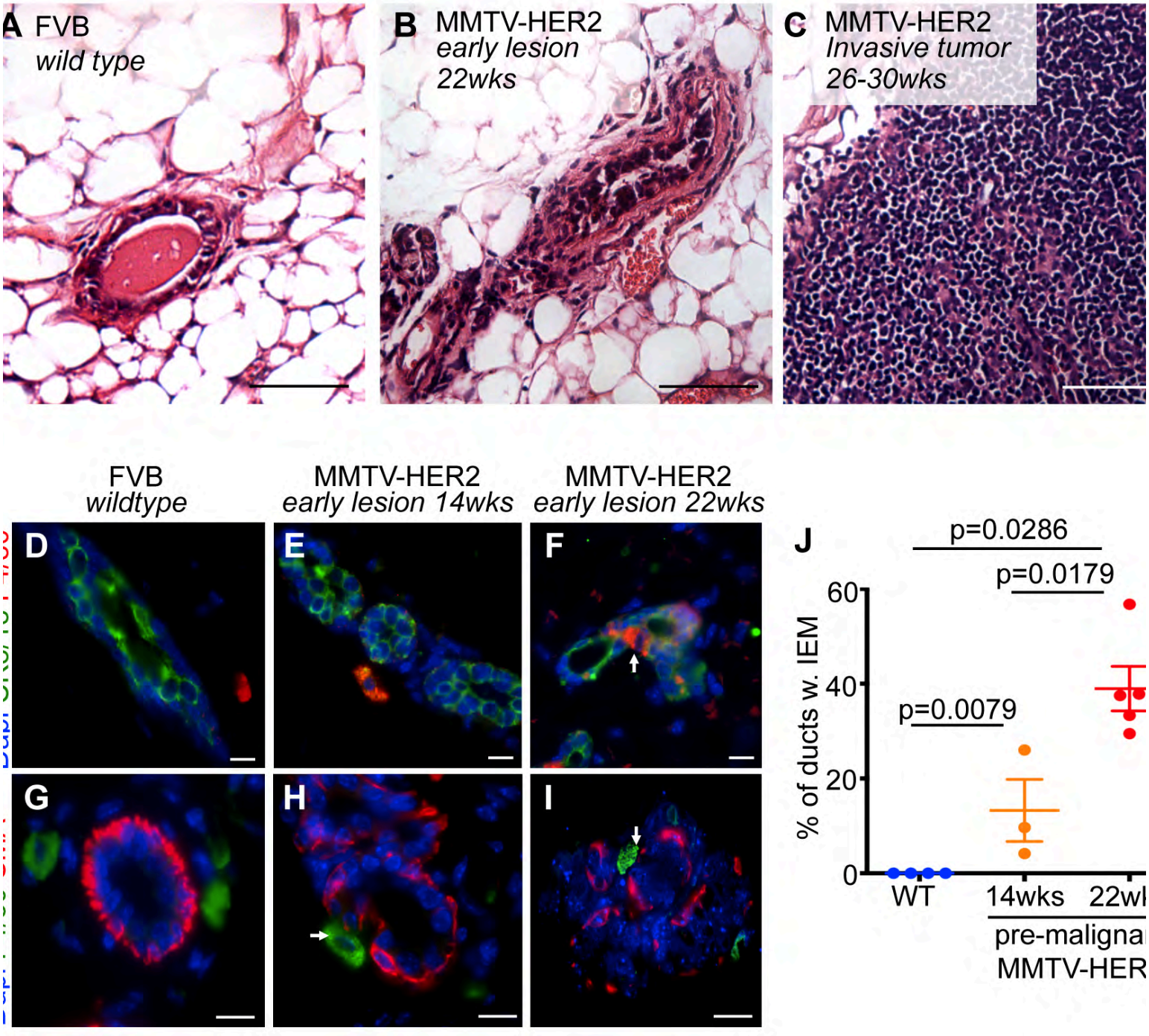

.inde et al. 2016 Figure 1

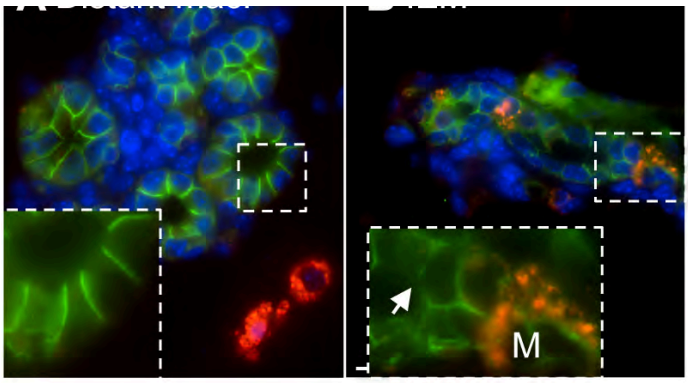

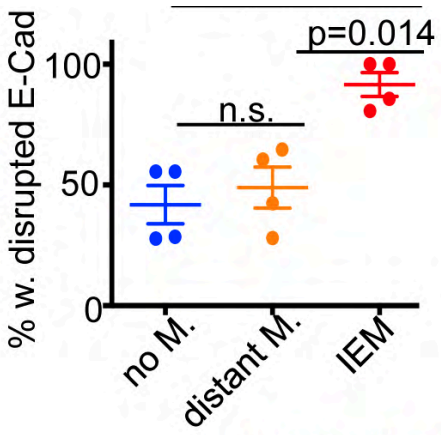

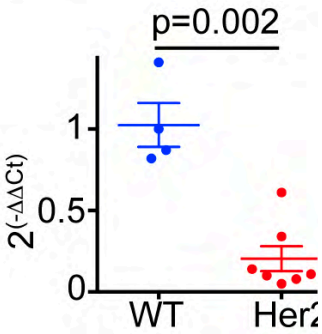

β-Catenin Iba1

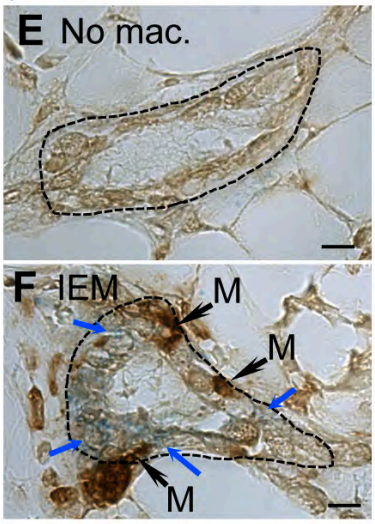

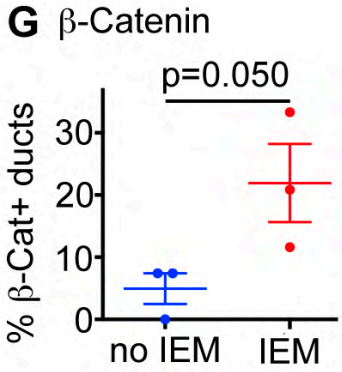

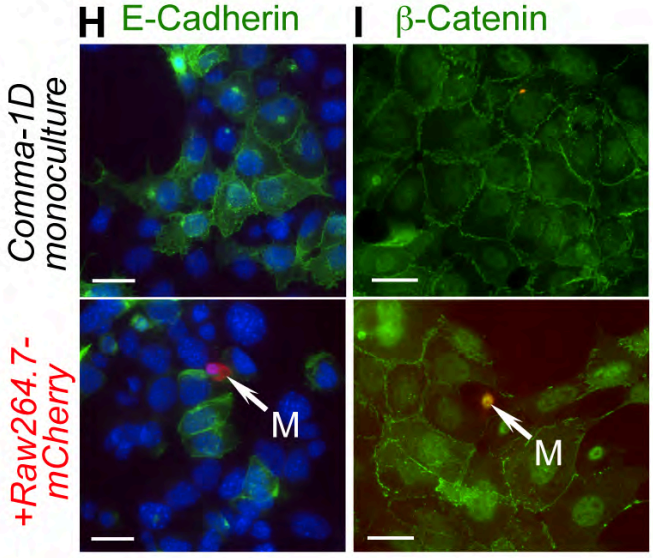

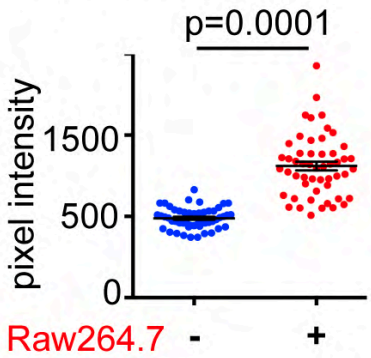

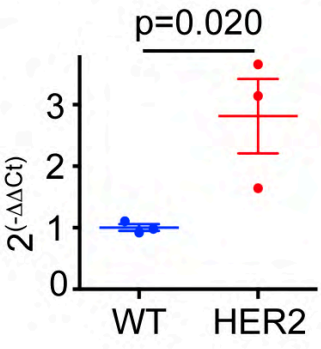

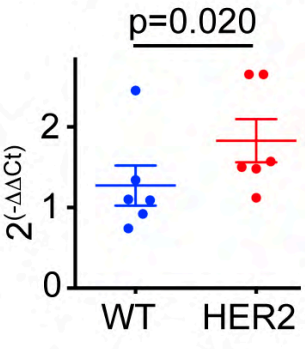

E-Cadherin mCherry

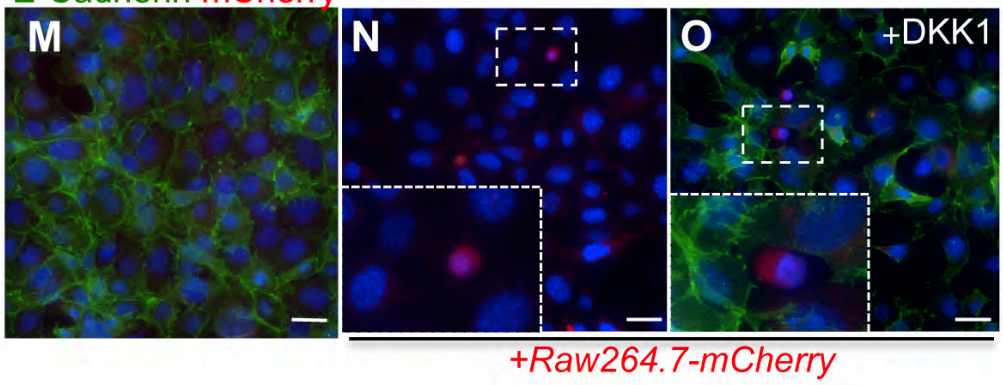

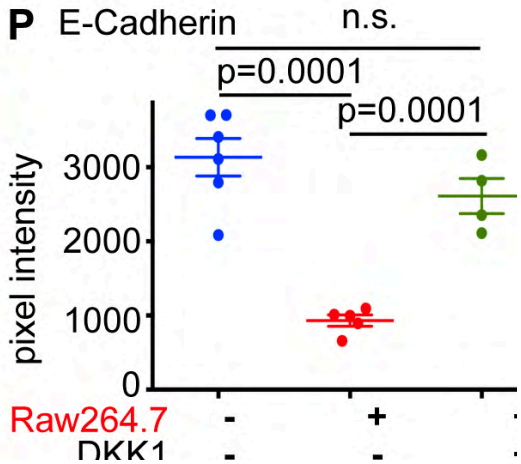

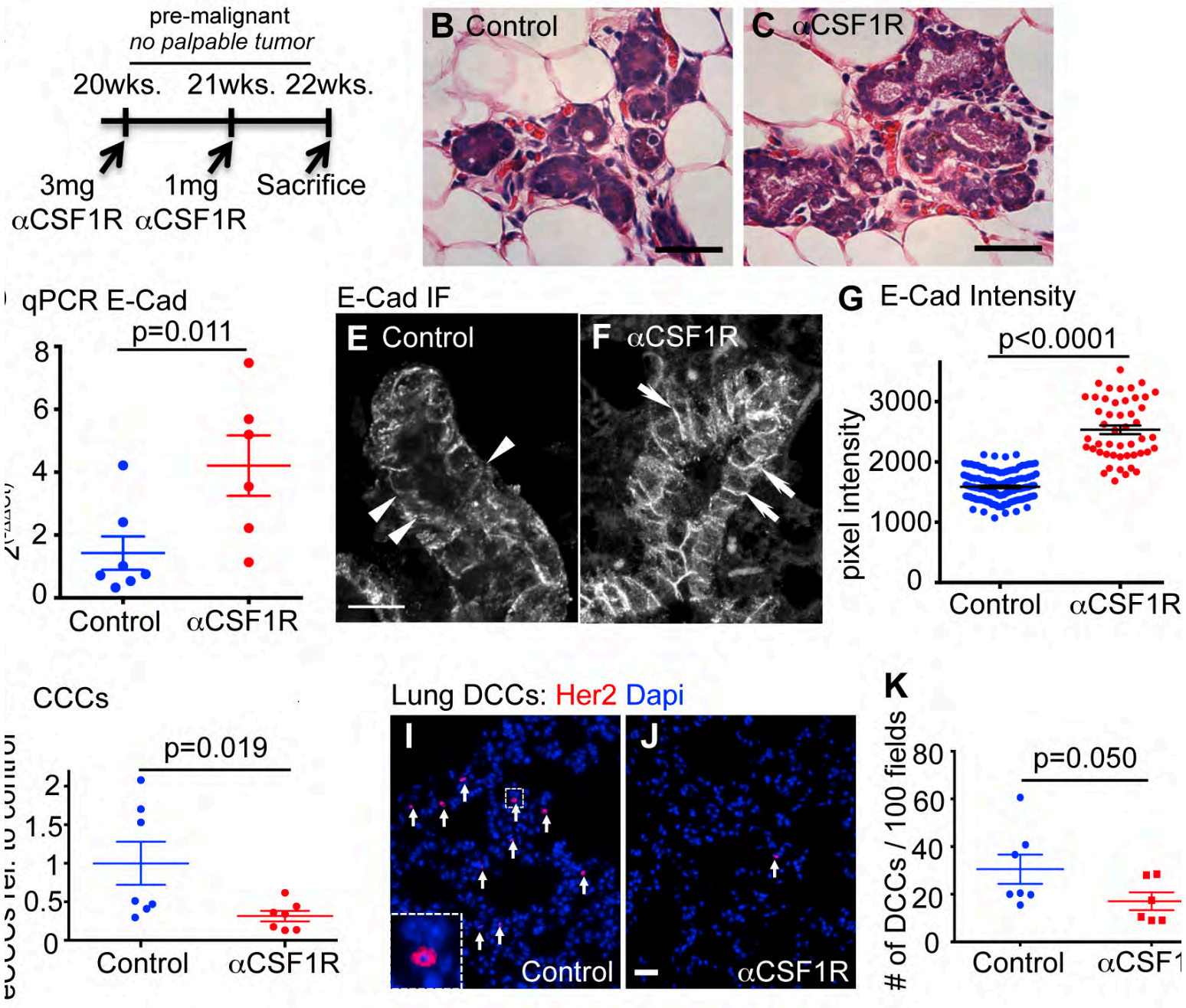

Linde et al. 2016 Figure 3

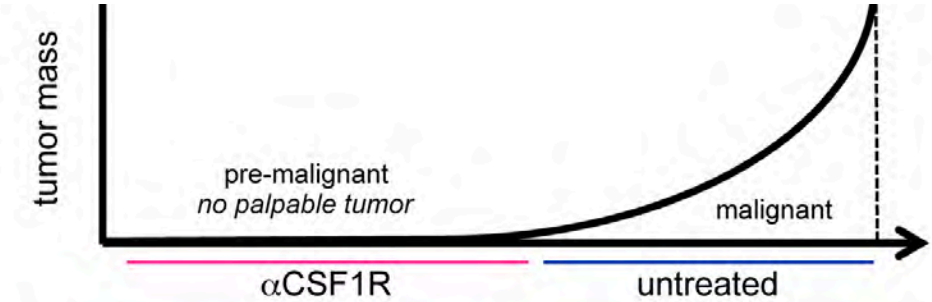
tumor mass
pre-malignant
no palpable tumor
malignant
αCSF1R
untreated

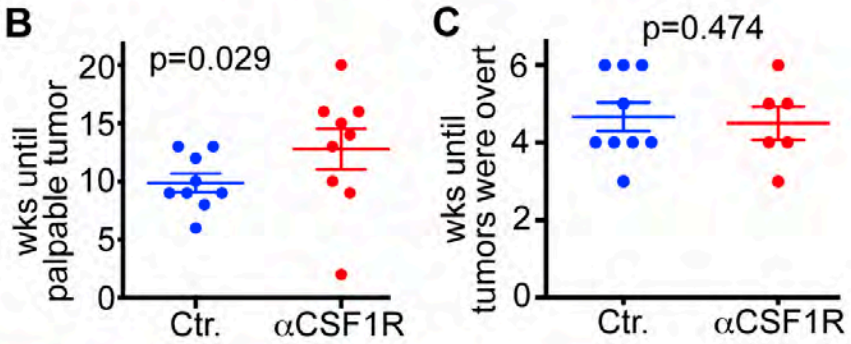
B
p=0.029
wks until palpable tumor
20
15
10
5
0
Ctr.
αCSF1R
C
p=0.474
wks until tumors were overt
6
4
2
0
Ctr.
αCSF1R

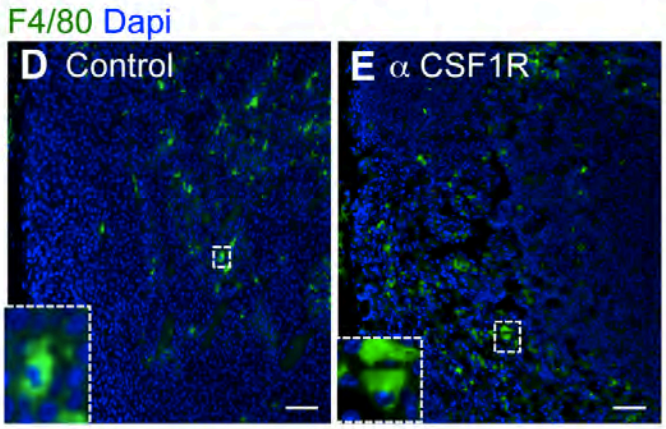
F4/80 Dapi
D Control
E α CSF1R

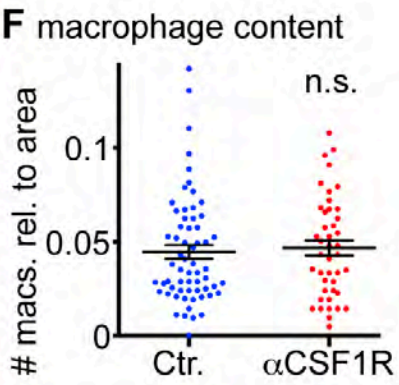
F macrophage content
macs. rel. to area
0.1
0.05
0
n.s.
Ctr.
αCSF1R

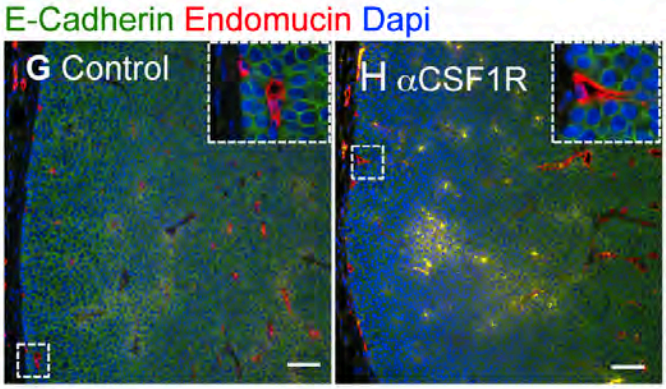
E-Cadherin Endomucin Dapi
G Control
H αCSF1R

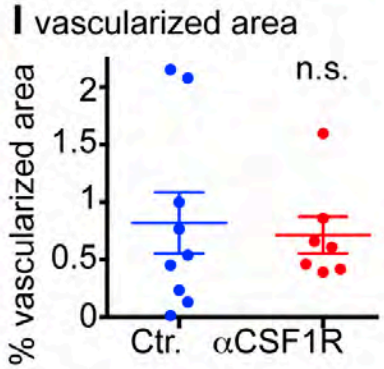
I vascularized area
% vascularized area
2
1.5
1
0.5
0
n.s.
Ctr.
αCSF1R

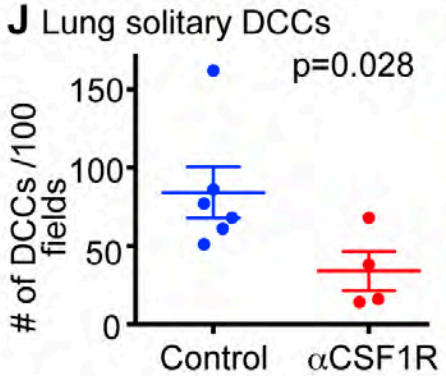
J Lung solitary DCCs
p=0.028
# of DCCs /100 fields
150
100
50
0
Control
αCSF1R

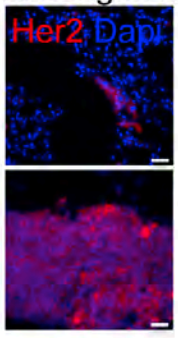
K Lung met
Her2 Dapi

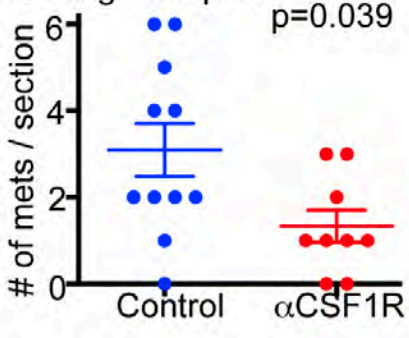
L Lung met quant.
p=0.039
# of mets / section
6
4
2
0
Control
αCSF1R

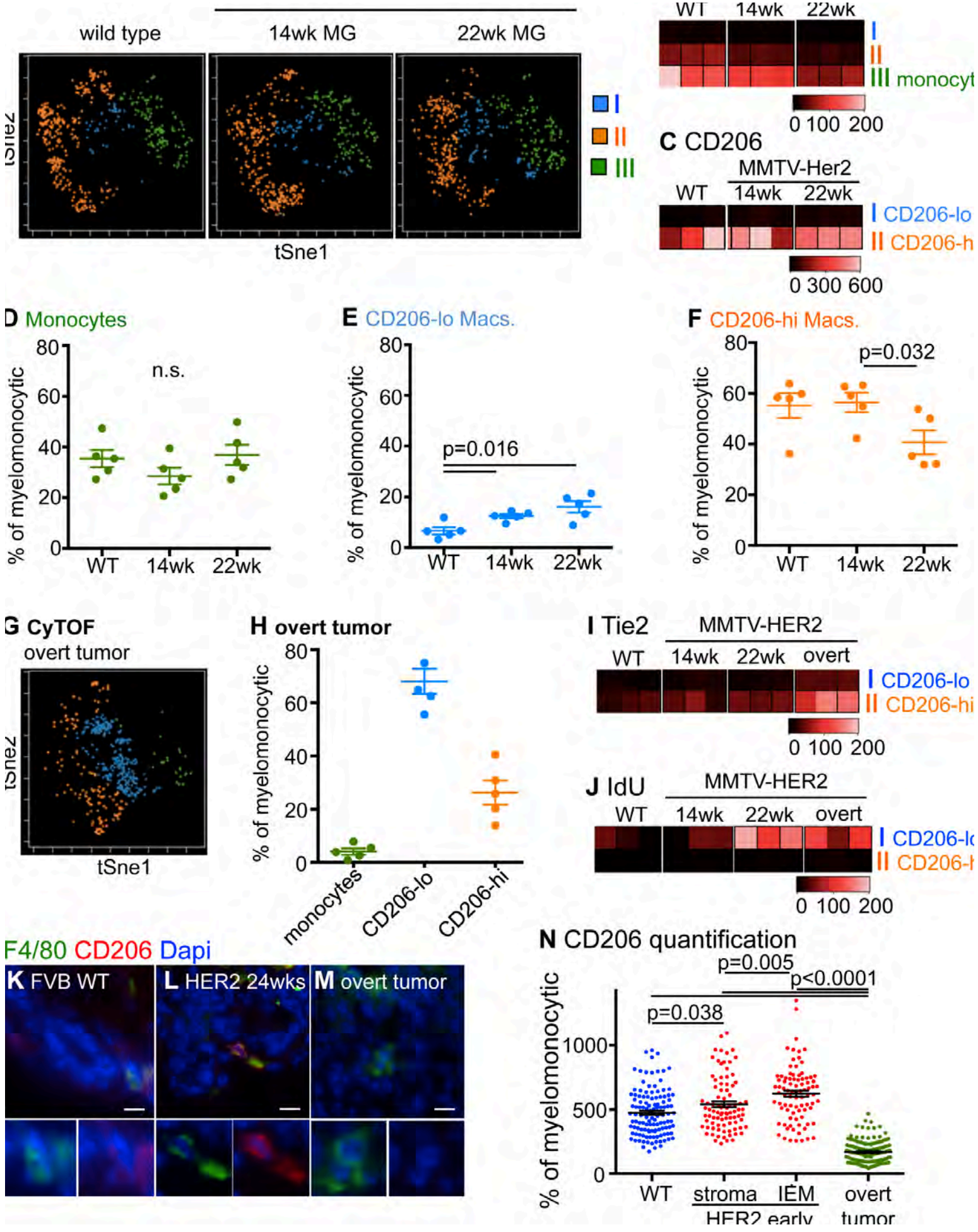
wild type
14wk MG
22wk MG
tSne2
tSne1
I
II
III
WT
14wk
22wk
monocyt
0 100 200
C CD206
MMTV-Her2
CD206-lo
CD206-h
0 300 600
D Monocytes
n.s.
% of myelomonocytic
E CD206-lo Macs.
p=0.016
F CD206-hi Macs.
p=0.032
G CyTOF
overt tumor
H overt tumor
monocytes
CD206-lo
CD206-hi
I Tie2
MMTV-HER2
overt
CD206-hi
J IdU
F4/80 CD206 Dapi
K FVB WT
L HER2 24wks
M overt tumor
N CD206 quantification
p=0.005
p<0.0001
p=0.038
stroma
IEM
HER2 early
tumor

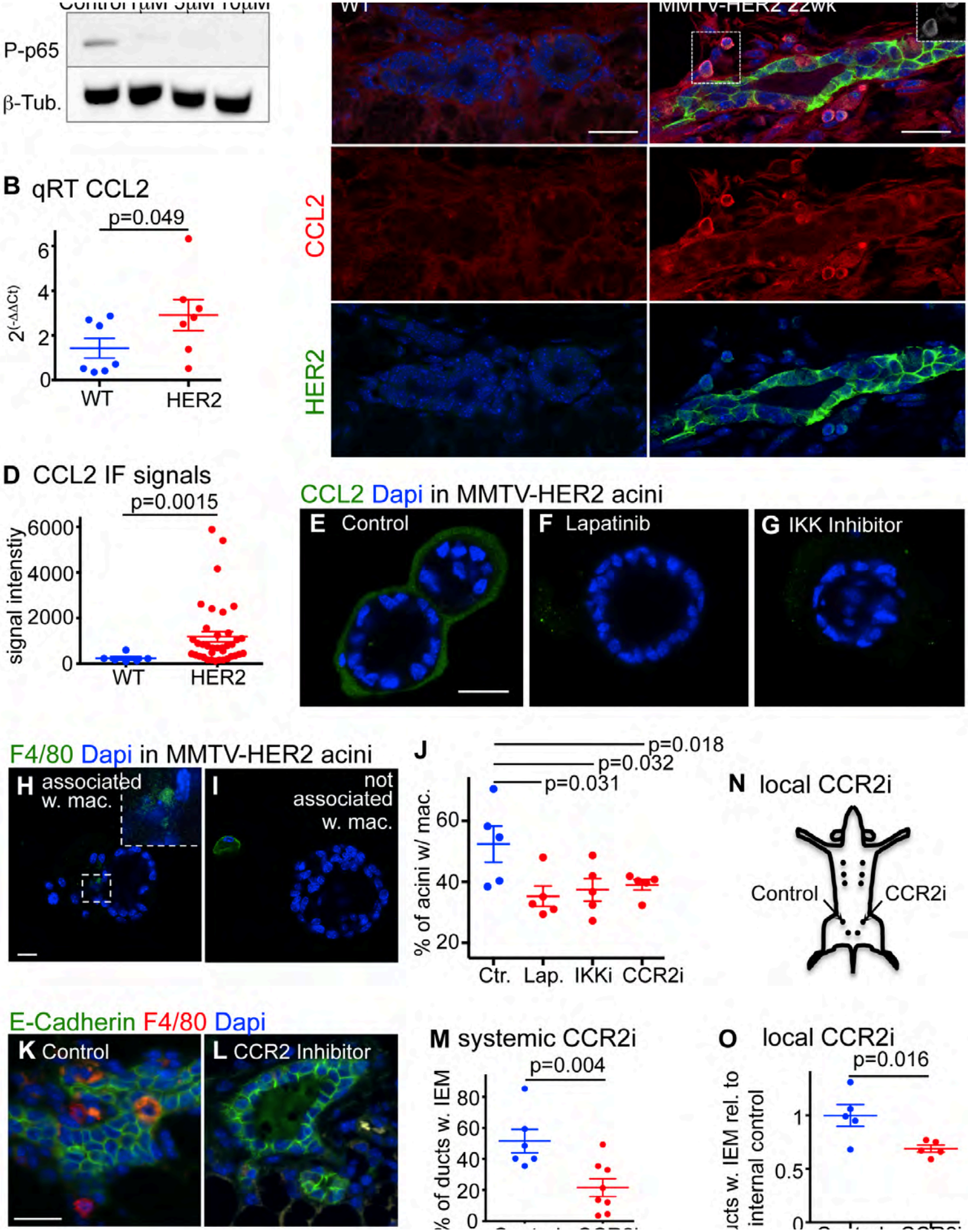
Control 1μM 5μM 10μM
P-p65
β-Tub.
B qRT CCL2
p=0.049
2(-ΔΔCt)
WT
HER2
WT
MMTV-HER2 22wk
CCL2
HER2
D CCL2 IF signals
p=0.0015
signal intenstiy
CCL2 Dapi in MMTV-HER2 acini
E Control
F Lapatinib
G IKK Inhibitor
F4/80 Dapi in MMTV-HER2 acini
H associated w. mac.
I not associated w. mac.
J
p=0.018
p=0.032
p=0.031
% of acini w/ mac.
Ctr.
Lap.
IKKi
CCR2i
N local CCR2i
Control
CCR2i
E-Cadherin F4/80 Dapi
K Control
L CCR2 Inhibitor
M systemic CCR2i
p=0.004
% of ducts w. IEM
O local CCR2i
p=0.016
ucts w. IEM rel. to internal control

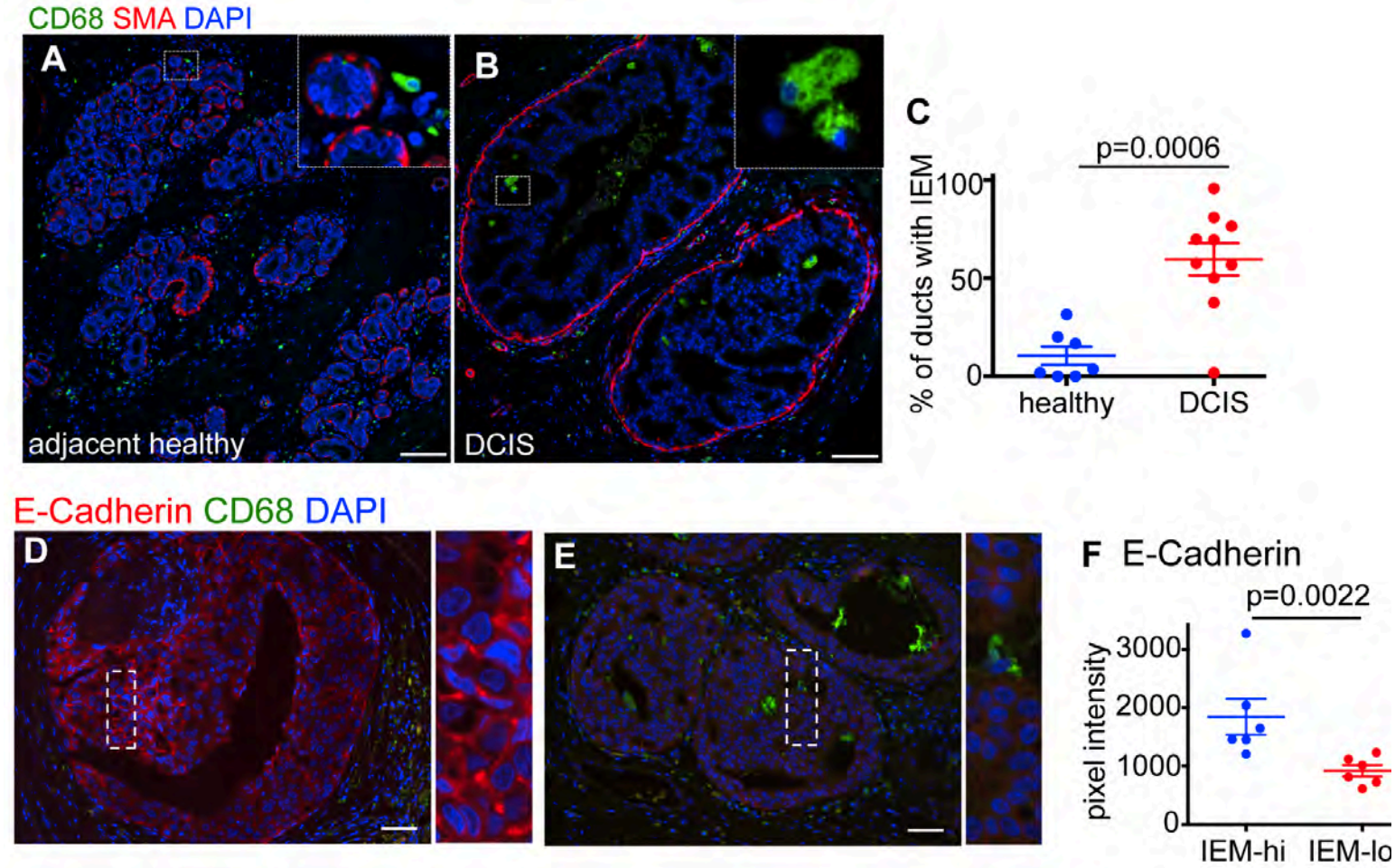

G Model of macrophage driven early dissemination

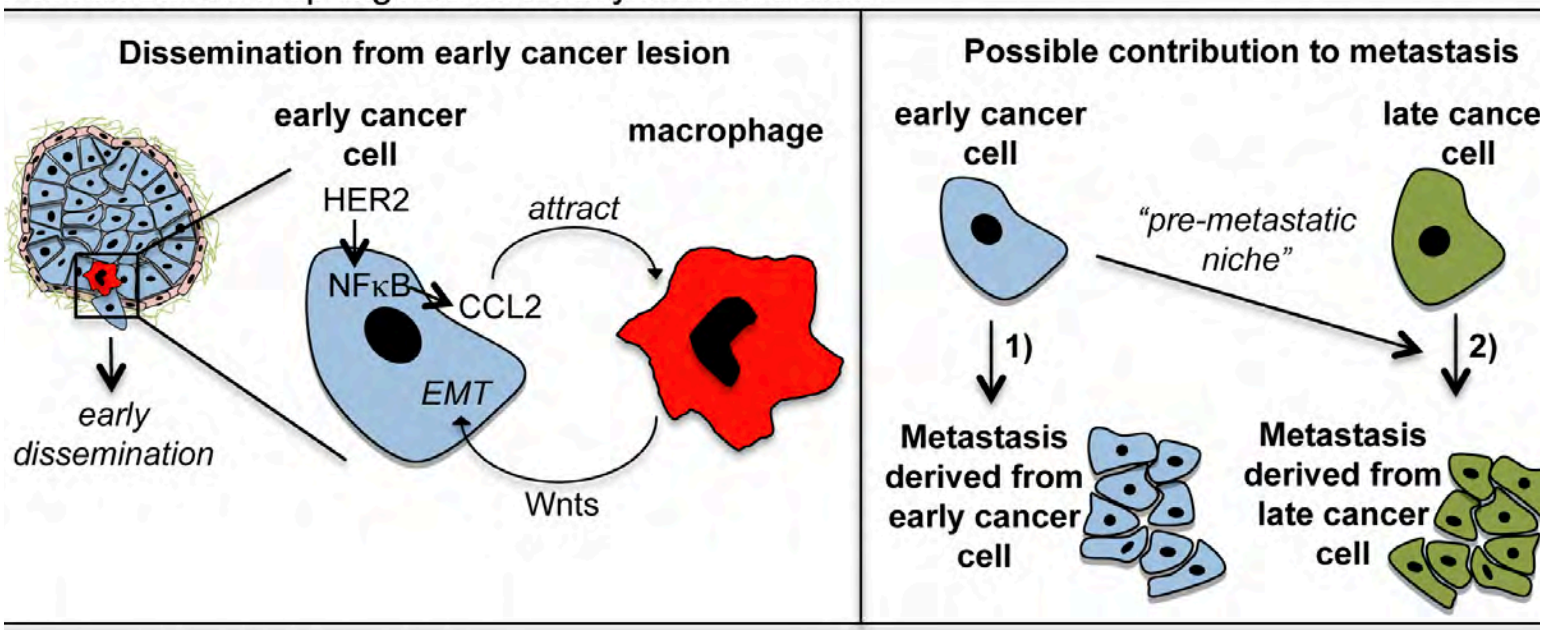

Linde et al. 2016 Figure 7